INVESTIGATION OF SOME NONLINEAR PROBLEMS IN MECHANICS

BY

WEI WANG

A dissertation submitted to the

School of Graduate Studies

Rutgers, The State University of New Jersey

In partial fulfillment of the requirements

For the degree of

Doctor of Philosophy

Graduate Program in Mechanical and Aerospace Engineering

Written under the direction of

Liping Liu

And approved by

_____

_____

_____

_____

New Brunswick, New Jersey

January, 2021

ABSTRACT OF THE DISSERTATION

Investigation of some nonlinear problems in Mechanics

by WEI WANG

Dissertation Director: Liping Liu

We investigate some nonlinear problems in mechanics, which include the dynamic problem with nonlinear interaction, the optimal design of multi-phase conductive composite, and the phase transition of lattice structures governed by non-convex energy functions.

The first nonlinear problem we investigate is the dynamics of a two-dimensional lattice with harmonic, weakly nonlinear, and strongly nonlinear interactions. Assuming the nearest neighbor interaction, we derive the continuum approximation of the discrete system in the long wavelength regime while keeping the Hamiltonian structure of the system. For a hexagonal lattice with nontrivial shear resistance, we surprisingly find that solitary wave solutions exist in certain directions related to the underlying symmetries of the lattice. The properties of the solitary waves are also studied by numerical simulations of the original discrete system. Besides being of fundamental scientific interest, the solitary wave solutions in nonlinear hexagonal lattices are anticipated to have applications in the design of shock absorbers, acoustic lens, non-destructive structural testing devices among many others.

Secondly, the optimal design of multiphase conductive composites by estimating Hashin-Shtrikman bounds (HS bounds) attainability in the constraint of volume fractions of the

constituent phases. We derive the necessary condition by null lagrangian and maximum principle. We address the sufficient condition of the HS bounds attainability by proposing a new class of coated sphere comprised of three-phase and four-phase isotropic conductive materials, and generalize the coated spheres to a larger number of phases. Combining the necessary and sufficient condition of HS bounds attainability, we can precisely characterize the G-closure and effective properties of multiphase conductive materials for a broader range.

Lastly, we design and characterize a two-dimensional (2D) crystal formed by a lattice structure, which consists of repeating structure elements called unit cells. Based on the minimization of total free energy of the unit cell, we find three stable phases coexist at the critical loading which turns out naturally result in the microstructure. The microstructure of the lattice structure may easily buckle while the macrostructure of the lattice structure is in compression, the properties of the lattice structure are also studied by numerical simulations in a 2D biaxial stress system. Such lattice structures can undergo "phase transitions" mimicking the Austenite-Martensite phase transition in shape memory alloys (SMAs). More importantly, they offer directly observable material models that can shed light on the fundamental mechanisms of the first-order non-diffusive phase transitions and shape memory effects, their interactions with defects, and the physical origins of hysteresis.

Acknowledgements

First and foremost I would like to express my sincere gratitude to my advisor Prof. Liping Liu for his continuous support and encouragement of my Ph.D. study and related research. I appreciate all his contributions of time, ideas, and funding to make my Ph.D. experience productive and stimulating. He has been supportive and has given me the freedom to pursue various projects without objection. He has also provided insightful discussions about the research. It is his guidance and constant feedback helped me accomplish this thesis. I also appreciate his consideration of my life.

Besides my advisor, I would like to thank my thesis committee: Prof. Howon Lee, Prof. Aaron Mazzeo, and Prof. Wujun Zhang for their insightful comments and suggestion. My sincere thanks also go to Prof. Howon Lee's group who provided me the knowledge of 3D printing. I would also thank Prof. Wujun Zhang for insightful discussions of my research of the curved beam, he gave me instruction of numerical analysis.

I thank my fellow Hanxiong Wang for the stimulating discussions and he provided me with a lot of help in completing the teaching assistance work. Wuhan Yuan and Zhizhong Dong have been so helpful when I attended a course at night, they drove me home until I bought a car, I will never forget their help.

Also, I thank my friends Tongfen Liang, Jingren Wang, Xiyue Zou, Xuehai Wu, Yang Wang, Xiaodong Xia, Xing Liu, and Wei Tang for providing support and friendship that I needed. I also thank my friends Xiang Kou, Rui Wang, Bowen Huang, Zhenzhou Wang, Ying Huang for spending a great time with me. My time at Rutgers was made enjoyable in large part due to their company which became a part of my life. I am grateful for time spent with Yan Liang, Minjing Wang, Ke Ke, Qiming Guan, Piao Zheng, Yanzhe Xu, Biyu Wen, the time spent with them is joyful and meaningful, their consideration and caring give me

the courage to go further.

I would also like to thank my family: my parents Jinghong Wang and Guiyin Tian and my parents-in-law Yaokang Deng and Xiaoping Bai for their unconditional love and care. My parents raised me with a love of science and supported me in all my pursuits. They take care of my baby, which gives me the time to spend on my research, their support makes me more dedicated to my research. I love them so much, and I would not have made it this far without them.

Last but not least, I am most appreciative of my husband Zupeng Deng, he always believed in me like nobody else and gave me endless support. His positive and motivate attitude affect me, which make me pursuing big progress in my research, There are no words to convey how much I love him.

Table of Contents

List of Figures

Chapter 1
Introduction

Nonlinear systems can be described as a system in which the principle of superposition does not hold. It is ubiquitous in nature and has been an important topic for engineers, biologists, physicists, mathematicians, and many other scientists [75]. Nonlinearities cover almost all parts of mechanics, and accordingly nonlinear systems of equations related to many problems have been discovered. Some of the principal examples include systems arising (1) in the formulation of the nonlinear dynamics of discrete systems, (2) in connection with nonlinear optimization problems, (3) in connection with phase transition problems. Since the form and properties of these nonlinear systems are strongly affected by the problem area and nonlinear sources, we focus ourselves in three specific mechanics problems, including the propagation of solitary waves in granular crystal, the optimal design of multi-phase conductive composites and the phase transition of lattice structures governed by non-convex energy functions.

In this dissertation, we first focus on dynamics in granular material with nonlinear interaction. The initial motivation to investigate strongly nonlinear dynamics of the discrete system was prompted by the challenges in the development of mitigating media to reduce high-amplitude compression pulses caused by impact or explosion[79]. Nesterenko first solved the problem by Korteweg-de Vries (KdV) equation with a weakly nonlinear one-dimensional chain of elastic spheres in the continuum approximation, However, this approach had a mathematical and physical problem when the amplitude of the wave was much larger than the initial precompression. Thus instead of a weakly nonlinear KdV type of equation, a more complex strongly nonlinear wave equation was proposed [77, 78]. As initiated by the seminal work of Fermi-Pasta-Ulam (FPU), it has been found that 1D

Hertzian granular crystals support the formation and propagation of highly nonlinear solitary waves (HNSWs) [77], therefore, extensive research has focused on the propagation of solitary waves in granular crystal.

Generic granular material is a collection of distinct macroscopic particles with varying shapes, sizes, and orientations. Some examples of granular materials are snow, nuts, coal, sand, rice, coffee, corn flakes, fertilizer, and bearing balls. Granular crystal is a special class of granular material since it is fabricated as tightly packed lattices or ordered solid particles. The dynamic response of granular crystal is scalable and tunable ranging from highly nonlinear to almost linear. For a one-dimensional (1D) granular crystals, i.e., a chain of balls, the equation of motion of the discrete system is derived by Hamilton's principle. Since the phase speed of a propagating disturbance is much larger than the particle velocities in the solitary wave, a complex long wave approximation is adopted, and by the standard first-variation calculation, the associated Euler-Lagrange general equation was found in the long-wavelength limit. However, few analytical calculations demonstrating the solitary wave solutions in higher dimensional granular crystals, which significantly limit the engineering of such granular crystals. We focus on a 2D hexagonal lattice with nontrivial shear resistance and general nonlinear interaction potentials. Aiming at analytical solutions, we pay close attention to approximating the discrete model in a systematic manner. For the final continuum equations, we surprisingly find exact longitudinal solitary wave solutions for systems with weakly nonlinear interactions and Hertzian interactions.

The second nonlinear problem we discuss is the optimal design of multiphase conductive composites. The quasi-convexification of the nonconvex function was proposed for the optimal design problem of multiphase composites, the quasiconvex functions have proven to be useful in describing, constructing and restricting microstructures [8], consequently, the optimal design problem can be reformulated as a vector variational problem of the minimization of the quasiconvex functions [85]. The optimal design problem has received a lot of attention because of its relevance to bounding the effective properties of multimaterial mixtures. However, characterizing the effective properties is not easy because it

depends on the detailed microstructure of composites. Therefore, much attention in this area has focused on the study of optimal bounds of the effective properties. The well-established strategy in seeking optimal bounds consists of two steps: the first is to derive a microstructure-independent bound and the second is to study if this bound is attainable and if so, by what kind of microstructures. Hashin et al. derived the Hashin–Shtrikman bounds (HS bounds) by variational principles and applied the bound on the effective elastic moduli of statistically isotropic heterogeneous materials [38, 39]. Moreover, the following groups construct microstructures to explore the optimality of the bounds, the optimal microstructures include spheres model [36], coated ellipsoids [68], finite rank laminates [63, 82, 69, 27], "Vigdergauz microstructures" [33, 104]. However, the HS bounds are not always optimal for more than two-phase composite based on the volume fractions of the constituent phases [68]. Therefore, more work is needed to investigate the optimal microstructures of multiphase composites and the attainment conditions of the HS bounds.

The first optimal three material microstructure is comprised of two kinds of Hashin–Shtrikman coated sphere [68]. Further, Sigmund et al. proposed several new designs of materials with extremal elastic properties using a numerical topology optimization approach [93, 94, 95, 92]. Besides constructing the optimal microstructure, the translation bounds were also introduced to reproduce the HS bounds for multiphase conducting composites [100, 76, 5]. Albin et al. expanded the attainable region of the translation bounds and introduced a general algorithm for constructing the structures of three components in two dimensions, and investigated the sufficient conditions of the attainability of HS bounds by multi-rank laminates [3]. What's more, Liu presented a new way derivation of the Hashin-Shtrikman bounds and prescribed the attainment condition [59]. Although plenty of works address the attainability of HS bounds for multiphase composite, there still lacks a systematic method to characterize all the attainable regimes. Followed by the previous work of Liu [59], we construct a new optimal three-phase coated sphere: the core sphere occupied by one-phase and the external coating occupied by two-phase periodic E-inclusion [61]. We demonstrate the optimality of the microstructure by applying local electrical fields

and present the sufficient condition of HS bounds attainment in terms of volume fractions of the constituent phases. We extend the microstructure to the optimal four-phase coated sphere and generalize to a larger number of phases. Combining the necessary and sufficient condition of HS bounds attainability, we summarize all the attainable region for three-dimensional multiphase conductive composites.

The last nonlinear problem is the phase transition of lattice structure governed by nonconvex energy functions. By characterizing a two-dimensional (2D) crystal formed by a lattice structure, we deal with phase transition to mimic the Austenite-Martensite phase transition in shape memory alloys. Shape memory alloys (SMAs) are a group of metallic alloys that can recover to their original shape when subjected to a certain stimulus such as thermomechanical or magnetic variations. This phase transition is characterized as a displacive, non-diffusive, first-order transition [9]. It is found that the free energy at critical temperatures, at which transition occurs, becomes a nonconvex function, which can be solved by the variational principle [26, 6, 17, 4]. From a microscopic point of view, the shape memory effect (SME) consists in a transition from a crystallographic phase stable at low temperature, i.e. martensite, to a different crystallographic phase stable at high temperature, namely austenite [99, 15, 83, 84], which makes SMAs have applications in numerous commercial fields [73, 98, 29, 53, 74]. However, most applications are limited to NiTi-based SMAs, and NiTi-based SMAs have two major limitations: high materials cost and the narrow temperature range. Therefore, it is important to understand the fundamental mechanisms of phase transition and shape memory effect to develop new materials.

To understand the shape memory effect between austenite and martensite, James developed a mathematical formulation based on free energy minimization to theoretical approach these fine phase mixtures [47, 49], they found that some of the common microstructures in shape memory materials were depending on the lattice parameters. Based on the energy minimization theory, Bhattacharya further illustrated that energy minimization with many variants naturally results in microstructure when the lattice parameters satisfying some significant restrictions. Remarkable progress in mathematically understanding the

relationship between the microstructure formation and lattice parameters of SMAs boosts the design of new materials [12]. Moreover, advances in the understanding of the relation between microscopic and macroscopic deformation also play a key role [50]. To mimic the shape memory effect, we adopt a two-dimensional lattice with a simple stress-induced phase transition [96, 103]. In this model, the microstructure of the lattice structure may easily buckle when the macrostructure of the lattice structure are in compression. By the Cauchy-Born rule, the free energy can be expressed as a function of the deformation gradient and temperature. Minimizing the total free energy based on the geometrically linear theory, we get four distinct stable configurations corresponding to four stable phases, and transitions between these phases are regarded as phase transformations of the lattice structure. Applying the Hadamard compatibility condition, we found that the microstructure forms when the lattice satisfies significant restrictions on the parameters.

The dissertation is organized as follows: in Chapter 2 we present the general scheme of deriving continuum approximations to a discrete dynamic system for square lattice and hexagonal lattice, and we derive explicit solitary wave solutions with respect to harmonic, weakly nonlinear and Hertzian interactions. Moreover, we study the properties of solitary waves and scaling laws by numerical simulations. In Chapter 3 we recall the general scheme of Hashin-Shtrikman bounds (HS bounds) and their attainment conditions to $(N+1)$-phase isotropic conductive materials. We derive a necessary condition such that HS bounds are attainable, and we derive a sufficient condition through constructing a new type of optimal three-phase and four-phase coated spheres. Combining the necessary and sufficient conditions of HS bounds, we present the G_θ-closure of multiphase conductive composites. Chapter 4 we design and characterize the stress-induced phase transition of a two-dimensional (2D) lattice structure. With the general deformation gradient, we derive the four-phase of the unit cell by minimization of free energy. By extending the scheme to 2D lattice structure, we discuss the microstructure formed by two different types of load, and numerically study the phase transformation of lattice structure under biaxial loading. Finally, we conclude and present an outlook of possible applications in Chapter 5.

Chapter 2

Solitary waves in two dimensional nonlinear lattices in the continuum limit

2.1 Introduction

Generic granular materials can be described as densely packed discrete particles with varying shapes, sizes, and orientations. In fact, granular materials are ubiquitous in nature and have broad applications ranging from man-made shock absorbers, bullet proof vests [34, 51] to non-destructive structural testing [108], shock energy absorbing [91, 23], sound scrambling [80, 22], and actuating devices [52]. Over the last several decades, considerable efforts have been devoted to analyzing the wave propagations in ordered granular materials (or granular crystals). However, many analytical works have been focused on one-dimensional (1D) granular crystals, i.e., a chain of balls. As initiated by the seminal work of Fermi-Pasta-Ulam (FPU), it has been found that 1D Hertzian granular crystals support the formation and propagation of highly nonlinear solitary waves (HNSWs) [77]. Such solitary waves have been experimentally validated [78, 90] and explored for a number of novel applications, e.g., detecting orthopaedic implant stability [108], and monitoring the hydration of cement [81]. It has also been found that heterogeneous chains robustly support the formation and propagation of HNSWs, and the periodicity of the chain highly affect the widths, propagation speed, and energy redistribution of the wave [42, 86]. The scalability and tunability of HNSWs in granular crystals are ideal for studying the fundamental physics of nonlinear system and promise novel designs of structures or devices that can be used for high-throughput waveguides, vibration mitigation, and energy trapping among many others.

In contrast to granular chains, there are few studies focusing on two-dimensional (2D) granular crystals. A particularly interesting question is whether there exist similar solitary wave solutions in an ordered 2D lattice with nonlinear interaction potential [46, 28]. Experimentally, it has been found that the dynamic properties of square packing of spheres are essentially one dimensional because of lack of shear resistance: an impulsive excitation gives rise to a solitary wave traveling only in the initially excited direction [57]. However, interesting dynamic properties of centered square packing of spheres and interstitial cylinders are experimentally observed in [56], including controllable wavefronts and propagation speeds. Recently, the group investigated the dynamic responses of hexagonal packed spheres and identified power laws between the propagation speed, propagation distance, and wave amplitude [55]. These recent studies on 2D granular crystals have generated considerable interest among the community and motivated the present study.

As shown in aforementioned works, propagating nonlinear waves in 2D granular crystals preserve much of features of HNSWs in 1D chains. There is, however, few analytical calculations demonstrating the solitary wave solutions in higher dimensional granular crystals, which significantly limits the engineering of such granular crystals. We are therefore motivated to systematically investigate the dynamic behaviors of 2D nonlinear lattice models and in particular, the formation and propagation of solitary waves in 2D granular crystals. Another motivation lies in the suitable strain-gradient (possibly nonlinear) for crystalline solids and complex granular media. It has been a widely accepted practice to understand the size-dependent elasticity and plasticity of solids by a strain-gradient theory [30, 45, 2]. Upon specifying interaction potentials, it will be of interest to systematically coarse-grain the atomistic model to achieve a nonlinear strain-gradient continuum model. Also, nonregular granular media such as desert dunes and pharmaceutical pills have broad applications in industry. In the modeling of their mechanical behaviors, we may question that, besides being consistent with thermodynamic constraints, are there any other constraints on a physically reasonable nonlinear strain-gradient model as implied by the underlying atomistic/discrete description?

In pursuit of answers to the above questions, we begin with a general discrete model for granular crystals, i.e., the classic spring-mass lattice connected by *nonlinear* springs. To some extent, such a model has been extensively explored in the literature which is too voluminous to recount here. Historically, the interest in the dynamics of nonlinear lattice models was initiated by the seminal work of Fermi-Pasta-Ulam (FPU) for their quest of time-scale to equipartition of energies after an initial excitation. For comprehensive historical references, the reader is referred to recent review papers of [90], [51], and the textbook of [24]. It turns out that similar technical problems appear in other scientific areas including quantum field theory [102], nonlinear optics [16], and telecommunications [62] among others. In the long wavelength limit, we coarse-grain the discrete microscopic models with the Hamiltonian structure preserved [89]. Such an energy-based approach has the advantage of obtaining the static and dynamic properties of the system in a unified manner. For explicit calculations, we focus on a 2D hexagonal lattice with nontrivial shear resistance and general nonlinear interaction potentials. Aiming at analytical solutions, we pay close attention to approximating the discrete model in a systematic manner. For the final continuum equations, we surprisingly find exact longitudinal solitary wave solutions for systems with weakly nonlinear interactions and Hertzian interactions. Specifically, the 2D solitary wave has planar wavefront, is confined in the propagation direction but not the other direction, and maintains its shape.

We also investigate the wave propagation properties in the 2D anharmonic lattices by numerical solutions. Though the analytical solution is found for an infinite system in the continuum limit, the numerical simulations can only be achieved for a finite system. To eliminate the boundary effect, we assume a localized initial excitation at the center and simulations are terminated once the wave reaches the boundary particles in the numerical model. Strictly speaking, the numerical solution we obtained has a circular wavefront and decays as it propagates since the total energy has to be conserved, and hence does not precisely mimic our analytic solution of the planar solitary wave. Nevertheless, if the radius of the numerical circular wavefront is large, we expect the dependence of the wave

propagation velocity on the wave amplitude in the numerical model well approximates the analytical solutions. Moreover, the scaling laws regarding the propagation speed, propagation distance and wave amplitude are explored by the numerical model which will be valuable for designing shock and energy absorbing system and wave-tailoring and protective materials.

The paper is organized as follows. First, in Section 2.2 we present the general scheme of deriving continuum approximations to a discrete dynamic system that preserves the Hamiltonian structure for square lattice (§ 2.2.2) and hexagonal lattice (§ 2.2.3). In Section 2.3 we present explicit wave solutions, in particular, solitary wave solutions, to the coarse-grained continuum models with respect to harmonic, weakly nonlinear and Hertzian interactions. In Section 4.3 we study the properties of solitary waves and scaling laws by two different numerical methods: the fourth-order Runge-Kutta scheme and the explicit Newmark scheme. Finally, we summarize and present an outlook of possible applications in Section 4.4.

Notation. We employ direct notation for brevity if possible. Vectors are denoted by bold symbols such as $\mathbf{e}, \mathbf{u}$, etc. When index notations are in use, the convention of summation over repeated index is followed. The inner (or dot) product of two vectors $\mathbf{a}, \mathbf{b} \in \mathbb{R}^3$ is defined as $\langle \mathbf{a}, \mathbf{b} \rangle \equiv \mathbf{a} \cdot \mathbf{b} := (\mathbf{a})_i (\mathbf{b})_i$ whereas the inner (or dot) product between matrices $\mathbf{A}$ and $\mathbf{B}$ of the same size is defined as $\mathbf{A} \cdot \mathbf{B} := \mathrm{Tr}(\mathbf{A}^T \mathbf{B}) = (\mathbf{A})_{ij} (\mathbf{B})_{ij}$. From the viewpoint of matrices, the i^{th} row vector of the gradient of a vector field, e.g., $\nabla \mathbf{u}$, is the gradient of the i^{th} component of $\mathbf{u}$ whereas the "div" operates on the row vectors of a matrix field. Therefore, $\mathrm{div} \nabla \mathbf{u} = \Delta \mathbf{u}$ and $\mathrm{div}[(\nabla \mathbf{u})^T] = \nabla(\mathrm{div} \mathbf{u})$. For a scaling parameter $\varepsilon \ll 1$, $O(\varepsilon)$ implies the asymptotic behavior $O(\varepsilon)/\varepsilon \to C \neq 0$ as $\varepsilon \to 0$ whereas $o(\varepsilon)/\varepsilon \to 0$ as $\varepsilon \to 0$.

2.2 Continuum approximations of 2D nonlinear lattices

2.2.1 Equations of motions of discrete systems

As shown in Fig. 2.1, we consider an infinite two-dimensional spring-mass system at the reference Bravais lattice points:

$$\mathbf{x}_{ij} = i\mathbf{a}_1 + j\mathbf{a}_2 \qquad (i, j \in \mathbb{Z}),$$

where $\mathbf{a}_1, \mathbf{a}_2 \in \mathbb{R}^2$ are lattice vectors. Let $\mathbf{u}_{ij}(t)$ be the displacement of the mass point (ij)

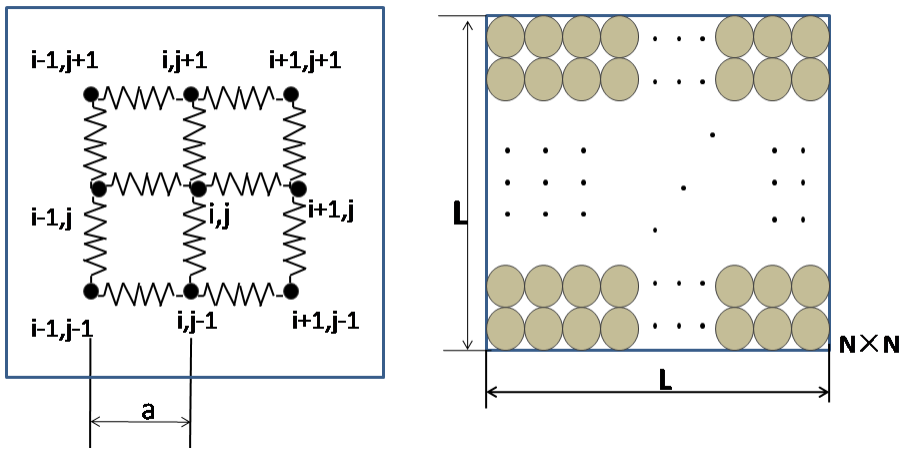

Figure 2.1: Two dimensional square packing lattice.

with respect to its reference position $i\mathbf{a}_1 + j\mathbf{a}_2$ and $\varphi : \mathbb{R} \to \mathbb{R}$ be the interaction potential between nearest neighbors. Denote by $\mathscr{N}$ the set of indicial differences of the nearest neighbors. For a square lattice, $\mathscr{N} = \{(1,0),(0,1),(-1,0),(0,-1)\}$. As usual, we assume that the interaction energy depends only on the change of distance, i.e., the interaction energy between (ij)-mass point with $(i+k\ j+l)$-mass point is given by

$$\varphi(|\mathbf{y}_{i+k\ j+l} - \mathbf{y}_{ij}| - |\mathbf{x}_{i+k\ j+l} - \mathbf{x}_{ij}|) \qquad \Big((kl) \in \mathscr{N}\Big), \tag{2.1}$$

where $\mathbf{y}_{ij} = \mathbf{x}_{ij} + \mathbf{u}_{ij}$ is the current positions of the (ij)-lattice point. For small displacement $|\mathbf{u}_{ij}| \ll |\mathbf{a}_i|$, a good approximation of the interaction potential energy (2.1) is given by

$$\varphi(|\mathbf{y}_{i+k\ j+l} - \mathbf{y}_{ij}| - |\mathbf{x}_{i+k\ j+l} - \mathbf{x}_{ij}|) \approx \varphi((\mathbf{u}_{i+k\ j+l} - \mathbf{u}_{ij}) \cdot \hat{\mathbf{r}}_{kl}),$$

where $\mathbf{r}_{kl} = \mathbf{x}_{i+k\,j+l} - \mathbf{x}_{ij} = k\mathbf{a}_1 + l\mathbf{a}_2$ and $\hat{\mathbf{r}}_{kl} = \mathbf{r}_{kl}/|\mathbf{r}_{kl}|$. Therefore, the total potential energy of the system is assumed as

$$V[\mathbf{u}_{ij}] = \frac{1}{2}\sum_{i,j\in\mathbb{Z}}\sum_{(kl)\in\mathscr{N}} \varphi((\mathbf{u}_{i+k\,j+l} - \mathbf{u}_{ij})\cdot\hat{\mathbf{r}}_{kl}). \tag{2.2}$$

In addition, we assume that the reference lattice is a stable equilibrium in the sense that

$$\frac{\partial V}{\partial \mathbf{u}_{ij}} = 0, \qquad \frac{\partial^2 V}{\partial \mathbf{u}_{ij}\partial \mathbf{u}_{ij}} = \mathbf{K}, \tag{2.3}$$

where the derivatives are evaluated at $\mathbf{u}_{ij} = 0$ for all $i, j \in \mathbb{Z}$, and the 2×2 symmetric matrix $\mathbf{K}$ is positive definite. Subsequently, we assume that

$$\varphi'(0) = 0, \qquad \varphi''(0) > 0, \tag{2.4}$$

which clearly guarantees the required constraints (2.3).

By definition, the Hamiltonian of the system can be written as

$$H[\mathbf{u}_{ij}] = T[\mathbf{u}_{ij}] + V[\mathbf{u}_{ij}], \tag{2.5}$$

where $T[\mathbf{u}_{ij}] = \sum_{i,j\in\mathbb{Z}} \frac{1}{2}m|\dot{\mathbf{u}}_{ij}|^2$ is the kinetic energy (m is mass). We are interested in the dynamic and static behaviors of this 2D spring-mass lattice and in particular, if the system sustains solitary waves when the interaction potential φ is nonlinear. By the Hamilton's principle or Newton's Second Law, the equations of motions for the discrete system can be written as (recall that $\mathbf{r}_{kl} = k\mathbf{a}_1 + l\mathbf{a}_2$)

$$m\ddot{\mathbf{u}}_{ij} = \sum_{(kl)\in\mathscr{N}} \varphi'((\mathbf{u}_{i+k\,j+l} - \mathbf{u}_{ij})\cdot\hat{\mathbf{r}}_{kl})\hat{\mathbf{r}}_{kl}. \tag{2.6}$$

The above ordinary differential equations (ODE), though exactly describes the dynamics of the system, are impractical for analytical solutions if the number of particles is large. Nevertheless, the behaviors of propagating waves in the discrete system (2.6) can be well described by a continuum theory in the long wavelength limit. To this end, we define the continuum displacement $\phi(\cdot,t) : \mathbb{R}^2 \to \mathbb{R}^2$ by interpolation such that

$$\phi(x_i, y_j, t) = \mathbf{u}_{ij}(t), \qquad (x_i = (i\mathbf{a}_1 + j\mathbf{a}_2)\cdot\mathbf{e}_x, \quad y_j = (i\mathbf{a}_1 + j\mathbf{a}_2)\cdot\mathbf{e}_y), \tag{2.7}$$

Also, we define the characteristic wavelength λ as $1/k_{\max}$ with $k_{\max}$ being the wave number that achieves the maximum of the spectrum density of $|\hat{\phi}(\mathbf{k})|^2$, $\hat{\phi}(\mathbf{k}) = \int_{\mathbb{R}^2} \phi(\mathbf{x}) e^{i\mathbf{k}\cdot\mathbf{x}} d\mathbf{x}$. Let $a \sim |\mathbf{a}_i|$ be the lengthscale of lattice spacing, $u \sim |\mathbf{u}_{ij}| \sim |\phi|$ be the lengthscale of amplitude, and c be the velocity of propagating wave. In the limit of long wavelength (i.e., $a/\lambda \ll 1$) and small excitation (i.e., $u/a \ll 1$), we can approximate summations by integrals and rewrite the kinetic energy of system as

$$T[\phi] \approx \sum_{i,j\in\mathbb{Z}} \frac{1}{2} m \phi_t^2(x_i, y_j) = \frac{1}{2} \int_{\mathbb{R}^2} \rho |\phi_t|^2 dxdy, \tag{2.8}$$

where $\rho = m/|\mathbf{a}_1 \times \mathbf{a}_2|$ is the mass density (per unit area) of the continuum medium. Next, we calculate the potential energy in terms of the continuum variable ϕ. There are two cases that will be discussed separately.

2.2.2 Square lattice

For a square lattice, the lattice vectors $\mathbf{a}_1 = a\mathbf{e}_x$, $\mathbf{a}_2 = a\mathbf{e}_y$ ($a > 0$ is the lattice spacing), and the set $\mathscr{N} = \{(1,0),(0,1),(-1,0),(0,-1)\}$. Our purpose here is to find an explicit expression of the potential energy functional $V[\phi]$. To this end, it suffices to consider displacements $\phi(\mathbf{x},t)$ that vanish if $|\mathbf{x}|$ is large enough. (In other words, ϕ is compactly supported.)

Since $a/\lambda \ll 1$, by Taylor expansion and keeping terms up to $O(a^3)$ we obtain

$$\begin{aligned}
\mathbf{u}_{i+1j} - \mathbf{u}_{ij} &= \phi(x_{i+1}, y_j) - \phi(x_i, y_j) \\
&\approx a\frac{\partial}{\partial x}\phi(x_i, y_j) + \frac{a^2}{2}\frac{\partial^2}{\partial x^2}\phi(x_i, y_j) + \frac{a^3}{6}\frac{\partial^3}{\partial x^3}\phi(x_i, y_j); \\
\mathbf{u}_{ij+1} - \mathbf{u}_{ij} &= \phi(x_i, y_{j+1}) - \phi(x_i, y_j) \\
&\approx a\frac{\partial}{\partial y}\phi(x_i, y_j) + \frac{a^2}{2}\frac{\partial^2}{\partial y^2}\phi(x_i, y_j) + \frac{a^3}{6}\frac{\partial^3}{\partial y^3}\phi(x_i, y_j).
\end{aligned} \tag{2.9}$$

For brevity we write the x-component and y-component of the vector field ϕ as

$$\xi = \phi \cdot \mathbf{e}_x, \qquad \zeta = \phi \cdot \mathbf{e}_y,$$

respectively. Inserting (2.9) into (2.2) and converting the summation into an integral, we obtain

$$\begin{aligned} V[\xi,\zeta] &\approx \int_{\mathbb{R}^2} \frac{1}{a^2}\big[\varphi(a\xi_x+\frac{a^2}{2}\xi_{xx}+\frac{a^3}{6}\xi_{xxx})+\varphi(a\zeta_y+\frac{a^2}{2}\zeta_{yy}+\frac{a^3}{6}\zeta_{yyy})\big]dxdy \\ &\approx \int_{\mathbb{R}^2} \frac{1}{a^2}\big[\varphi(a\xi_x)+\varphi'(a\xi_x)(\frac{a^2}{2}\xi_{xx}+\frac{a^3}{6}\xi_{xxx})+\frac{1}{2}\varphi''(a\xi_x)(\frac{a^2}{2}\xi_{xx}+\frac{a^3}{6}\xi_{xxx})^2 \\ &\quad +\varphi(a\zeta_y)+\varphi'(a\zeta_y)(\frac{a^2}{2}\zeta_{yy}+\frac{a^3}{6}\zeta_{yyy})+\frac{1}{2}\varphi''(a\zeta_y)(\frac{a^2}{2}\zeta_{yy}+\frac{a^3}{6}\zeta_{yyy})^2\big]dxdy, \end{aligned} \tag{2.10}$$

where the second approximation follows from the Taylor expansion of φ. By the divergence theorem and (2.4) we find that

$$\begin{aligned} &\int_{\mathbb{R}^2}\varphi'(\xi_x)\xi_{xx}dxdy=\int_{\mathbb{R}^2}\mathbf{e}_x\cdot\nabla[\varphi(\xi_x)]dxdy=0, \\ &\int_{\mathbb{R}^2}\varphi'(\xi_x)\xi_{xxx}dxdy=\int_{\mathbb{R}^2}\mathbf{e}_x\cdot\nabla[\varphi'(\xi_x)\xi_{xx}]dxdy-\int_{\mathbb{R}^2}\varphi''(\xi_x)(\xi_{xx})^2dxdy. \end{aligned}$$

Inserting the above equations and corresponding equations for ζ into (2.10), we obtain that

$$V[\xi,\zeta]=\int_{\mathbb{R}^2}\frac{1}{a^2}\big[\varphi(a\xi_x)-\frac{a^4}{24}\varphi''(a\xi_x)(\xi_{xx})^2+\varphi(a\zeta_y)-\frac{a^4}{24}\varphi''(a\zeta_y)(\zeta_{yy})^2\big]dxdy. \tag{2.11}$$

Therefore, the action functional of the system is given by

$$\begin{aligned} S[\xi,\zeta]=\int_0^\infty T[\xi,\zeta]-V[\xi,\zeta]dt=\int_0^\infty\int_{\mathbb{R}^2}\Big\{&\frac{1}{2}\rho(\xi_t^2+\zeta_t^2) \\ &-\frac{1}{a^2}\big[\varphi(a\xi_x)-\frac{a^4}{24}\varphi''(a\xi_x)(\xi_{xx})^2+\varphi(a\zeta_y)-\frac{a^4}{24}\varphi''(a\zeta_y)(\zeta_{yy})^2\big]\Big\}dxdydt. \end{aligned}$$

According to the Hamilton's Principle, the actual motion of the system shall be a stationary state of the action functional, satisfying that for all admissible perturbation of the system ϕ_1,

$$\frac{d}{d\delta}S[\phi+\delta\phi_1]\Big|_{\delta=0}=0 \qquad \forall\,\phi_1.$$

By the standard first-variation calculation, we find the associated Euler-Lagrange general equation for the system:

$$\begin{cases} \xi_{tt}-\dfrac{1}{a\rho}\dfrac{d}{dx}\{\varphi'(a\xi_x)+\dfrac{a^4}{24}\varphi'''(a\xi_x)\xi_{xx}^2+\dfrac{a^3}{12}\varphi''(a\xi_x)\xi_{xxx}\}=0, \\ \zeta_{tt}-\dfrac{1}{a\rho}\dfrac{d}{dy}\Big\{\varphi'(a\zeta_y)+\dfrac{a^4}{24}\varphi'''(a\zeta_y)\zeta_{yy}^2+\dfrac{a^3}{12}\varphi''(a\zeta_y)\zeta_{yyy}\Big\}=0. \end{cases} \tag{2.12}$$

From the above equation, we observe that the motions in two directions are decoupled because of lack of shear resistance in a square lattice. Therefore, the system behaves exactly like a 1D system as discussed in [78].

2.2.3 Hexagonal lattice

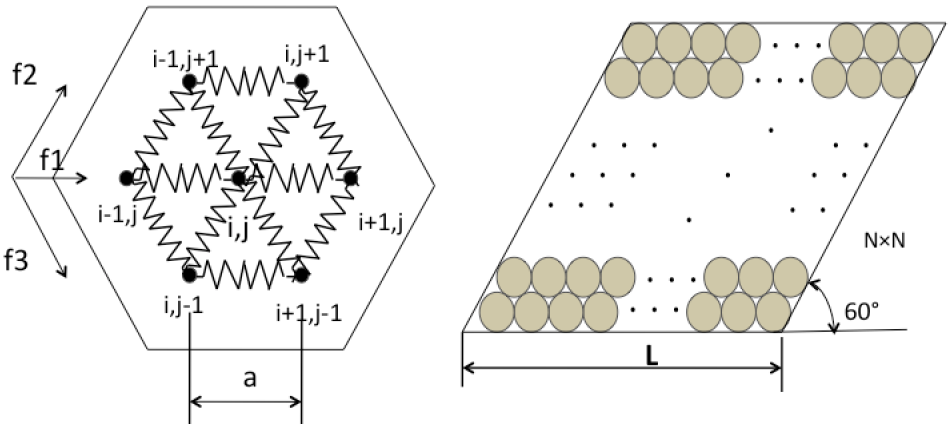

Figure 2.2: Two dimensional hexagonal packing lattice.

The static and dynamic properties of hexagonal lattices are fundamentally different from square lattices due to their nontrivial shear resistance. As shown in Fig. 2.2, let

$$\mathbf{f}_1 = \mathbf{e}_x, \quad \mathbf{f}_2 = \frac{1}{2}\mathbf{e}_x + \frac{\sqrt{3}}{2}\mathbf{e}_y$$

be the lattice vectors and consider a 2D hexagonal crystal with lattice points given by

$$\mathbf{x}_{ij} = a(i\mathbf{f}_1 + j\mathbf{f}_2) \qquad (i, j \in \mathbb{Z}).$$

Each lattice point at $\mathbf{x}_{ij}$ has six nearest neighbors $\mathbf{x}_{i+k\ j+l}$ with

$$(kl) \in \mathscr{N} := \{(1,-1),(1,0),(0,1),-(1,-1),-(1,0),-(0,1)\},$$

and in particular three nearest neighbor on its right with $\mathbf{x}_{i+k\ j+l} = \mathbf{x}_{ij} + \mathbf{r}_{kl}$:

$$\mathbf{r}_{kl} = k\mathbf{f}_1 + l\mathbf{f}_2 = \begin{cases} \mathbf{f}_1 & \text{if } (kl) = (1,0), \\ \mathbf{f}_2 & \text{if } (kl) = (0,1), \\ \mathbf{f}_3 := \mathbf{f}_1 - \mathbf{f}_2 & \text{if } (kl) = (1,-1). \end{cases}$$

To compute the potential energy of the hexagonal lattice in the long wavelength limit as in (2.10), we introduce notation (see Section 2.6 for detailed expressions for $m = 1,2$)

$$\Lambda^m_\alpha = \langle D^m\phi, \underbrace{\mathbf{f}_\alpha \otimes \cdots \otimes \mathbf{f}_\alpha}_{m+1} \rangle \equiv (\phi)_{i_1,i_2\cdots i_{m+1}} (\mathbf{f}_\alpha)_{i_1} (\mathbf{f}_\alpha)_{i_2} \cdots (\mathbf{f}_\alpha)_{i_{m+1}}. \tag{2.13}$$

Then by Taylor expansion we have

$$(\mathbf{u}_{i+k\ j+l}-\mathbf{u}_{ij})\cdot\hat{\mathbf{r}}_{kl}=a\Lambda_\alpha^1+\frac{a^2}{2}\Lambda_\alpha^2+\frac{a^3}{6}\Lambda_\alpha^3+o(a^3),$$

where $\alpha=1$ (resp. 2, 3) if $(kl)=(1,0)$ (resp. $(0,1)$, $(1,-1)$). Therefore,

$$\sum_{(kl)\in\mathcal{N}}\varphi((\mathbf{u}_{i+k\ j+l}-\mathbf{u}_{ij})\cdot\hat{\mathbf{r}}_{kl})\approx\sum_{\alpha=1}^{3}\varphi(a\Lambda_\alpha^1+\frac{a^2}{2}\Lambda_\alpha^2+\frac{a^3}{6}\Lambda_\alpha^3). \tag{2.14}$$

Inserting the above equations into (2.2) and converting the summation into integral, we obtain

$$\begin{aligned}V[\phi]&\approx\frac{1}{2}\sum_{i,j\in\mathbb{Z}}\sum_{\alpha=1}^{3}\varphi(a\Lambda_\alpha^1+\frac{a^2}{2}\Lambda_\alpha^2+\frac{a^3}{6}\Lambda_\alpha^3)\approx\frac{1}{A_c}\int_{\mathbb{R}^2}\sum_{\alpha=1}^{3}\varphi(a\Lambda_\alpha^1+\frac{a^2}{2}\Lambda_\alpha^2+\frac{a^3}{6}\Lambda_\alpha^3)dxdy\\&\approx\frac{1}{A_c}\int_{\mathbb{R}^2}\sum_{\alpha=1}^{3}[\varphi(a\Lambda_\alpha^1)+\varphi'(a\Lambda_\alpha^1)(\frac{a^2}{2}\Lambda_\alpha^2+\frac{a^3}{6}\Lambda_\alpha^3)+\frac{1}{2}\varphi''(a\Lambda_\alpha^1)(\frac{a^2}{2}\Lambda_\alpha^2+\frac{a^3}{6}\Lambda_\alpha^3)^2]dxdy,\end{aligned}$$

where $A_c=\frac{\sqrt{3}}{4}a^2$ is the unit cell area. By the divergence theorem we find that

$$\begin{aligned}\int_{\mathbb{S}}\varphi'(a\Lambda_\alpha^1)\Lambda_\alpha^2dxdy&=\int_{\mathbb{S}}\mathbf{f}_\alpha\cdot\nabla[\varphi(a\Lambda_\alpha^1)]dxdy=0\\\int_{\mathbb{S}}\varphi'(a\Lambda_\alpha^1)\Lambda_\alpha^3dxdy&=\int_{\mathbb{S}}\mathbf{f}_\alpha\cdot\nabla[\varphi'(a\Lambda_\alpha^2)]dxdy-\int_{\mathbb{S}}\varphi''(a\Lambda_\alpha^1)(\Lambda_\alpha^2)^2dxdy.\end{aligned}$$

Therefore, the potential energy can be rewritten as

$$V[\phi]=\frac{1}{A_c}\int_{\mathbb{S}}\sum_{\alpha=1}^{3}[\varphi(a\Lambda_\alpha^1)-\frac{1}{24}\varphi''(a\Lambda_\alpha^1)(a^2\Lambda_\alpha^2)^2]dxdy. \tag{2.15}$$

Again, we denote the x and y-components of ϕ by

$$\xi=\phi\cdot\mathbf{e}_x,\qquad\zeta=\phi\cdot\mathbf{e}_y.$$

Then the action functional of the system is given by

$$\begin{aligned}S[\xi,\zeta]&=\int_0^\infty T[\xi,\zeta]-V[\xi,\zeta]dt\\&=\int_0^\infty\int_{\mathbb{S}}\frac{1}{2}\rho(\xi_t^2+\zeta_t^2)-\frac{1}{A_c}\sum_{\alpha=1}^{3}[\varphi(a\Lambda_\alpha^1)-\frac{1}{24}\varphi''(a\Lambda_\alpha^1)(a^2\Lambda_\alpha^2)^2]dxdydt.\end{aligned} \tag{2.16}$$

According to the Hamilton's Principle, the equation of motion is determined by

$$\frac{d}{d\delta}S[\phi+\delta\phi_1]|_{\delta=0}=0\qquad\forall\,\phi_1,$$

where $\phi_1 = (\xi_1, \zeta_1)$ is an admissible perturbation. By the standard first variation calculation, we obtain the associated Euler-Lagrange equations as

$$\begin{cases} \rho\xi_{tt} + \mathrm{div}[\tau_x(\phi)] - \nabla\nabla\cdot[\Sigma_x(\phi)] = 0, \\ \rho\zeta_{tt} + \mathrm{div}[\tau_y(\phi)] - \nabla\nabla\cdot[\Sigma_y(\phi)] = 0, \end{cases} \tag{2.17}$$

where, for brevity, we introduce notation:

$$\begin{aligned} \tau_x(\phi) &= \sum_{\alpha=1}^{3}[-\frac{1}{a}\varphi'(a\Lambda_\alpha^1) + \frac{a^3}{24}\varphi'''(a\Lambda_\alpha^1)(\Lambda_\alpha^2)^2]\ell_{x\alpha}, \\ \tau_y(\phi) &= \sum_{\alpha=1}^{3}[-\frac{1}{a}\varphi'(a\Lambda_\alpha^1) + \frac{a^3}{24}\varphi'''(a\Lambda_\alpha^1)(\Lambda_\alpha^2)^2]\ell_{y\alpha}, \\ \Sigma_x(\phi) &= \sum_{\alpha=1}^{3}[\frac{a^2}{12}\varphi''(a\Lambda_\alpha^1)(\Lambda_\alpha^2)\mathbf{M}_{x\alpha}], \\ \Sigma_y(\phi) &= \sum_{\alpha=1}^{3}[\frac{a^2}{12}\varphi''(a\Lambda_\alpha^1)(\Lambda_\alpha^2)\mathbf{M}_{y\alpha}], \end{aligned}$$

and vectors $\ell_{x\alpha}, \ell_{y\alpha} \in \mathbb{R}^2$ and symmetric matrices $\mathbf{M}_{x\alpha}, \mathbf{M}_{y\alpha} \in \mathbb{R}^{2\times 2}$ are such that

$$\begin{aligned} \Lambda_\alpha^1 &= \ell_{x\alpha}\cdot\nabla\xi + \ell_{y\alpha}\cdot\nabla\zeta, \\ \Lambda_\alpha^2 &= \mathbf{M}_{x\alpha}\cdot\nabla\nabla\xi + \mathbf{M}_{y\alpha}\cdot\nabla\nabla\zeta. \end{aligned} \tag{2.18}$$

We remark that the vectors $\ell_{x\alpha}, \ell_{y\alpha} \in \mathbb{R}^2$ and matrices $\mathbf{M}_{x\alpha}, \mathbf{M}_{y\alpha} \in \mathbb{R}^{2\times 2}$ depend on geometric properties of the hexagonal lattice and are explicitly calculated in the Section 2.6.

2.3 Explicit solutions to hexagonal lattice

2.3.1 Harmonic interaction

For the harmonic interaction potential $\varphi(x) = \frac{1}{2}Kx^2$, by (2.15) we find the potential energy:

$$V[\phi] = \int_{\mathbb{S}}[Q(\nabla\phi) - a^2\Gamma(\nabla\nabla\phi)], \tag{2.19}$$

where $Q : \mathbb{R}^{2\times 2} \to \mathbb{R}$ and $\Gamma : \mathbb{R}^{2\times 2\times 2} \to \mathbb{R}$ are quadratic forms given by

$$Q(\nabla\phi) := \frac{K}{2}\sum_{\alpha=1}^{3}(\Lambda_\alpha^1)^2 = \frac{3K}{16}\Big[|\nabla\phi|^2 + \mathrm{Tr}(\nabla\phi)^2 + (\mathrm{Tr}\nabla\phi)^2\Big] \tag{2.20}$$

and

$$\Gamma(\nabla\nabla\phi) := \frac{K}{24}\sum_{\alpha=1}^{3}(\Lambda_\alpha^2)^2 = \frac{K}{24}\Big[\frac{33}{32}\xi_{xx}^2 + \frac{3}{16}\xi_{xx}\xi_{yy} + \frac{3}{8}\xi_{xy}^2 + \frac{9}{32}\xi_{yy}^2 + \frac{3}{32}\zeta_{xx}^2 + \frac{9}{8}\zeta_{xy}^2 + \frac{27}{32}\zeta_{yy}^2 + \frac{9}{16}\zeta_{xx}\zeta_{yy} + \frac{3}{8}\xi_{xx}\zeta_{xy} + \frac{3}{8}\xi_{xy}\zeta_{xx} + \frac{9}{8}\xi_{xy}\zeta_{yy} + \frac{9}{8}\xi_{yy}\zeta_{xy}\Big], \tag{2.21}$$

respectively. From the above quadratic forms, we identify two tensors: the forth-order stiffness tensor $\mathbf{C} : \mathbb{R}^{2\times 2} \to \mathbb{R}^{2\times 2}$

$$(\mathbf{C})_{piqj} = \frac{3}{8}K\Big[(\delta_{pq}\delta_{ij} + \delta_{pj}\delta_{iq}) + \frac{3}{8}\delta_{pi}\delta_{qj}\Big], \tag{2.22}$$

and the sixth-order *dispersion* tensor $\mathbb{D} : \mathbb{R}^{2\times 2\times 2} \to \mathbb{R}^{2\times 2\times 2}$ such that (cf., (2.52))

$$\frac{1}{2}\nabla\nabla\phi \cdot \mathbb{D}\nabla\nabla\phi = \Gamma(\nabla\nabla\phi). \tag{2.23}$$

Therefore, the potential energy (2.19) can be rewritten as

$$V[\phi] = \int_{\mathbb{S}}\Big[\frac{1}{2}\nabla\phi\cdot\mathbf{C}\nabla\phi - \frac{1}{2}a^2\nabla\nabla\phi\cdot\mathbb{D}\nabla\nabla\phi\Big], \tag{2.24}$$

and we rewrite the general equation of motion (2.17) as

$$\rho\phi_{tt} = \mathrm{div}(\mathbf{C}\nabla\phi) + a^2\nabla\nabla\cdot\mathbb{D}\nabla\nabla\phi. \tag{2.25}$$

To find the dispersion relation, we consider a trial plane wave solution of the form [1]:

$$\phi(\mathbf{x},t) = \phi_0 e^{i(\mathbf{k}\cdot\mathbf{x}-\omega t)},$$

where $\phi_0 \in \mathbb{C}^2$ is some nonzero complex vector, $\mathbf{k} \in \mathbb{R}^2$ is the wave vector, and $\omega > 0$ is the frequency. Inserting the above trial solution into (2.25), we obtain the secular equation for determining the dispersion relation as follows:

$$[(\mathbf{C})_{piqj}k_ik_j - a^2(\mathbb{D})_{pijqlm}k_ik_jk_lk_m - \rho\omega^2\delta_{pq}](\phi_0)_q = 0. \tag{2.26}$$

For plane waves propagating along the x-direction with $\mathbf{k} = (k_1, 0)$, by (2.22) and (2.23) we rewrite (2.26) in a matrix form ($c^2 = K/\rho$):

$$\begin{bmatrix} \frac{9}{8}c^2k_1^2 - \frac{11}{128}c^2a^2k_1^4 - \omega^2 & 0 \\ 0 & \frac{3}{8}c^2k_1^2 - \frac{1}{128}c^2a^2k_1^4 - \omega^2 \end{bmatrix}\phi_0 = 0.$$

Immediately, we find two nontrivial solutions:

$$\begin{cases} \omega_1 = c\sqrt{\frac{9}{8}k_1^2 - \frac{11}{128}a^2k_1^4}, & \phi_0 = (1,0), \\ \omega_2 = c\sqrt{\frac{3}{8}k_1^2 - \frac{1}{128}a^2k_1^4} & \phi_0 = (0,1). \end{cases} \tag{2.27}$$

The former of the above solution corresponds to the longitudinal wave with dispersion relation $v_1 := \omega_1/k_1 = c\sqrt{\frac{9}{8} - \frac{11}{128}a^2k_1^2}$ whereas the latter describes the shear wave with dispersion relation $v_2 := \omega_2/k_1 = c\sqrt{\frac{3}{8} - \frac{1}{128}a^2k_1^2}$. Incidentally, we find that if $ak_1 \ll 1$, we have $v_1 \approx \frac{3c}{2\sqrt{2}}$ and $v_2 \approx \frac{c}{2}\sqrt{\frac{3}{2}}$. Moreover, due to the six-fold symmetry, we conclude that similar longitudinal and shear wave solutions can be found for propagating directions $\hat{\mathbf{k}} = \pm\mathbf{f}_1, \pm\mathbf{f}_2, \pm\mathbf{f}_3$.

2.3.2 Weakly nonlinear interaction

We now consider a weakly nonlinear potential energy $\varphi = \frac{1}{2}Kx^2 + \frac{1}{3}\kappa x^3$.By (2.15) and (2.18) we find that the potential energy is given by

$$V[\phi] = \frac{1}{2}K\nabla\phi\cdot\mathbf{C}\nabla\phi - \frac{1}{2}Ka^2\nabla\nabla\phi\cdot\mathbb{D}\nabla\nabla\phi + \frac{\kappa a}{3}\sum_{\alpha=1}^{3}(\ell_{x\alpha}\cdot\nabla\xi + \ell_{y\alpha}\cdot\nabla\zeta)^3, \tag{2.28}$$

and the equation of motion (2.17) can be written as

$$\begin{aligned} \rho\phi_{tt} =& \operatorname{div}(\mathbf{C}\nabla\phi) + a^2\nabla\nabla\cdot\mathbb{D}\nabla\nabla\phi \\ &+ 2a\kappa\begin{bmatrix} \sum_{\alpha=1}^{3}(\ell_{x\alpha}\cdot\nabla\xi + \ell_{y\alpha}\cdot\nabla\zeta)(\ell_{x\alpha}\otimes\ell_{x\alpha}\cdot\nabla\nabla\xi + \ell_{x\alpha}\otimes\ell_{y\alpha}\cdot\nabla\nabla\zeta) \\ \sum_{\alpha=1}^{3}(\ell_{x\alpha}\cdot\nabla\xi + \ell_{y\alpha}\cdot\nabla\zeta)(\ell_{y\alpha}\otimes\ell_{x\alpha}\cdot\nabla\nabla\xi + \ell_{y\alpha}\otimes\ell_{y\alpha}\cdot\nabla\nabla\zeta) \end{bmatrix}. \end{aligned} \tag{2.29}$$

To find a traveling wave solution to (2.29), we consider a trial solution of the form:

$$\phi(\mathbf{x},t) = [\hat{\xi}(s), 0], \qquad s = x - V_g t, \tag{2.30}$$

where $V_g > 0$ is the (longitudinal) wave speed. Inserting (2.30) into $(2.29)_1$ we obtain

$$V_g^2\rho\hat{\xi}_{ss} = \frac{9}{8}K\hat{\xi}_{ss} + \frac{11}{128}Ka^2\hat{\xi}_{ssss} + \frac{33}{16}\kappa a\hat{\xi}_s\hat{\xi}_{ss}.$$

We also verify that the second of (2.29) is trivially satisfied by (2.30). Further, the above equation can be rewritten as

$$[(V_g^2\rho - \frac{9}{8}K)\hat{\xi}_s - \frac{11}{128}Ka^2\hat{\xi}_{sss} - \frac{33}{32}\kappa a(\hat{\xi}_s^2)]_s = 0,$$

implying that for some constant c_1,

$$(V_g^2\rho-\frac{9}{8}K)\hat{\xi}_s-\frac{11}{128}Ka^2\hat{\xi}_{sss}-\frac{33}{32}\kappa a\hat{\xi}_s^2=c_1.$$

Setting $w=\hat{\xi}_s$ and multiplying w_s on both sides, we obtain

$$\frac{d}{ds}\Big[\frac{1}{2}(V_g^2\rho-\frac{9}{8}K)w^2-\frac{11}{256}Ka^2(w_s)^2-\frac{11}{32}\kappa aw^3-c_1w\Big]=0.$$

Let $\eta=\sqrt{\frac{4\kappa}{Ka}}s$ and $\beta=\frac{64}{11\kappa a}(\frac{1}{2}V_g^2\rho-\frac{9}{16}K)$. The above equation is equivalent to

$$\frac{d}{d\eta}\Big[(w_\eta)^2-\beta w^2+2w^3-c_1'w\Big]=0,$$

and hence for some integration constant c_2,

$$w_\eta^2-\beta w^2+2w^3=c_1'w+c_2. \tag{2.31}$$

By definition, a solitary wave requires that $w,w_s,w_{ss}\to 0$ as $x\to\infty$, implying that $c_1=0$, $c_1'=0$ and $c_2=0$. Therefore, (2.31) can be rewritten as

$$d\eta=\frac{dw}{\sqrt{\beta w^2-2w^3}},$$

and upon integration, yields

$$w(\eta)=\frac{\beta}{2}\mathrm{sech}^2(\frac{\sqrt{\beta}}{2}\eta). \tag{2.32}$$

It is clear that (2.32) represents a solitary wave solution to (2.29). In terms of strain $\hat{\xi}_s(s)$ and particle velocity $v(s)=\frac{d}{dt}\hat{\xi}(s)$ ($s=x-V_gt$), the solitary wave solution (2.32) can be rewritten as

$$\hat{\xi}_s(s)=\frac{\beta}{2}\mathrm{sech}^2(\frac{\sqrt{\beta}}{2}\sqrt{\frac{4\kappa}{Ka}}s),\qquad v(s)=-V_g\frac{\beta}{2}\mathrm{sech}^2(\frac{\sqrt{\beta}}{2}\sqrt{\frac{4\kappa}{Ka}}s). \tag{2.33}$$

2.3.3 Hertzian interactions

For granular crystals with Hertzian interaction, the potential energy is given by $\varphi=\frac{2}{5}K|x|^{\frac{5}{2}}$. By (2.15) and (2.18) we find the potential energy

$$\begin{aligned}V[\phi]=&\frac{2}{5}Ka^{\frac{1}{2}}\sum_{\alpha=1}^{3}(\ell_{x\alpha}\cdot\nabla\xi+\ell_{y\alpha}\cdot\nabla\zeta)^{\frac{5}{2}}\\&-\frac{1}{16}Ka^{\frac{5}{2}}\sum_{\alpha=1}^{3}(\ell_{x\alpha}\cdot\nabla\xi+\ell_{y\alpha}\cdot\nabla\zeta)^{\frac{1}{2}}\sum_{\alpha=1}^{3}(\mathbf{M}_{x\alpha}\cdot\nabla\nabla\xi+\mathbf{M}_{y\alpha}\cdot\nabla\nabla\zeta)^2.\end{aligned} \tag{2.34}$$

Then the equation of motion (2.17) can be written as (see Section 2.6 for explicit expressions of vectors $\ell_{x\alpha}, \ell_{y\alpha}$ and matrices $\mathbf{M}_{x\alpha}$, $\mathbf{M}_{y\alpha}$)

$$\begin{aligned}\rho\xi_{tt} + K\sum_{\alpha=1}^{3}\Big\{\ell_{x\alpha}\cdot\nabla\Big[-a^{\frac{1}{2}}(\ell_{x\alpha}\cdot\nabla\xi+\ell_{y\alpha}\cdot\nabla\zeta)^{\frac{3}{2}} \\ +\frac{a^{\frac{5}{2}}}{32}(\ell_{x\alpha}\cdot\nabla\xi+\ell_{y\alpha}\cdot\nabla\zeta)^{-\frac{1}{2}}(\mathbf{M}_{x\alpha}\cdot\nabla\nabla\xi+\mathbf{M}_{y\alpha}\cdot\nabla\nabla\zeta)^2\Big] \\ -\frac{a^{\frac{5}{2}}}{8}\mathbf{M}_{x\alpha}\cdot\nabla\nabla\Big[(\ell_{x\alpha}\cdot\nabla\xi+\ell_{y\alpha}\cdot\nabla\zeta)^{\frac{1}{2}}(\mathbf{M}_{x\alpha}\cdot\nabla\nabla\xi+\mathbf{M}_{y\alpha}\cdot\nabla\nabla\zeta)\Big]\Big\}=0,\end{aligned} \tag{2.35}$$

$$\begin{aligned}\rho\zeta_{tt} + K\sum_{\alpha=1}^{3}\Big\{\ell_{y\alpha}\cdot\nabla\Big[-a^{\frac{1}{2}}(\ell_{x\alpha}\cdot\nabla\xi+\ell_{y\alpha}\cdot\nabla\zeta)^{\frac{3}{2}} \\ +\frac{a^{\frac{5}{2}}}{32}(\ell_{x\alpha}\cdot\nabla\xi+\ell_{y\alpha}\cdot\nabla\zeta)^{-\frac{1}{2}}(\mathbf{M}_{x\alpha}\cdot\nabla\nabla\xi+\mathbf{M}_{y\alpha}\cdot\nabla\nabla\zeta)^2\Big] \\ -\frac{a^{\frac{5}{2}}}{8}\mathbf{M}_{y\alpha}\cdot\nabla\nabla\Big[(\ell_{x\alpha}\cdot\nabla\xi+\ell_{y\alpha}\cdot\nabla\zeta)^{\frac{1}{2}}(\mathbf{M}_{x\alpha}\cdot\nabla\nabla\xi+\mathbf{M}_{y\alpha}\cdot\nabla\nabla\zeta)\Big]\Big\}=0.\end{aligned} \tag{2.36}$$

For a traveling wave solution, we again consider a trial solution of the form (2.30). By (2.35) we obtain

$$\begin{aligned}\frac{\rho}{K}V_g^2\hat{\xi}_{ss} - \frac{51}{32}a^{\frac{1}{2}}(-\hat{\xi}_s)^{\frac{1}{2}}\hat{\xi}_{ss} + \frac{33}{1024}a^{\frac{5}{2}}(-\hat{\xi}_s)^{-\frac{3}{2}}\hat{\xi}_{ss}^3 \\ +\frac{33}{128}a^{\frac{5}{2}}(-\hat{\xi}_s)^{-\frac{1}{2}}\hat{\xi}_{ss}\hat{\xi}_{sss} - \frac{33}{128}a^{\frac{5}{2}}(-\hat{\xi}_s)^{\frac{1}{2}}\hat{\xi}_{ssss} = 0.\end{aligned}$$

Also, equation (2.36) is automatically satisfied due to symmetries of $\ell_{x\alpha}$, $\ell_{y\alpha}$, $\mathbf{M}_{x\alpha}$ and $\mathbf{M}_{y\alpha}$. Setting $p = -\hat{\xi}_s \geq 0$ we rewrite the above equation as

$$V_g^2 p_s - c^2[\frac{17}{16}p^{\frac{3}{2}} + \frac{33}{160}a^2 p^{\frac{1}{4}}(p^{\frac{5}{4}})_{ss}]_s = 0, \tag{2.37}$$

where $c^2 = \frac{K}{\rho}a^{\frac{1}{2}}$. Upon a change of variable $p \to z^{\frac{4}{5}}$ and integration, we obtain that for some constant c_6,

$$V_g^2 z^{\frac{4}{5}} = c^2[\frac{17}{16}z^{\frac{6}{5}} + \frac{33}{160}a^2 z^{\frac{1}{5}}z_{ss}] + c_6.$$

Further, setting $z = (\frac{4V_g}{\sqrt{17}c})^5 y$ and $s = \sqrt{\frac{33}{170}}a\eta$, we write the above equation into a dimensionless form as

$$y^{\frac{4}{5}} = y^{\frac{6}{5}} + y^{\frac{1}{5}}y_{\eta\eta} + c_7 \quad \Longleftrightarrow \quad y_{\eta\eta} = -\frac{\partial}{\partial y}N(y), \tag{2.38}$$

where (c_7, c_8 are constants)

$$N(y) = -\frac{5}{8}y^{\frac{8}{5}} + \frac{1}{2}y^2 + c_8 y^{\frac{4}{5}}. \tag{2.39}$$

The particular form of (2.38) prompts the analogy with particle motion in a potential ($N(y)$) with η being the "time" and y being the "coordinate" [54]. If $c_8 = 0$, it is not hard to check that $y(\eta) = (4/5)^{-5/2}\cos^5(\eta/5)$ satisfies (2.38) with $c_7 = 0$. In other words,

$$\hat{\xi}_s(s) = -(\frac{20V_g^2}{17c^2})^2 \cos^4(\frac{\sqrt{170}}{5a\sqrt{33}}s), \tag{2.40}$$

satisfies (2.37). However, the above solution represents a periodic traveling wave solution instead of a soliton. As argued in [77], problem (2.38) does admit a solitary wave solution if $0 < c_8 < 5/27$, which can be implicitly represented as

$$\eta = \eta_0 + \int_{y_0}^{y} \frac{dy}{\sqrt{-2[N(y) - N(y_{max})]}}, \tag{2.41}$$

where y_{max} is related to the maximum strain of the solitary wave. However, since the hexagonal lattice is initially uncompressed (or very weakly compressed), we shall prescribe $0 < c_8 \ll 1$. Then the propagating wave is expected to remain as a solitary wave (as represented by (2.41)) whose profile is well approximated by one "hump" of the periodic wave (2.42) with particle velocity $v(s) = -V_g\hat{\xi}_s$ given by one "hump" of

$$v(s) = V_g(\frac{20V_g^2}{17c^2})^2 \cos^4(\frac{\sqrt{170}}{5a\sqrt{33}}s). \tag{2.42}$$

2.4 Numerical results

It is enlightening to numerically simulate the dynamic responses of a hexagonal lattice of size 100×100. As shown in Fig. 2.3, the initial condition of the system is prescribed as that the six spheres around the center sphere ($i, j = 50$) have a velocity $v_0 = 0.5m/s$ with the direction along with $\mathbf{f}_1, \mathbf{f}_2, \mathbf{f}_3$ and $-\mathbf{f}_1, -\mathbf{f}_2, -\mathbf{f}_3$, respectively. We employ both the fourth-order Runge-Kutta and explicit Newmark method to solve the discrete equations of motion:

$$\begin{aligned} m\dot{\mathbf{v}}_{i,j} = {} & \varphi'|2a\mathbf{f}_1 + \mathbf{u}_{i-1,j} - \mathbf{u}_{i,j}| - \varphi'|2a\mathbf{f}_1 + \mathbf{u}_{i,j} - \mathbf{u}_{i+1,j}| + \varphi'|2a\mathbf{f}_2 + \mathbf{u}_{i,j-1} - \mathbf{u}_{i,j}| \\ & - \varphi'|2a\mathbf{f}_2 + \mathbf{u}_{i,j} - \mathbf{u}_{i,j+1}| + \varphi'|2a\mathbf{f}_3 + \mathbf{u}_{i-1,j+1} - \mathbf{u}_{i,j}| - \varphi'|2a\mathbf{f}_3 + \mathbf{u}_{i,j} - \mathbf{u}_{i+1,j-1}|. \end{aligned} \tag{2.43}$$

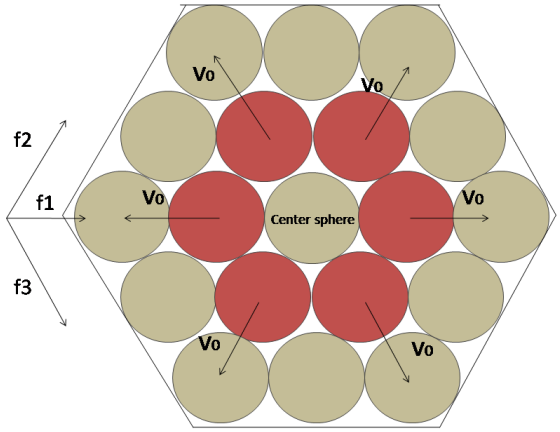

Figure 2.3: Initial particle velocity in the lattice

where $\mathbf{v}, \mathbf{u}$ is the velocity and displacement of the sphere, respectively (see Appendix A for detailed code) .

We show typical wave velocity profiles of the system with harmonic interactions in Fig. 2.4(a)-(c) and that with weakly nonlinear interactions in Fig. 2.4(d)-(f), respectively. The harmonic potential is chosen as $\varphi(x) = \frac{K|x|^2}{2}$ with $K = \frac{\pi aE}{4} = 3.6 \times 10^7 N/m$, $a = 4.76mm$, and mass $m = 4.4 \times 10^{-4} kg$, whereas the weakly nonlinear potential is given by $\varphi(x) = \frac{K|x|^2}{2} + \frac{\kappa|x|^3}{3}$ with the same K and $\kappa = 9 \times 10^{11} N/m^2$. Since we are only interested in the properties of propagating waves, the simulation is terminated once the wavefront reaches the boundary spheres in the system. Numerically, the wavefront velocity amplitude (V_p) is identified as the maximum particle velocity and the wavefront is defined as the surface on which the particle velocity achieves the maximum. The wave propagation speed (V_g) is defined as the propagation speed of wavefront (i.e., group velocity). In the systems with both harmonic and weakly nonlinear interactions, we see that propagating waves are generated in response to the initial impulse. As shown in Fig. 2.4, the wavefront roughly remains to be circular and the velocity amplitude decreases as the wave propagates away from the center. Also, as illustrated in Fig. 2.4 and Fig. 2.5 it is found that the interior particles have relatively large velocity which is unphysical since the energy of the system should be conserved. This issue arises from the accumulation of numerical errors in the iterations

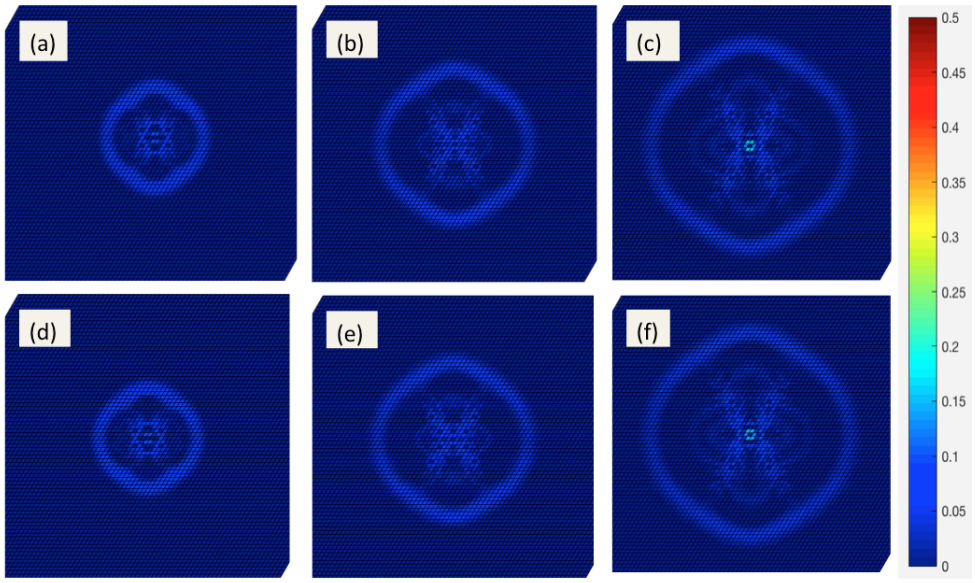

Figure 2.4: (Color online) Numerical simulations of wave formation and propagation in a hexagonal lattice with harmonic and weakly nonlinear interactions: velocity profile in a harmonic lattice ($K = 3.6 \times 10^7 N/m$) at (a) $t = 40\mu s$, (b) $t = 60\mu s$, and (c) $t = 80\mu s$; velocity profile in a weakly nonlinear lattice ($K = 3.6 \times 10^7 N/m$, $\kappa = 9 \times 10^{11} N/m^2$) at (d) $t = 40\mu s$, (e) $t = 60\mu s$, (f) $t = 80\mu s$. The colorbar indicates particle velocity magnitude in m/s.)

against discretized time steps. Nevertheless, the properties of the outermost wavefront can be confidentially obtained as evident in the comparisons with analytical results for a harmonic lattice (c.f., Fig. 2.6(a)-2.7(a)).

We next consider strongly nonlinear lattices with Hertzian potential $\varphi(x) = \frac{2K|x|^{\frac{5}{2}}}{5}$, where $K = \frac{2E}{1-\nu^2}\sqrt{\frac{a}{2}}$. We remark that this particular K value corresponds to 2D granular crystals formed by stainless steel spheres of diameter $a = 4.76mm$, densities $\rho = 7780kg/m^3$, Young's modulus $E = 193GPa$, and Poisson ratio $\nu = 0.3$. Figure 2.5(a)-(f) show the formation and propagation of a wavefront. In response to the initial impulse, the wave spatially spread about 4 sphere diameters and propagates in the direction normal to the wavefront. We also observe that the wavefront preserves the shape of hexagonal in a short period of time, and becomes smoother and more circular as time increases.

To have a better understanding of properties of the propagating waves, in Fig. 2.6(a), (b), and (c) we plot the velocity amplitude versus the wavefront position of harmonic,

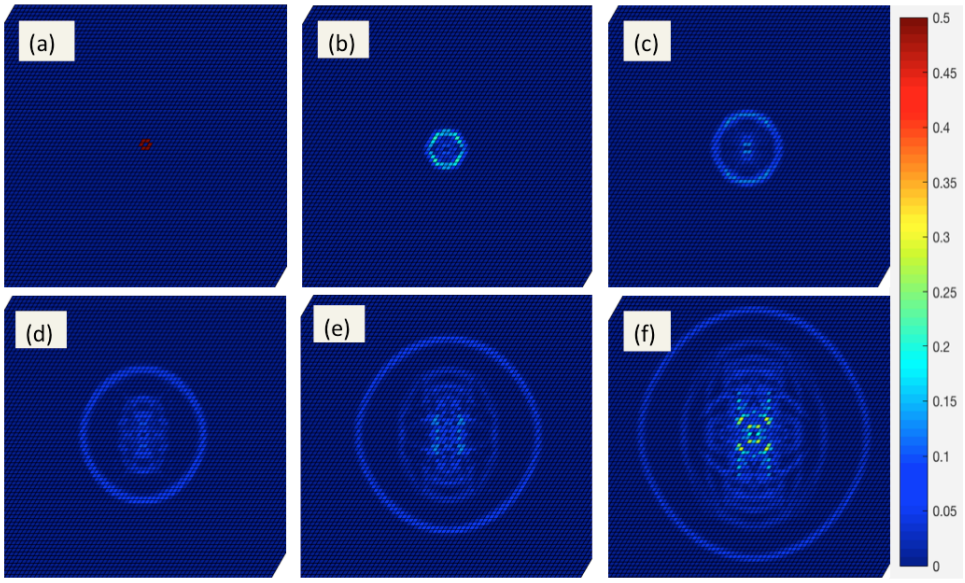

Figure 2.5: (Color online) Numerical simulations of soliton formation and propagation in a hexagonal lattice with the Hertzian interaction: velocity profiles at (a) $t = 2\mu s$, (b) $t = 20\mu s$, (c) $t = 40\mu s$, (d) $t = 80\mu s$, (e) $t = 120\mu s$, and (f) $t = 160\mu s$. The colorbar indicates particle velocity magnitude in m/s.

weakly nonlinear, and Hertzian interactions, respectively. In an ideal harmonic lattice, the kinetic energy of a propagating wave equals to the potential energy and remains to be constant, implying that

$$\frac{1}{2}mV_p^2\frac{2\pi R}{2a} \sim const. \quad \Rightarrow \quad V_p \propto R^{-1/2}. \tag{2.44}$$

Also, the propagation speed V_g shall be constant, independent of position and wavefront velocity amplitude. Indeed, we find these expected behaviors in our numerical simulations as shown in Fig. 2.6(a) and Fig. 2.7(a). The agreement between numerical results and theoretical results for the harmonic lattice, to some extent, validates our numerical schemes in capturing the properties of propagating wavefronts in spite of some numerical artifacts near the center. For weakly nonlinear and Hertzian lattices, there is no simple argument to show the scaling law analogous to (2.44). Numerically, we find that the wavefront velocity amplitudes still depend on propagation distance according to power laws: $V_p \propto R^{-1/1.9}$ for weakly nonlinear interaction (Fig. 2.6(b)) and $V_p \propto R^{-1/2.4}$ for Hertzian interaction (Fig. 2.6(c)).

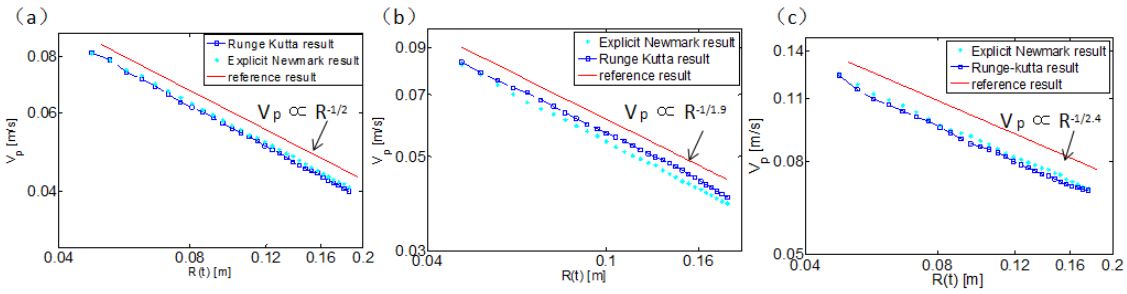

Figure 2.6: (Color online)The log-log plot of the maximum particle velocity (or wavefront velocity amplitude) versus wavefront position: (a) harmonic interaction, (b) weakly nonlinear interaction, and (c) Hertzian interaction.

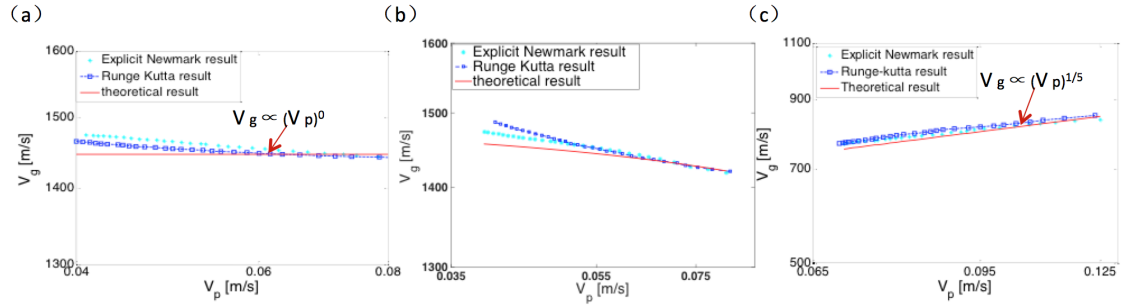

Figure 2.7: (Color online) The log-log plot of the propagation velocity versus the maximum particle velocity (or wavefront velocity amplitude): (a) harmonic interaction, (b) weakly nonlinear interaction, and (c) Hertzian interaction.

Figure 2.7(a), (b) and (c) show the propagation speed versus the wavefront velocity amplitude for systems with harmonic, weakly nonlinear, and Hertzian interaction, respectively. For a harmonic lattice, the propagation velocity is clearly independent of the wavefront velocity amplitude and consistent with the theoretical prediction (2.27):

$$V_g \propto V_p^0. \tag{2.45}$$

For a weakly nonlinear lattice, the propagation velocity depends on the wavefront velocity as shown in Fig. 2.7(b). Incidentally, we notice that the dependence agrees well with (2.33):

$$V_p \propto \frac{16\rho}{11\kappa a} V_g^3 - \frac{18K}{11\kappa a} V_g, \tag{2.46}$$

which is obtained for 2D planar solitary waves. The agreement is particularly well when V_p is small or $R(t)$ is large. This is consistent with the intuition that circular wavefronts better approximate a planar wavefront if the radius of the circular wavefront is large. Finally, for

a Hertzian lattice we plot the simulated propagation velocity versus the wavefront velocity in Fig. 2.7(c). Again, we compare the numerical result with the analytic prediction (2.42):

$$V_g \propto V_p^{\frac{1}{5}}. \tag{2.47}$$

The agreement seems to be reasonable in spite of the fact that the wavefront in numerics is circular while the wavefront in analysis is planar. We also highlight that the scaling laws (2.45)-(2.47) are obtained in a single simulation instead of multiple simulations with different initial velocity. Similar simulations have been performed for different initial velocity $v_0 = 0.2, 0.4 m/s$. The relations between the group velocity V_g and velocity wave amplitude V_p extracted from these simulations are consistent with the theoretical results as illustrated by Fig. 2.7 with similar trends (in a different regime of V_p).

2.5 Conclusion

The present work has focused on dynamic responses of a two-dimensional lattice with harmonic, weakly nonlinear, and Hertzian interactions by analytical and numerical approach. In the theoretical analysis, we have systematically derived the continuum approximations to the discrete system in a square lattice and in a hexagonal lattice. For the hexagonal lattice, we surprisingly find some nontrivial exact longitudinal solitary wave solutions along certain symmetric directions for systems with weakly nonlinear and Hertzian interactions. By numerical simulations, we have studied the properties of propagating waves and found the scaling laws between the wavefront velocity amplitudes and propagation distance: $V_p \propto R^{-1/1.9}$ for a weakly nonlinear lattice and $V_p \propto R^{-1/2.4}$ for a Hertzian lattice. The closed-form solitary wave solutions and scaling laws are expected to be valuable for the design of shock absorbers, acoustic lens, non-destructive structural testing devices among many others.

2.6 Appendix : calculations of relevant tensors of hexagonal lattices

From the definition (2.13), we find that

$$\begin{cases} \Lambda_1^1 = \langle D\phi, \mathbf{f}_1 \otimes \mathbf{f}_1 \rangle = \dfrac{\partial \phi}{\partial x} \cdot \mathbf{f}_1 = \dfrac{\partial \xi}{\partial x}, \\ \Lambda_2^1 = \langle D\phi, \mathbf{f}_2 \otimes \mathbf{f}_2 \rangle = [\dfrac{1}{2}\dfrac{\partial \phi}{\partial x} + \dfrac{\sqrt{3}}{2}\dfrac{\partial \phi}{\partial y}] \cdot \mathbf{f}_2 \\ \quad = \dfrac{1}{4}\dfrac{\partial \xi}{\partial x} + \dfrac{\sqrt{3}}{4}\dfrac{\partial \xi}{\partial y} + \dfrac{\sqrt{3}}{4}\dfrac{\partial \zeta}{\partial x} + \dfrac{3}{4}\dfrac{\partial \zeta}{\partial y}, \\ \Lambda_3^1 = \langle D\phi, \mathbf{f}_3 \otimes \mathbf{f}_3 \rangle = [\dfrac{1}{2}\dfrac{\partial \phi}{\partial x} - \dfrac{\sqrt{3}}{2}\dfrac{\partial \phi}{\partial y}] \cdot \mathbf{f}_3 \\ \quad = \dfrac{1}{4}\dfrac{\partial \xi}{\partial x} - \dfrac{\sqrt{3}}{4}\dfrac{\partial \xi}{\partial y} - \dfrac{\sqrt{3}}{4}\dfrac{\partial \zeta}{\partial x} + \dfrac{3}{4}\dfrac{\partial \zeta}{\partial y}. \end{cases} \tag{2.48}$$

In addition, direct but tedious calculations yield that

$$\begin{cases} \Lambda_1^2 = \langle D^2\phi, \mathbf{f}_1 \otimes \mathbf{f}_1 \otimes \mathbf{f}_1 \rangle = \dfrac{\partial^2 \phi}{\partial x^2} \cdot \mathbf{f}_1 = \dfrac{\partial^2 \xi}{\partial x^2}, \\ \Lambda_2^2 = \dfrac{1}{8}\dfrac{\partial^2 \xi}{\partial x^2} + \dfrac{\sqrt{3}}{4}\dfrac{\partial^2 \xi}{\partial x \partial y} + \dfrac{3}{8}\dfrac{\partial^2 \xi}{\partial y^2} + \dfrac{\sqrt{3}}{8}\dfrac{\partial^2 \zeta}{\partial x^2} + \dfrac{3}{4}\dfrac{\partial^2 \zeta}{\partial x \partial y} + \dfrac{3\sqrt{3}}{8}\dfrac{\partial^2 \zeta}{\partial y^2}, \\ \Lambda_3^2 = \dfrac{1}{8}\dfrac{\partial^2 \xi}{\partial x^2} - \dfrac{\sqrt{3}}{4}\dfrac{\partial^2 \xi}{\partial x \partial y} + \dfrac{3}{8}\dfrac{\partial^2 \xi}{\partial y^2} - \dfrac{\sqrt{3}}{8}\dfrac{\partial^2 \zeta}{\partial x^2} + \dfrac{3}{4}\dfrac{\partial^2 \zeta}{\partial x \partial y} - \dfrac{3\sqrt{3}}{8}\dfrac{\partial^2 \zeta}{\partial y^2}. \end{cases} \tag{2.49}$$

From (2.48), (2.49) and (2.18), we identify the vectors $\ell_{x\alpha}, \ell_{y\alpha}$ and symmetric matrices $\mathbf{M}_{x\alpha}, \mathbf{M}_{y\alpha}$ explicitly as

$$\begin{aligned} \mathbf{l}_{x1} &= \begin{bmatrix} 1 & 0 \end{bmatrix}, \qquad \mathbf{l}_{x2} = \begin{bmatrix} \frac{1}{4} & \frac{\sqrt{3}}{4} \end{bmatrix}, \qquad \mathbf{l}_{x3} = \begin{bmatrix} \frac{1}{4} & -\frac{\sqrt{3}}{4} \end{bmatrix}, \\ \mathbf{l}_{y1} &= \begin{bmatrix} 0 & 1 \end{bmatrix}, \qquad \mathbf{l}_{y2} = \begin{bmatrix} \frac{\sqrt{3}}{4} & \frac{3}{4} \end{bmatrix}, \qquad \mathbf{l}_{y3} = \begin{bmatrix} -\frac{\sqrt{3}}{4} & \frac{3}{4} \end{bmatrix}, \end{aligned} \tag{2.50}$$

and

$$\begin{aligned} \mathbf{M}_{x1} &= \begin{bmatrix} 1 & 0 \\ 0 & 0 \end{bmatrix}, \qquad \mathbf{M}_{x2} = \begin{bmatrix} \frac{1}{8} & \frac{\sqrt{3}}{8} \\ \frac{\sqrt{3}}{8} & \frac{3}{8} \end{bmatrix}, \qquad \mathbf{M}_{x3} = \begin{bmatrix} \frac{1}{8} & -\frac{\sqrt{3}}{8} \\ -\frac{\sqrt{3}}{8} & \frac{3}{8} \end{bmatrix}, \\ \mathbf{M}_{y1} &= \begin{bmatrix} 0 & 0 \\ 0 & 1 \end{bmatrix}, \qquad \mathbf{M}_{y2} = \begin{bmatrix} \frac{\sqrt{3}}{8} & \frac{3}{8} \\ \frac{3}{8} & \frac{3\sqrt{3}}{8} \end{bmatrix}, \qquad \mathbf{M}_{y3} = \begin{bmatrix} -\frac{\sqrt{3}}{8} & \frac{3}{8} \\ \frac{3}{8} & -\frac{3\sqrt{3}}{8} \end{bmatrix}, \end{aligned} \tag{2.51}$$

respectively. Further, from the definition (2.21) we identify the six-order tensor $\mathbb{D}$ by the following quadratic form:

$$\begin{aligned}\Gamma(\nabla\nabla\phi) &= \frac{1}{2}\nabla\nabla\phi\cdot\mathbb{D}\nabla\nabla\phi = \frac{K}{24}\sum_{\alpha=1}^{3}(\Lambda_\alpha^2)^2 \\ &= \frac{K}{24}\begin{bmatrix}\xi_{xx}\\ \xi_{yy}\\ \xi_{xy}\\ \zeta_{xx}\\ \zeta_{yy}\\ \zeta_{xy}\end{bmatrix}^T \begin{bmatrix}\mathbf{D}_1 & \mathbf{D}_2\\ \mathbf{D}_2^T & \mathbf{D}_3\end{bmatrix} \begin{bmatrix}\xi_{xx}\\ \xi_{yy}\\ \xi_{xy}\\ \zeta_{xx}\\ \zeta_{yy}\\ \zeta_{xy}\end{bmatrix},\end{aligned} \tag{2.52}$$

where

$$\mathbf{D}_1 = \begin{bmatrix}\frac{33}{32} & \frac{3}{32} & 0\\ \frac{3}{32} & \frac{9}{32} & 0\\ 0 & 0 & \frac{12}{32}\end{bmatrix}, \qquad \mathbf{D}_2 = \begin{bmatrix}0 & 0 & \frac{6}{32}\\ 0 & 0 & \frac{18}{32}\\ \frac{6}{32} & \frac{18}{32} & 0\end{bmatrix}, \qquad \mathbf{D}_3 = \begin{bmatrix}\frac{3}{32} & \frac{9}{32} & 0\\ \frac{9}{32} & \frac{27}{32} & 0\\ 0 & 0 & \frac{36}{32}\end{bmatrix}.$$

Chapter 3

New classes of extremal microstructures and G_θ-closure for isotropic multiphase conductive composites

3.1 Introduction

Composite material have attract tremendous attention due to their advanced properties in recent years. The continuous expansion of composite materials in many fields show the great need for developing a methodology to determine their effective properties. However, characterizing the effective properties of a composite is not easy, the effective properties requires solutions to partial differential equations which are generally impractical for realistic microstructures. Since the seminal works of [105, 87, 41, 38, 39], much of the attention in this area has focused on the study of optimal bounds on the effective properties with or without constraint on the volume fractions of the constituent phases. Among them, one of the most celebrated results in the theory of composite is Hashin–Shtrikman bounds (HS bounds) [38, 39]. Hashin et al. derived the bounds by variational principles and indicated the bounds were attainable for all two-phase bulk modulus by applying the bounds on the effective elastic moduli of isotropic composites [37]. Walpole extended the HS bounds to the arbitrarily anisotropic composite utilizing a similar variational method [107]. HS bounds restrict the effective properties in a range, that is, there exist composite with optimal properties when the HS bounds are attainable. In order to analyze the optimality of the HS bounds, the following groups constructed diverse microstructures. Hashin constructed the first microstructure by a composite spheres model, which attained the optimal bulk modulus bounds [36]. Milton proposed composites comprised of coated ellipsoids and illustrated the attainability of HS bounds [68]. The following group proved

that all the properties allowed by the optimal bounds are attainable by proposing finite rank laminates [63, 82, 69, 27]. Moreover, Vigdergauz constructed a new square symmetric composites("Vigdergauz microstructures") to attain the HS bounds [33, 104]. All the above microstructures can achieve the optimal properties in two phase composites. However, the HS bound are not always be optimal for more than two phase composite based on the volume fraction and constituent phases [68]. Therefore, more work is needed to understand the attainment condition of the HS bounds and improve the HS bounds for the multiphase composites.

In order to explore the optimal property of multiphase composite, considerable efforts have been devoted to constructing new microstructures and identifying the attainment condition of HS bounds. Milton first suggested a three material microstructure, which was comprised of two kinds of Hashin–Shtrikman coated sphere [68], and indicated that HS bounds were the most restrictive bounds within the constraint. Sigmund et al. proposed several new design of materials with extremal elastic properties using a numerical topology optimization approach [93, 94, 95, 92]. Although many attempts have been made to find the optimal microstructure, there is still a lack of a systematic approach to construct such structure. For two-dimension multiphase composites, the attainable regimes of HS bounds was restricted, so an improved bounds (translation bounds) was introduced to reproduce the HS bounds for multiphase conducting composites [100, 76, 5]. Albin et al. expanded the attainable region of the translation bound and introduced a general algorithm for constructing the structures of three components in two dimension, they investigated the sufficient conditions of the attainability of HS bounds by multi-rank laminates [3]. To further identify the attainment condition of HS bounds, Gibiansky and Sigmund [31] described sufficient conditions of the HS bounds attainability by combinations of coated sphere and laminates for three-phase composites. Liu presented a novel derivation of the Hashin-Shtrikman (HS) bounds for multi-phase composites and the associated attainment condition [59]. Cherkaev found an explicit form of bounds for effective conductivity for three-phase isotropic and anisotropic composites and extend to the exact lower bound on the effective elastic energy

of two-dimensional three-material composite [18, 20, 19]. Although plenty of works address the attainability of HS bounds for multiphase composite, there still lack systematic method to characterize all the attainable regimes. In the construction of multiphase composites, we may question that, besides coated spheres[36], coated ellipsoids[68], finite-rank laminates[63, 82, 69, 27], and "Vigdergauz microstructures"[104], are there any other microstructure with optimal properties can attain the HS bounds ?

In pursuit of answers to the above questions, we follow the usual approach of finding optimal bounds as the following steps: first we present a necessary condition for the HS bounds attainability of multiphase composites in the constraint of volume fractions of the constituent phases. Addressed by using a null lagrangian, the necessary condition gives new restrictions on the attainability of HS bounds. Further, we construct a new optimal three-phase coated sphere: the core sphere occupied by one-phase and the external coating occupied by two-phase periodic E-inclusion[61], which is the mathematically natural generalization of an ellipsoid. We demonstrate the optimality of the microstructure by applying local electrical fields and present the sufficient condition of HS bounds attainment in terms of volume fractions of the constituent phases, our attainability condition recover the results of Albin et al. [3]. We extend the optimal microstructure to a four-phase coated sphere and demonstrate the optimal conductivity of both lower bounds and upper bounds, and generalize the optimal coated sphere to a larger number phases. Moreover, we construct a new optimal microstructure by combining the three-phase coated sphere with two-phase periodic E-inclusion. By assuming each constituent part is optimal with $\triangle c_e = \triangle c_{HS}$, we systematically derive the sufficient condition for the attainability of HS bounds. Combining the necessary and sufficient condition of HS bounds attainability, we precisely illustrate the G-closure, which characterize the effective tensors with given material in prescribed volume fractions. Specialized to three-phase composites, the G-closure is described in closed form since the necessary condition and the sufficient condition are coincide. For four-phase composites, the G-closure labeled "attainable" is filled by both the new optimal microstructures and the four-phase coated sphere.

The paper is organized as follows. First, in Section 3.2 we recall the general scheme of Hashin-Shtrikman bounds and their attainment conditions to $(N+1)$-phase isotropic conductive materials. In Section 3.3 we derive a necessary condition such that Hashin-Shtrikman bounds are attainable. In Section 3.4 we present a new type of optimal three-phase and four-phase coated spheres in detail and extend the optimal microstructure to N phases. in Section 3.5 we construct a new optimal microstructure comprised of three-phase coated spheres and two-phase periodic E-inclusions, we derive a sufficient condition such that Hashin-Shtrikman bounds are attainable. In Section 3.6 we present the G_θ-closure of multiphase conductive composites. Finally, we summarize and present an outlook of possible applications in Section 3.7.

Notation. We introduce some notation for future convenience. Denote by $W^{\kappa,p}_{per}(Y)$ the set $\{\mathbf{u}|\mathbf{u}:\mathbb{R}^n \to \mathbb{R}^m$ is periodic on Y and $\int_Y \sum_{|\alpha|\leq\kappa} |D^\alpha \mathbf{u}|^{\mathbf{p}} < +\infty\}$

3.2 The Hashin-Shtrikman bounds and their attainment conditions

In this section, we recall the Hashin-Shtrikman bounds attainment conditions of $(N+1)$-phase isotropic conductive materials. Let Ω_i $(i = 0, \cdots, N)$ with $|\partial\Omega_i| = 0$ a measurable disjoint subdivision of the unit cell $Y = (0,1)^n$, and $\theta_i = |\Omega_i|/|Y| \neq 0$ the volume fractions. Without loss of generality, we assume $\Omega_1, \cdots, \Omega_N$ is closed but Ω_0 is open in Y. Consider multiphase composite of isotropic materials with conductivities $0 < k_0 < k_1 < ... < k_{N-1} < k_N$,

$$\mathbf{A}(\mathbf{x}, \mathscr{O}) = k_i \mathbf{I} \qquad \text{if } \mathbf{x} \in \Omega_i \qquad (i = 0, 1, \cdots, N), \tag{3.1}$$

where $\mathbf{I}$ is the identity matrix in $\mathbb{R}^{n\times n}$, $\mathscr{O} = (\Omega_1, \cdots, \Omega_N)$ is called the microstructure of the composite, and $(\theta_0, \cdots, \theta_N)$ denote the volume fractions of $\Omega_0, \cdots, \Omega_N$ in the unit cell Y with $\sum_{i=0}^N \theta_i = 1$. The effective tensor $\mathbf{A}^e(\mathscr{O}) = K^e\mathbf{I}$ admits rigorous bounds [37], which are independent of the detailed microstructure $\mathscr{O}$. We have the Hashin and Strikman bounds in the following form with the superscript $L(U)$ represent lower(upper) bounds, detailed

description can be found in [59],

$$k_0 + nk_0/\triangle c_{HS}^L = k^L \leq k^e \leq k^U = k_N + nk_N/\triangle c_{HS}^U \tag{3.2}$$

where

$$\begin{cases} \triangle c_i^L = \frac{nk_0}{k_i - k_0}, \quad \triangle c_{HS}^L = \frac{\theta_0 + \sum_{i=1}^N \theta_i \triangle c_i^L/(1+\triangle c_i^L)}{\sum_{i=1}^N \theta_i/(1+\triangle c_i^L)}, \\ \triangle c_i^U = \frac{nk_N}{k_i - k_N}, \quad \triangle c_{HS}^U = \frac{\theta_N + \sum_{i=0}^{N-1} \theta_i \triangle c_i^U/(1+\triangle c_i^U)}{\sum_{i=0}^{N-1} \theta_i/(1+\triangle c_i^U)}. \end{cases} \tag{3.3}$$

The above equation hold as equalities if, and only if the following overdetermined problem admits a solution $\xi \in W_{per}^{2,2}(Y)$,

$$\begin{cases} \Delta\xi = \sum_{i=0}^N p_i \chi_{\Omega_i} & \text{on } Y \\ \nabla\nabla\xi = \mathbf{Q}_i & \text{on } \Omega_i,\ i = 1, \cdots, N \\ \text{periodic boundary conditions} & \text{on } \partial Y \end{cases} \tag{3.4}$$

where χ_{Ω_i} is the characteristic function of $\Omega_i (i = 1,...,N)$, the overdetermined conditions $\mathbf{Q}_i (i = 1,...,N)$ are given by

$$\mathbf{Q}_i = \nabla\nabla\xi = \frac{p_i}{n}\mathbf{I}, \tag{3.5}$$

and the constant p_i for the lower and upper HS bounds as

$$\begin{cases} p_i^L = \mathrm{Tr}\mathbf{Q}_i^L = \frac{\triangle c_i^L - \triangle c_{HS}^L}{1+\triangle c_i^L} & i = 1,...,N, \\ p_i^U = \mathrm{Tr}\mathbf{Q}_i^U = \frac{\triangle c_i^U - \triangle c_{HS}^U}{1+\triangle c_i^U} & i = 0,...,N-1. \end{cases} \tag{3.6}$$

3.3 Restrictions on the attainable Hashin-Shtrikman bounds

3.3.1 Necessary condition for the lower HS bounds

We derive a necessary condition such that the lower Hashin-Shtrikman(HS) bounds are attainable. Based on HS bounds attainment conditions (3.2), finding a microstructure with given volume fraction θ_i and constants $p_i (i = 0, 1, ..., N)$ is not always possible due to strong

restrictions by the overdetermined problem (3.5). Below we derive a necessary condition such that (3.2) admits a solution $\xi \in W^{2,2}_{per}(Y)$. In (3.6), we have

$$p_i^L = \frac{\triangle c_i^L - \triangle c_{\mathrm{HS}}^L}{1+\triangle c_i^L}, \quad p_0^L = 1, \quad 0 < \triangle c_N^L < \triangle c_{\mathrm{HS}}^L < \triangle c_0^L. \tag{3.7}$$

where by(3.3) we have $\triangle c_i^L = \frac{nk_0}{k_i - k_0}$.

Assume ξ satisfies

$$\begin{cases} \Delta\xi = \sum_{i=0}^N p_i^L \chi_{\Omega_i} \\ \nabla\nabla\xi = \frac{p_i^L}{n}\mathbf{I} \qquad \text{on } \Omega_i,\ i = 1,\cdots,N. \end{cases}$$

It is clear that the boundary value of $\nabla\nabla\xi$ approached from interior Ω_0 to Ω_i is given by

$$\nabla\nabla\xi = \frac{p_i^L}{n}\mathbf{I} + (p_0^L - p_i^L)\mathbf{m}\otimes\mathbf{m} \qquad \text{on } \partial\Omega_i \cap \partial\Omega_0.$$

where $\mathbf{m}$ is the unit normal on $\partial\Omega_0$. Let $\mathbf{e} \in \mathbb{R}^n$ be an unit vector and $u_{\mathbf{e}} = \mathbf{e}\cdot(\nabla\nabla\xi)\mathbf{e}$. We verify

$$\begin{cases} \Delta u_{\mathbf{e}} = 0 & \text{on } \Omega_0, \\ u_{\mathbf{e}} = \frac{p_i^L}{n} + (p_0^L - p_i^L)(\mathbf{e}\cdot\mathbf{m})^{\mathbf{2}} & \text{on } \partial\Omega_i \cap \partial\Omega_0. \end{cases}$$

By the maximum principle applied to $u_{\mathbf{e}}$ on Ω_0, we have

$$u_{\mathbf{e}} \geq \lambda_{\min} = \min_{\alpha\in[0,1]} \{\frac{p_i^L}{n} + (p_0^L - p_i^L)\alpha, \quad i = 1,\cdots,N\}.$$

Since the mapping $\triangle c_i^L \mapsto p_i^L = \frac{\triangle c_i^L - \triangle c_{\mathrm{HS}}^L}{1+\triangle c_i^L}$ is strictly increasing, we have $p_1^L > p_2^L > \cdots > p_N^L$, $p_1^L > 0$ and $p_N^L < 0$, upon inspection we observe that

$$\lambda_{\min} = \frac{p_N^L}{n}. \tag{3.8}$$

Further, noticing that $\det : \mathbb{R}^{n\times n} \to \mathbb{R}$ is a null lagrangian [7]. By the divergence theorem, we have

$$\begin{aligned} \det(-\lambda_{\min}\mathbf{I}) &= \fint_Y \det(\nabla\nabla\xi - \lambda_{\min}\mathbf{I}) \\ &= \sum_{i=1}^N \theta_i \fint_{\Omega_i} \det(\nabla\nabla\xi - \lambda_{\min}\mathbf{I}) + \theta_0 \fint_{\Omega_0} \det(\nabla\nabla\xi - \lambda_{\min}\mathbf{I}), \end{aligned}$$

where $⨍_V = \frac{1}{volume(V)} \int_V$ is the average value of the integrand in region V. Since $\nabla\nabla\xi - \lambda_{\min}\mathbf{I}$ is positive semi-definite on Ω_0, we have

$$\det(-\lambda_{\min}\mathbf{I}) \geq \sum_{i=1}^{N} \theta_i ⨍_{\Omega_i} \det(\nabla\nabla\xi - \lambda_{\min}\mathbf{I}).$$

Inserting (3.8) into above inequalities, we obtain

$$\sum_{i=1}^{N} \theta_i (1 - \frac{p_i^L}{p_N^L})^n \leq 1. \tag{3.9}$$

By (3.7) and (3.3), the above inequalities (3.9) can be rewritten in terms of volume fraction of each constituent phases as

$$\left[\theta_0 + \sum_{i=1}^{N-1} \theta_i \frac{\triangle c_i^L - \triangle c_N^L}{1 + \triangle c_i^L}\right]^{-n} \sum_{i=1}^{N-1} \theta_i \left[\frac{\triangle c_i^L - \triangle c_N^L}{1 + \triangle c_i^L}\right]^n \leq 1, \tag{3.10}$$

which is a necessary condition for the lower HS bounds (3.2) to be attainable.

3.3.2 Necessary condition for the upper HS bounds

Following the similar procedure, we derive a necessary condition such that the upper Hashin-Strikman bounds are attainable. In (3.6), we have

$$p_i^U = \frac{\triangle c_i^U - \triangle c_{\mathrm{HS}}^U}{1 + \triangle c_i^U}, \quad p_N^U = 1, \quad \triangle c_N^U < \triangle c_{\mathrm{HS}}^U < \triangle c_0^U < 0. \tag{3.11}$$

where by(3.3) we have $\triangle c_i^U = \frac{nk_N}{k_i - k_N}$.

Assume ξ satisfies

$$\begin{cases} \Delta\xi = \sum_{i=0}^{N} p_i^U \chi_{\Omega_i} \\ \nabla\nabla\xi = \frac{p_i^U}{n}\mathbf{I} \qquad \text{on } \Omega_i,\ i = 0, \cdots, N-1. \end{cases}$$

It is clear that the boundary value of $\nabla\nabla\xi$ approached from interior Ω_N to Ω_i is given by

$$\nabla\nabla\xi = \frac{p_i^U}{n}\mathbf{I} + (p_N^U - p_i^U)\mathbf{m}\otimes\mathbf{m} \qquad \text{on } \partial\Omega_i \cap \partial\Omega_N.$$

where $\mathbf{m}$ is the unit normal on $\partial\Omega_N$. Let $\mathbf{e} \in \mathbb{R}^n$ be an unit vector and $u_{\mathbf{e}} = \mathbf{e}\cdot(\nabla\nabla\xi)\mathbf{e}$. We verify

$$\begin{cases} \Delta u_{\mathbf{e}} = 0 & \text{on } \Omega_N, \\ u_{\mathbf{e}} = \frac{p_i^U}{n} + (p_N^U - p_i^U)(\mathbf{e}\cdot\mathbf{m})^2 & \text{on } \partial\Omega_i \cap \partial\Omega_N. \end{cases}$$

By the maximum principle applied to $u_{\mathbf{e}}$ on Ω_N, we obtain that

$$u_{\mathbf{e}} \geq \lambda_{\min} = \min_{\alpha\in[0,1]} \{p_i^U/n + (p_N^U - p_i^U)\alpha, \quad i = 0, \cdots, N-1\}.$$

Since the mapping $\triangle c_i^U \mapsto \frac{\triangle c_i^U - \triangle c_{\mathrm{HS}}^U}{1+\triangle c_i^U}$ is strictly decreasing, we have $p_0^U < p_1^U < \cdots < p_{N-1}^U$, $p_0^U < 0$ and $p_{N-1}^U > 0$, upon inspection we observe that

$$\lambda_{\min} = \frac{p_0^U}{n}. \tag{3.12}$$

Further, noticing that $\det : \mathbb{R}^{n\times n} \to \mathbb{R}$ is a null lagrangian [7], we have

$$\begin{aligned}\det(-\lambda_{\min}\mathbf{I}) &= \fint_Y \det(\nabla\nabla\xi - \lambda_{\min}\mathbf{I}) \\ &= \sum_{i=0}^{N-1} \theta_i \fint_{\Omega_i} \det(\nabla\nabla\xi - \lambda_{\min}\mathbf{I}) + \theta_N \fint_{\Omega_N} \det(\nabla\nabla\xi - \lambda_{\min}\mathbf{I}).\end{aligned}$$

Since $\nabla\nabla\xi - \lambda_{\min}\mathbf{I}$ is positive semi-definite on Ω_N, we have

$$\det(-\lambda_{\min}\mathbf{I}) \geq \sum_{i=0}^{N-1} \theta_i \fint_{\Omega_i} \det(\nabla\nabla\xi - \lambda_{\min}\mathbf{I}).$$

Inserting (3.12) into above inequalities, we obtain

$$\sum_{i=0}^{N-1} \theta_i (1 - \frac{p_i^U}{p_0^U})^n \leq 1. \tag{3.13}$$

By (3.11)and (3.3), the above inequalities can be written as

$$\left[\theta_N + \sum_{i=1}^{N-1} \theta_i \frac{\triangle c_i^U - \triangle c_0^U}{1+\triangle c_i^U}\right]^{-n} \sum_{i=1}^{N-1} \theta_i \left[\frac{\triangle c_i^U - \triangle c_0^U}{1+\triangle c_i^U}\right]^n \leq 1, \tag{3.14}$$

which is a necessary condition for the upper HS bounds (3.2) to be attainable.

3.4 Construction of the optimal multiphase coated spheres

3.4.1 Construction of the optimal three-phase coated spheres

In this section we construct the optimal three-phase coated spheres to attain HS bounds. We describe in details the microstructure of the three-phase coated sphere of the α, β, γ phases.

Again, we denote by $k_\alpha, k_\beta, k_\gamma$ ($\min\{k_\alpha, k_\gamma\} < k_\beta < \max\{k_\alpha, k_\gamma\}$) the conductivities of the three phases and $\theta_\alpha, \theta_\beta, \theta_\gamma$ their corresponding volume fractions within the coated sphere. For future convenience, we introduce notation by (3.3) as

$$\triangle c_\gamma = \frac{nk_\alpha}{k_\gamma - k_\alpha}, \qquad \triangle c_\beta = \frac{nk_\alpha}{k_\beta - k_\alpha}. \tag{3.15}$$

As shown in Fig 3.1, we assume that the coated sphere has an inner radius R_1 and outer radius R_2, the core sphere is occupied by the β-phase, and external coating is occupied by a composite of the α, γ phases, so that the corresponding volume fractions are given by

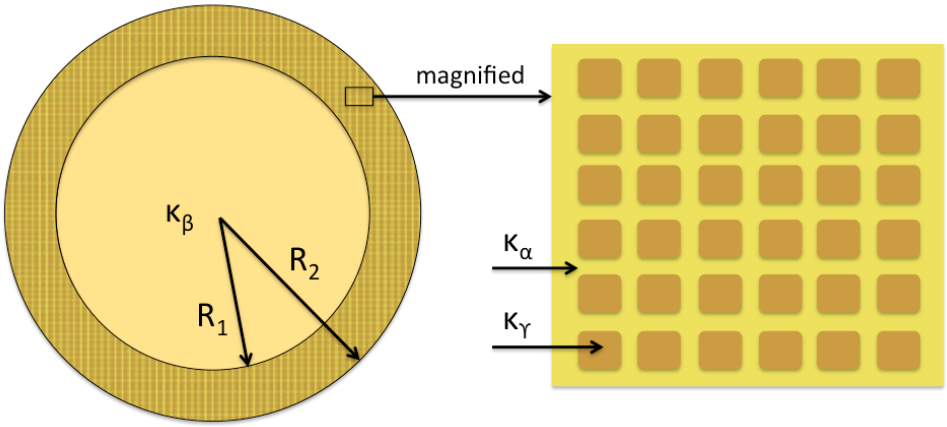

Figure 3.1: The microstructure of a three-phase coated sphere to attain HS bounds: the core sphere is occupied by phase-β; the external coating is occupied by two-phase periodic E-inclusion with local shape matrix $\mathbf{Q}(\mathbf{x})$ and local volume fraction $\rho(r)$, and the inclusions are occupied by the γ-phase, the matrix is occupied by the α-phase.

$$\theta_\beta = (\frac{R_1}{R_2})^n, \qquad \theta_\alpha + \theta_\beta + \theta_\gamma = 1. \tag{3.16}$$

The microstructure of the composite is locally a periodic E-inclusion [61] corresponding to the symmetric matrix $\mathbf{Q}(\mathbf{x})$ and local volume fraction $\rho(\mathbf{x})$, and the inclusions are occupied by the γ-phase, the matrix is occupied by the α-phase. The dependence of $\mathbf{Q}(\mathbf{x})$ and $\rho(\mathbf{x})$ on position $\mathbf{x}$ is assumed to be of the following form:

$$\mathbf{Q}(\mathbf{x}) = q_v(r)\mathbf{e}_r \otimes \mathbf{e}_r + q_\tau(r)[\mathbf{I} - \mathbf{e}_r \otimes \mathbf{e}_r], \qquad \rho(\mathbf{x}) = \rho(r), \tag{3.17}$$

where the subscript ν (τ) represents the radian (tangential) direction, $r = |\mathbf{x}|$, $\mathbf{e}_r = \mathbf{x}/r$, and $q_\nu(r), q_\tau(r)$ satisfy

$$q_\nu,\ q_\tau \geq 0, \qquad q_\nu + (n-1)q_\tau = \mathrm{Tr}(\mathbf{Q}(\mathbf{x})) = 1. \tag{3.18}$$

More precisely, let $\mathbf{A}(\mathbf{x})$ describes the conductivity tensor of the coated sphere and the ambient homogeneous medium of conductivity k^e, $a^e\mathbf{I}$ ($a^e \in \mathbb{R}$) be the applied electric fields, $\mathbf{v} : \mathbb{R}^n \to \mathbb{R}^n$ be the potential fields whose i-th component is the electric potential corresponding to an applied electric field given by the i-th row vector of the matrix $a^e\mathbf{I}$. Then the solution to

$$\begin{cases} \mathrm{div}(\mathbf{A}(\mathbf{x})\nabla\mathbf{v}) = 0 & \text{on } \mathbb{R}^n, \\ \nabla\mathbf{v} \to a^e\mathbf{I} & \text{as } |\mathbf{x}| \to +\infty, \end{cases} \tag{3.19}$$

satisfies

$$\nabla\mathbf{v} = a^e\mathbf{I} \qquad \text{outside the coated sphere.} \tag{3.20}$$

That is, the presence of the inhomogeneous coated sphere does not perturb the electric fields in the ambient medium. The field on the periodic E-inclusion [61] is uniform and given by

$$\nabla\mathbf{w} + \mathbf{F} = [\mathbf{I} - (\mathbf{I} + \frac{\triangle c_b}{(1-\theta_b)n}\mathbf{Q}^{-1})^{-1}]\mathbf{F}, \tag{3.21}$$

where $\mathbf{w} : Y \to \mathbb{R}^n$ are the electric potentials and $\mathbf{F} \in \mathbb{R}^{n\times n}$ is an average applied field. The effective conductivity tensor of a periodic E-inclusions is given by the following closed-form [58]

$$\mathbf{A}^e/k_a = \mathbf{I} + \frac{n\theta_b}{\triangle c_b}\mathbf{I} - \theta_a\theta_b\mathbf{Q}[\frac{\theta_a\triangle c_b}{n}\mathbf{Q} + \frac{\triangle c_b^2}{n^2}\mathbf{I}]^{-1}. \tag{3.22}$$

where the subscript a and b represent the matrix and inclusions, respectively. For the overall medium including the core, the external coating, and the surrounding medium, the

conductivity tensors are given by

$$\mathbf{A}(\mathbf{x}) = \begin{cases} k_\beta \mathbf{I} & \text{if } r < R_1, \\ k_\nu(r)\mathbf{e}_r \otimes \mathbf{e}_r + k_\tau(r)(\mathbf{I} - \mathbf{e}_r \otimes \mathbf{e}_r) & \text{if } R_1 < |\mathbf{x}| < R_2, \\ k^e \mathbf{I} & \text{if } r > R_2. \end{cases} \tag{3.23}$$

Inserting (3.17) into (3.22), we have k_ν and k_τ on the external coating by

$$\begin{aligned} \frac{k_\nu(r)}{k_\alpha} &= 1 + \frac{n\rho(r)}{n(1-\rho(r))q_\nu(r) + \triangle c_\gamma}, \\ \frac{k_\tau(r)}{k_\alpha} &= 1 + \frac{n\rho(r)}{n(1-\rho(r))q_\tau(r) + \triangle c_\gamma}. \end{aligned} \tag{3.24}$$

By symmetry, we observe that the solution to (3.19) is given by

$$\mathbf{v} = \nabla u, \qquad u = u(r) \qquad \text{if } r \le R_2. \tag{3.25}$$

Then the gradient field is given by

$$\nabla \mathbf{v} = \nabla\nabla u = u'' \mathbf{e}_r \otimes \mathbf{e}_r + \frac{u'}{r}(\mathbf{I} - \mathbf{e}_r \otimes \mathbf{e}_r), \tag{3.26}$$

and hence the current on the shell $\{R_1 < r < R_2\}$ is given by

$$\mathbf{A}(\mathbf{x})\nabla \mathbf{v} = k_\nu(r)u''(r)\mathbf{e}_r \otimes \mathbf{e}_r + k_\tau(r)\frac{u'}{r}(\mathbf{I} - \mathbf{e}_r \otimes \mathbf{e}_r). \tag{3.27}$$

Therefore, the first of (3.19) can be written as

$$(k_\nu(r)u'')' + \frac{n-1}{r}[k_\nu(r)u'' - \frac{k_\tau(r)}{r}u'] = 0. \tag{3.28}$$

The field on the periodic E-inclusions can be calculated as follows, for a fixed point in the external coating, the local field is given by $\nabla \mathbf{v} = \nabla\nabla u$, which is the average applied field for the underlying composite. Since the microstructures are periodic E-inclusions corresponding to symmetric matrix $\mathbf{Q}(\mathbf{x})$ and volume fraction $\rho(r)$ (cf., (3.17)), by (3.21) we find the microscopic field on the periodic E-inclusions is given by

$$\begin{aligned} &[\mathbf{I} - (\mathbf{I} + \frac{k_\alpha}{(1-\rho)(k_\gamma - k_\alpha)}\mathbf{Q}^{-1})^{-1}]\nabla\nabla u = \\ &\frac{u''\triangle c_\gamma}{\triangle c_\gamma + n(1-\rho)q_\nu}\mathbf{e}_r \otimes \mathbf{e}_r + \frac{\triangle c_\gamma u'/r}{\triangle c_\gamma + n(1-\rho)q_\tau}[\mathbf{I} - \mathbf{e}_r \otimes \mathbf{e}_r]. \end{aligned}$$

To attain the HS bound, from the attainment condition we shall require that

$$\frac{u''\triangle c_\gamma}{\triangle c_\gamma + n(1-\rho)q_v} = \frac{\triangle c_\gamma u'/r}{\triangle c_\gamma + n(1-\rho)q_\tau} = a_\gamma \qquad \text{if } r \in (R_1, R_2), \tag{3.29}$$

where $a_\gamma \in \mathbb{R}$ is to be determined. Plugging (3.24) and (3.29) into (3.28), we obtain

$$[(1-\rho)q_v + \rho]' + \frac{(n-1)(1-\rho)}{r}(q_v - q_\tau) = 0 \qquad \text{if } r \in (R_1, R_2). \tag{3.30}$$

Eliminating q_v in (3.30), by (3.18) we are left with

$$-\rho' q_\tau r + (1-\rho) r q_\tau' - (1-\rho)(1-q_\tau n) = 0 \qquad \text{if } r \in (R_1, R_2). \tag{3.31}$$

The three ordinary differential equations (ODE) in (3.29) and (3.30) imply only one ODE (3.31) for q_τ, ρ. Though equations (3.31) admit infinitely many different solutions to q_τ, ρ, we focus on two simple solutions which will be discussed in the following two sections.

Optimal three-phase coated spheres of the first type

By assuming q_τ is independent of r, the first simple solution to (3.31) is given by

$$q_\tau = const, \qquad \rho = 1 - cr^\delta, \;\; \delta = \frac{1}{q_\tau} - n, \tag{3.32}$$

where $q_v = 1-(n-1)q_\tau$ (cf., (3.18)) and $c \in \mathbb{R}$ is an integration constant to be determined. Inserting the above equation to (3.29), and by integrating we find

$$u(r) = \frac{1}{2} a_\gamma r^2 + \frac{cna_\gamma q_\tau}{(\delta+2)\triangle c_\gamma} r^{\delta+2} + d \qquad \text{if } r \in (R_1, R_2), \tag{3.33}$$

where d is an irrelevant constant such that u is continuous at $r = R_1$. To show the coated sphere is a neutral inclusion [66] for an appropriate ambient medium, we need to solve (3.29) for u. Again, from symmetry we infer the interior solution to (3.19) is given by (3.25) and we have

$$u(r) = \frac{1}{2} a_\beta r^2 \qquad \text{if} \quad r < R_1, \tag{3.34}$$

where $a_\beta \in \mathbb{R}$ is to be determined. Then the continuity of $\mathbf{v} = \nabla u$ and the continuity of normal current at the interface $\{r = R_1\}$ imply

$$\begin{cases} a_\beta R_1 = u'(R_1+), \\ k_\beta a_\beta = k_\nu u''(R_1+). \end{cases} \tag{3.35}$$

Inserting (3.24), (3.29) and (3.32) into (3.35), we obtain

$$\begin{cases} \frac{a_\beta}{a_\gamma} = 1 + \frac{cnq_\tau R_1^\delta}{\triangle c_\gamma}, \\ \frac{k_\beta a_\beta}{k_\alpha a_\gamma} = 1 + \frac{n}{\triangle c_\gamma} - \frac{cn(n-1)q_\tau R_1^\delta}{\triangle c_\gamma}. \end{cases}$$

Solving the above equation, we get

$$\frac{a_\beta}{a_\gamma} = \frac{1+1/\triangle c_\gamma}{1+1/\triangle c_\beta}, \qquad c = \frac{\triangle c_\gamma}{nq_\tau R_1^\delta}\left[\frac{1+1/\triangle c_\gamma}{1+1/\triangle c_\beta} - 1\right]. \tag{3.36}$$

Additionally, by (3.16), we have the volume fractions $\theta_\alpha, \theta_\beta, \theta_\gamma$ satisfy that $\theta_\beta = \left(\frac{R_1}{R_2}\right)^n$,

$$\frac{\theta_\gamma}{\theta_\alpha + \theta_\gamma} = \frac{n}{R_2^n - R_1^n}\int_{R_1}^{R_2} r^{n-1}\rho(r)dr = 1 - \frac{\triangle c_\gamma}{(n+\delta)q_\tau}[\frac{1+1/\triangle c_\gamma}{1+1/\triangle c_\beta} - 1]\frac{\theta_\beta^{-\delta/n} - \theta_\beta}{1-\theta_\beta}.$$

Noticing that $n+\delta = 1/q_\tau$ (cf., (3.32)) and $\theta_\alpha + \theta_\gamma = 1 - \theta_\beta$, we rewrite the above equation as

$$\begin{cases} \theta_\alpha = \triangle c_\gamma[\frac{1+1/\triangle c_\gamma}{1+1/\triangle c_\beta} - 1](\theta_\beta^{-\delta/n} - \theta_\beta), \\ \theta_\gamma = 1 - \frac{\triangle c_\beta - \triangle c_\gamma}{1+\triangle c_\beta}\theta_\beta^{-\delta/n} - \frac{1+\triangle c_\gamma}{1+\triangle c_\beta}\theta_\beta. \end{cases} \tag{3.37}$$

Since $q_\tau \geq 0$ and $q_\nu = 1-(n-1)q_\tau \geq 0$, we obtain the constraints $q_\tau \in [0, 1/(n-1)]$. In particular, we observe that when $q_\tau = 1/(n-1)$ (and so $\delta = 1/q_\tau - n = -1$, $q_\nu = 0$), the constructed three-phase coated sphere requires the least volume fraction of α-phase. In the following section, we apply $q_\tau = 1/(n-1)$ and $\delta = -1$ directly without further discussion. Below we calculate the conductivity of the ambient medium such that the coated sphere is a neutral inclusion [66]. First, the average electric field on the coated sphere $\{r < R_2\}$ is given by

$$⨍_{\{r<R_2\}} \nabla \mathbf{v} = ⨍_{\{r<R_2\}} \nabla\nabla u = \frac{\mathbf{I}}{n}⨍_{\{r<R_2\}} \Delta u = \frac{\mathbf{I}}{\omega_n R_2^n}\int_{\{r=R_2\}} u',$$

where the last equality follows from the divergence theorem, ω_n is the surface area of the unit sphere in $\mathbb{R}^n$, and hence $\omega_n R_2^n/n$ is the volume of the sphere $\{r<R_2\}$. Inserting (3.33) and (3.36) into the above equation and with $\theta_\beta = \left(\frac{R_1}{R_2}\right)^n$, we obtain

$$\fint_{\{r<R_2\}} \nabla \mathbf{v} = \bar{a}\mathbf{I}, \quad \bar{a} = \frac{u'}{r}|_{r=R_2} = a_\gamma \left[1 + \left(\frac{1+1/\triangle c_\gamma}{1+1/\triangle c_\beta} - 1\right)\theta_\beta^{-\delta/n}\right]. \tag{3.38}$$

Indeed, setting

$$u(r) = \frac{1}{2}\bar{a}r^2 + d' \qquad \text{if } r > R_2, \tag{3.39}$$

(d' is an irrelevant constant such that $u(r)$ is continuous at $r = R_2$) we verify the continuity of $\mathbf{v} = \nabla u$ and the continuity of normal current at the interface $\{r = R_2\}$ that

$$\begin{cases} u'(R_2-) = \bar{a}R_2, \\ k_\nu u''(R_2-) = k^e \bar{a}. \end{cases}$$

Finally, we have the effective conductivity k^e in the following form

$$\frac{k^e}{k_\alpha} = \frac{\triangle c_\gamma + n - (n-1)\theta_\beta^{-\delta/n}\triangle c_\gamma[\frac{1+1/\triangle c_\gamma}{1+1/\triangle c_\beta} - 1]}{\triangle c_\gamma + \theta_\beta^{-\delta/n}\triangle c_\gamma[\frac{1+1/\triangle c_\gamma}{1+1/\triangle c_\beta} - 1]}.$$

By (3.15), the above equation can be written as

$$\triangle c_e := \frac{nk_\alpha}{k^e - k_\alpha} = \frac{\triangle c_\alpha + \theta_\alpha + \triangle c_\gamma[\frac{1+1/\triangle c_\gamma}{1+1/\triangle c_\beta} - 1]\theta_\beta}{\theta_\beta + \theta_\gamma - \triangle c_\gamma[\frac{1+1/\triangle c_\gamma}{1+1/\triangle c_\beta} - 1]\theta_\beta},$$

which, unsurprisingly with volume fraction given by (3.37), coincides with the HS lower bounds if $k_\gamma > k_\alpha$ and the HS upper bounds if $k_\gamma < k_\alpha$. Particularly if $\delta = -1$, the above equation can be rewritten as

$$\triangle c_e = \frac{\triangle c_\gamma + \theta_\beta^{1/n}[\frac{\triangle c_\beta - \triangle c_\gamma}{1+\triangle c_\beta}]}{1 - \theta_\beta^{1/n}[\frac{\triangle c_\beta - \triangle c_\gamma}{1+\triangle c_\beta}]}. \tag{3.40}$$

Optimal three-phase coated spheres of the second type

Parallel to the last section, we obtain the second simple solution to (3.31) as

$$\begin{cases} q_\tau = \frac{1}{n} + cr^{-n}, \\ q_\nu = \frac{1}{n} - c(n-1)r^{-n}, \end{cases} \qquad \rho = const, \tag{3.41}$$

where $c \in \mathbb{R}$ is an integration constant. Inserting the above equations to (3.29), we find

$$u(r) = \frac{1}{2}a_\gamma(1+\frac{1-\rho}{\triangle c_\gamma})r^2 - \frac{cn(1-\rho)a_\gamma}{\triangle c_\gamma(n-2)r^{n-2}} + d \qquad \text{if } r \in (R_1, R_2), \tag{3.42}$$

where d is a constant such that u is continuous at $r = R_1$. Inserting (3.41) into (3.35) we obtain

$$\begin{cases} \frac{a_\beta}{a_\gamma} = \frac{1}{\triangle c_\gamma}[\triangle c_\gamma + 1 - \rho + \frac{cn(1-\rho)}{R_1^n}], \\ \frac{k_\beta a_\beta}{k_\alpha a_\gamma} = \frac{1}{\triangle c_\gamma}[\triangle c_\gamma + 1 + (n-1)\rho - \frac{cn(n-1)(1-\rho)}{R_1^n}]. \end{cases}$$

Solving the above equation, we have,

$$\frac{a_\beta}{a_\gamma} = \frac{1+1/\triangle c_\gamma}{1+1/\triangle c_\beta}, \qquad c = \frac{\big(\triangle c_\gamma(\frac{1+1/\triangle c_\gamma}{1+1/\triangle c_\beta} - 1) - (1-\rho)\big)R_1^n}{n(1-\rho)}. \tag{3.43}$$

Additionally, by (3.16), we have the volume fractions $\theta_\alpha, \theta_\beta, \theta_\gamma$ satisfy that $\theta_\beta = \left(\frac{R_1}{R_2}\right)^n$,

$$\frac{\theta_\gamma}{\theta_\alpha + \theta_\gamma} = \frac{n}{R_2^n - R_1^n}\int_{R_1}^{R_2} r^{n-1}\rho\, dr = \rho.$$

Noticing that $\theta_\alpha + \theta_\gamma = 1 - \theta_\beta$, we rewrite the above equation as

$$\begin{cases} \theta_\alpha = (1-\rho)(1-\theta_\beta), \\ \theta_\gamma = \rho(1-\theta_\beta). \end{cases} \tag{3.44}$$

Below we calculate the conductivity of the ambient medium such that the coated sphere is a neutral inclusion [66]. By (3.42) and (3.43) we get the average electric field on the coated sphere $\{r < R_2\}$ as

$$\begin{aligned} &\fint_{\{r\le R_2\}} \nabla\nabla u = \frac{\mathbf{I}}{n}\fint_{\{r\le R_2\}} \Delta u = \bar{a}\mathbf{I}, \\ &\bar{a} = \frac{u'}{r}|_{r=R_2} = a_\gamma[1 + \frac{1-\rho}{\triangle c_\gamma}(1-\theta_\beta) + (\frac{1+1/\triangle c_\gamma}{1+1/\triangle c_\beta} - 1)\theta_\beta]. \end{aligned} \tag{3.45}$$

Indeed, setting

$$u(r) = \frac{1}{2}\bar{a}r^2 + d' \qquad \text{if } r > R_2, \tag{3.46}$$

(d' is an irrelevant constant such that $u(r)$ is continuous at $r = R_2$) we verify the continuity of $\mathbf{v} = \nabla u$ and the continuity of normal current at the interface $\{r = R_2\}$ that

$$\begin{cases} u'(R_2-) = \bar{a}R_2, \\ k_\nu u''(R_2-) = k^e \bar{a}. \end{cases}$$

Finally, by (3.43) we express k^e as

$$\frac{k^e}{k_\alpha} = \frac{\triangle c_\gamma + n\rho + (1-\rho) - (n-1)[\triangle c_\gamma(\frac{1+1/\triangle c_\gamma}{1+1/\triangle c_\beta} - 1) - (1-\rho)]\theta_\beta}{\triangle c_\gamma + (1-\rho) + [\triangle c_\gamma(\frac{1+1/\triangle c_\gamma}{1+1/\triangle c_\beta} - 1) - (1-\rho)]\theta_\beta}.$$

Further, we can get

$$\triangle c_e := \frac{nk_\alpha}{k^e - k_\alpha} = \frac{\triangle c_\gamma + (1-\rho) + [\triangle c_\gamma(\frac{1+1/\triangle c_\gamma}{1+1/\triangle c_\beta} - 1) - (1-\rho)]\theta_\beta}{\rho - [\triangle c_\gamma(\frac{1+1/\triangle c_\gamma}{1+1/\triangle c_\beta} - 1) - (1-\rho)]\theta_\beta},$$

which, unsurprisingly with volume fraction given by (3.44), coincides with the HS lower bounds if $k_\gamma > k_\alpha$ and the HS upper bounds if $k_\gamma < k_\alpha$.

3.4.2 Construction of the optimal four-phase coated spheres

In this section, we explore the optimal microstructure of the four-phase coated sphere, and generalize the optimal microstructure to a larger number of phases following the similar procedure.

Construction of four-phase coated spheres attaining lower HS bounds

We construct a microstructure of four-phase coated sphere to attain the lower HS bounds. Again, we denote by k_0, k_1, k_2, k_3 ($k_0 < k_1 < k_2 < k_3$) the conductivities of the four phases and $\theta_0, \theta_1, \theta_2, \theta_3$ the corresponding volume fraction. For future convenience, we introduce notation by (3.3) as

$$\triangle c_1^L = \frac{nk_0}{k_1 - k_0}, \qquad \triangle c_2^L = \frac{nk_0}{k_2 - k_0}, \qquad \triangle c_3^L = \frac{nk_0}{k_3 - k_0}. \tag{3.47}$$

As shown in Fig 3.2, we constructed a four-phase coated sphere to attain the lower HS bounds. We assume that the coated sphere has an inner radius R_1, first outer layer of radius

R_2, and second outer layer of radius R_3. The core sphere is occupied by the 1-phase, the external coating is occupied by two layers of composites, the first layer of external coating($R_1 < r < R_2$) is occupied by 0-phase as matrix and 2-phase as inclusions, and the second layer of external coating($R_2 < r < R_3$) is occupied by 0-phase as matrix and 3-phase as inclusions. The corresponding volume fractions $\theta_1, \theta_0^2, \theta_2, \theta_0^3, \theta_3$ are given by

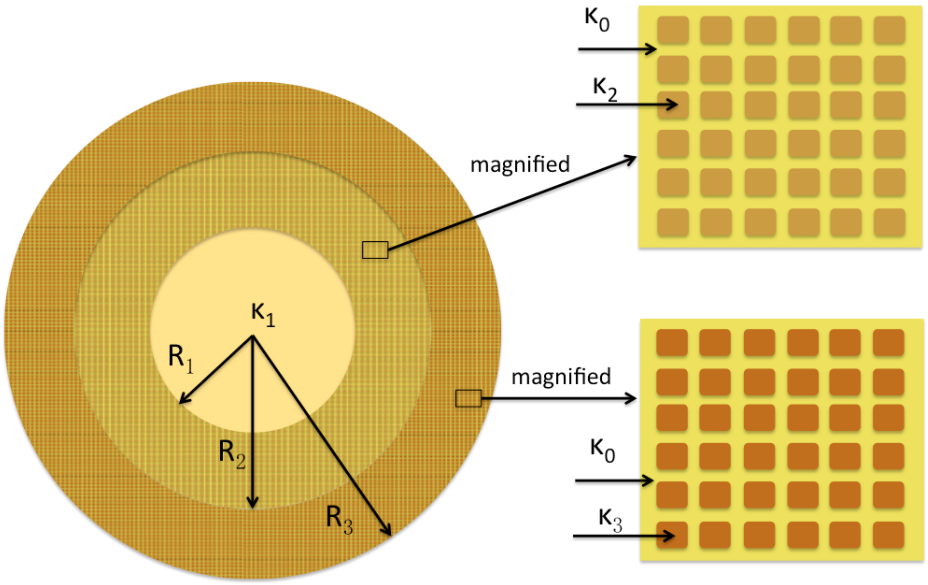

Figure 3.2: The microstructure of a four-phase coated sphere to attain lower HS bounds: the core sphere is occupied by phase-1; the external coating is occupied by two layers of composites, the microstructure of the composite is a periodic E-inclusion with local shape matrix $\mathbf{Q}(\mathbf{x})$ and local volume fraction $\rho(r)$, the first layer of external coating is occupied by $2,0$-phase(the inclusions are occupied by the 2-phase, the matrix is occupied by the 0-phase), and the second layer of external coating is occupied by $3,0$-phase(the inclusions are occupied by the 3-phase, the matrix is occupied by the 0-phase)

$$\begin{aligned} &\theta_1 = (\frac{R_1}{R_3})^n, \qquad \theta_1 + \theta_0^2 + \theta_2 = (\frac{R_2}{R_3})^n, \\ &\theta_1 + \theta_0^2 + \theta_2 + \theta_0^3 + \theta_3 = 1, \qquad \theta_0 = \theta_0^2 + \theta_0^3. \end{aligned} \tag{3.48}$$

where θ_0^2 and θ_0^3 are the volume fraction of matrix in the first and second layers of external coating respectively. The microstructure of the external coating is locally a periodic E-inclusion corresponding to the symmetric matrix $\mathbf{Q}_(\mathbf{x})$ and volume fraction $\rho_(\mathbf{x})$. The dependence of $\mathbf{Q}(\mathbf{x})$ and $\rho(\mathbf{x})$ on position $\mathbf{x}$ is assumed to be of the following form:

$$\mathbf{Q}(\mathbf{x}) = q_v(r)\mathbf{e}_r \otimes \mathbf{e}_r + q_\tau(r)[\mathbf{I} - \mathbf{e}_r \otimes \mathbf{e}_r], \quad \rho(\mathbf{x}) = \rho(r), \quad \text{if } r \in (R_1, R_3), \tag{3.49}$$

where the subscript ν (τ) represents the radian (tangential) direction, $r = |\mathbf{x}|$, $\mathbf{e}_r = \mathbf{x}/r$, and $q_\nu(r), q_\tau(r)$ satisfy

$$q_\nu,\ q_\tau \geq 0, \qquad q_\nu + (n-1)q_\tau = \mathrm{Tr}(\mathbf{Q}(\mathbf{x})) = 1. \tag{3.50}$$

More precisely, let $\mathbf{A}(\mathbf{x})$ describes the conductivity tensor of the coated sphere and the ambient homogeneous medium of conductivity k^e, $a^e\mathbf{I}$ ($a^e \in \mathbb{R}$) be the applied electric fields, $\mathbf{v} : \mathbb{R}^n \to \mathbb{R}^n$ be the potential fields whose i-th component is the electric potential corresponding to an applied electric field given by the i-th row vector of the matrix $a^e\mathbf{I}$. Then the solution to

$$\begin{cases} \mathrm{div}(\mathbf{A}(\mathbf{x})\nabla\mathbf{v}) = 0 & \text{on } \mathbb{R}^n, \\ \nabla\mathbf{v} \to a^e\mathbf{I} & \text{as } |\mathbf{x}| \to +\infty, \end{cases} \tag{3.51}$$

satisfies

$$\nabla\mathbf{v} = a^e\mathbf{I} \qquad \text{outside the coated sphere.} \tag{3.52}$$

That is, the presence of the inhomogeneous coated sphere does not perturb the electric fields in the ambient medium. The field on the periodic E-inclusion [61] is uniform and given by

$$\nabla\mathbf{w} + \mathbf{F} = [\mathbf{I} - (\mathbf{I} + \frac{\triangle c_b}{(1-\theta_b)n}\mathbf{Q}^{-1})^{-1}]\mathbf{F}, \tag{3.53}$$

where $\mathbf{w} : Y \to \mathbb{R}^n$ are the electric potentials and $\mathbf{F} \in \mathbb{R}^{n\times n}$ is an average applied field. The effective conductivity tensor of a periodic E-inclusions is given by the following closed-form [58]

$$\mathbf{A}^e/k_a = \mathbf{I} + \frac{n\theta_b}{\triangle c_b}\mathbf{I} - \theta_a\theta_b\mathbf{Q}[\frac{\theta_a\triangle c_b}{n}\mathbf{Q} + \frac{\triangle c_b^2}{n^2}\mathbf{I}]^{-1}. \tag{3.54}$$

where the subscript a and b represent the matrix phase and inclusions, respectively. For the overall medium including the core, the external coating, and the surrounding medium, the

conductivity tensors are given by

$$\mathbf{A}(\mathbf{x}) = \begin{cases} k_1\mathbf{I} & \text{if } r < R_1, \\ k_v(r)\mathbf{e}_r \otimes \mathbf{e}_r + k_\tau(r)(\mathbf{I} - \mathbf{e}_r \otimes \mathbf{e}_r) & \text{if } R_1 < r < R_3, \\ k^e\mathbf{I} & \text{if } r > R_3. \end{cases} \tag{3.55}$$

Inserting (3.49) into (3.54), we can find the effective conductivity tensors on the external coating by

$$\begin{aligned} \frac{k_v(r)}{k_0} &= 1 + \frac{n\rho(r)}{n(1-\rho(r))q_v(r) + \triangle c_\gamma(r)}, \\ \frac{k_\tau(r)}{k_0} &= 1 + \frac{n\rho(r)}{n(1-\rho(r))q_\tau(r) + \triangle c_\gamma(r)}, \end{aligned} \tag{3.56}$$

where

$$\triangle c_\gamma(r) = \begin{cases} \triangle c_2^L & \text{if } r \in (R_1, R_2), \\ \triangle c_3^L & \text{if } r \in (R_2, R_3). \end{cases}$$

By symmetry, we observe that the solution to (3.51) is given by

$$\mathbf{v} = \nabla u, \qquad u = u(r) \qquad \text{if } r \leq R_3. \tag{3.57}$$

Then the gradient field is given by

$$\nabla\mathbf{v} = \nabla\nabla u = u''\mathbf{e}_r \otimes \mathbf{e}_r + \frac{u'}{r}(\mathbf{I} - \mathbf{e}_r \otimes \mathbf{e}_r), \tag{3.58}$$

and hence the current on the shell $\{R_1 < r < R_3\}$ is given by

$$\mathbf{A}(\mathbf{x})\nabla\mathbf{v} = k_v(r)u''(r)\mathbf{e}_r \otimes \mathbf{e}_r + k_\tau(r)\frac{u'}{r}(\mathbf{I} - \mathbf{e}_r \otimes \mathbf{e}_r). \tag{3.59}$$

Therefore, the first of (3.51) can be written as

$$(k_v(r)u'')' + \frac{n-1}{r}[k_v(r)u'' - \frac{k_\tau(r)}{r}u'] = 0. \tag{3.60}$$

Further, the field on the periodic E-inclusions can be calculated as follows. For a fixed point in the external coating, the local field is given by $\nabla\mathbf{v} = \nabla\nabla u$, which is the average applied

field for the underlying composite. Since the microstructures are periodic E-inclusions corresponding to symmetric matrix $\mathbf{Q}(\mathbf{x})$ and volume fraction $\rho(r)$ (cf., (3.49)), from (3.53) we find the microscopic field on the periodic E-inclusions is given by

$$[\mathbf{I}-(\mathbf{I}+\frac{k_0}{(1-\rho)(k_\gamma-k_0)}\mathbf{Q}^{-1})^{-1}]\nabla\nabla u = \\ \frac{u''\triangle c_\gamma}{\triangle c_\gamma+n(1-\rho)q_\nu}\mathbf{e}_r\otimes\mathbf{e}_r+\frac{\triangle c_\gamma u'/r}{\triangle c_\gamma+n(1-\rho)q_\tau}[\mathbf{I}-\mathbf{e}_r\otimes\mathbf{e}_r].$$

To attain the HS bound, from the attainment condition we shall require that

$$\frac{u''\triangle c_\gamma}{\triangle c_\gamma+n(1-\rho)q_\nu}=\frac{\triangle c_\gamma u'/r}{\triangle c_\gamma+n(1-\rho)q_\tau}=a(r), \tag{3.61}$$

where

$$a(r)=\begin{cases} a_2 & \text{if } r\in(R_1,R_2),\\ a_3 & \text{if } r\in(R_2,R_3),\end{cases}$$

where $a_2,a_3\in\mathbb{R}$ are to be determined. Inserting (3.56) and (3.61) into (3.60), we obtain

$$[(1-\rho)q_\nu+\rho]'+\frac{(n-1)(1-\rho)}{r}(q_\nu-q_\tau)=0 \qquad \text{if } r\in(R_1,R_3). \tag{3.62}$$

Eliminating q_ν in (3.62), by (3.50) we are left with

$$-\rho' q_\tau r+(1-\rho)rq_\tau'-(1-\rho)(1-q_\tau n)=0 \qquad \text{if } r\in(R_1,R_3). \tag{3.63}$$

Thus, the three ordinary differential equations (ODE) in (3.61) and (3.62) imply only one ODE (3.63) for q_τ,ρ. Though equations (3.63) admit infinitely many different solutions, we focus on a simple solution as discussed in Section 3.4.1. By assuming q_τ is constant in region of $r\in(R_1,R_3)$, the first simple solution to (3.63) is given by

$$q_\tau=\frac{1}{n-1} \qquad \text{if } r\in(R_1,R_3), \qquad \rho(r)=\begin{cases}1-c^2r^{-1} & \text{if } r\in(R_1,R_2),\\ 1-c^3r^{-1} & \text{if } r\in(R_2,R_3),\end{cases} \tag{3.64}$$

where $q_\nu=1-(n-1)q_\tau=0$ (cf., (3.50)) and $c^2,c^3\in\mathbb{R}$ are integration constants to be determined. Inserting the above equation into (3.61), and by integrating we find

$$u(r)=\begin{cases}\frac{1}{2}a_2r^2+\frac{c^2na_2}{(n-1)\triangle c_2^L}r+d_1 & \text{if } r\in(R_1,R_2),\\ \frac{1}{2}a_3r^2+\frac{c^3na_3}{(n-1)\triangle c_3^L}r+d_2 & \text{if } r\in(R_2,R_3),\end{cases} \tag{3.65}$$

where d_1, d_2 are irrelevant constant such that u is continuous at $r = R_1, r = R_2$, respectively. To show the coated sphere is a neutral inclusion [66] for an appropriate ambient medium, we need to solve (3.61) for u. Again, from symmetry we infer the interior solution to (3.51) is given by (3.57) and we have

$$u(r) = \frac{1}{2} a_1 r^2 \qquad \text{if} \quad r < R_1, \tag{3.66}$$

where $a_1 \in \mathbb{R}$ is to be determined. Then the continuity of $\mathbf{v} = \nabla u$ and the continuity of normal current at the interface $\{r = R_1\}$ imply

$$\begin{cases} a_1 R_1 = u'(R_1+), \\ k_1 a_1 = k_\nu(R_1+) u''(R_1+), \end{cases} \tag{3.67}$$

Inserting (3.61) and (3.64) into (3.67) we obtain

$$\begin{cases} \frac{a_1}{a_2} = 1 + \frac{c^2 n}{(n-1)\triangle c_2^L R_1}, \\ \frac{k_1 a_1}{k_0 a_2} = 1 + \frac{n}{\triangle c_2^L} - \frac{c^2 n}{\triangle c_2^L R_1}, \end{cases}$$

Solving the above equation, we get

$$\frac{a_1}{a_2} = \frac{1 + 1/\triangle c_2^L}{1 + 1/\triangle c_1^L}, \qquad c^2 = \frac{(n-1)R_1}{n} \frac{\triangle c_1^L - \triangle c_2^L}{1 + \triangle c_1^L}. \tag{3.68}$$

Further the continuity of $\mathbf{v} = \nabla u$ and the continuity of normal current at the interface $\{r = R_2\}$ imply

$$\begin{cases} u'(R_2-) = u'(R_2+), \\ k_\nu(R_2-) u''(R_2-) = k_\nu(R_2+) u''(R_2+). \end{cases} \tag{3.69}$$

Inserting (3.61) and (3.64) into (3.69) we obtain

$$\begin{cases} \frac{a_2}{a_3} = \frac{\triangle c_2^L((n-1)\triangle c_3^L R_2 + nc^3)}{\triangle c_3^L((n-1)\triangle c_2^L R_2 + nc^2)}, \\ \frac{a_2}{a_3} = \frac{\triangle c_2^L(\triangle c_3^L R_2 + nR_2 - nc^3)}{\triangle c_3^L(\triangle c_2^L R_2 + nR_2 - nc^2)}. \end{cases}$$

Solving the above equation, we get

$$\begin{aligned} &\frac{a_2}{a_3} = \frac{1 + 1/\triangle c_3^L}{1 + 1/\triangle c_2^L}, \\ &c^3 = \frac{R_2(n-1)}{n} \frac{\triangle c_2^L - \triangle c_3^L}{1 + \triangle c_2^L} + \frac{R_1(n-1)}{n} \frac{(1 + \triangle c_3^L)(\triangle c_1^L - \triangle c_2^L)}{(1 + \triangle c_2^L)(1 + \triangle c_1^L)}. \end{aligned} \tag{3.70}$$

Additionally, by (3.48), we have the volume fractions $\theta_1, \theta_0^2, \theta_2, \theta_0^3, \theta_3$ satisfy that

$$\begin{aligned}
&\theta_1 = \left(\frac{R_1}{R_3}\right)^n, \qquad \theta_1 + \theta_0^2 + \theta_2 = \left(\frac{R_2}{R_3}\right)^n, \\
&\frac{\theta_2}{\theta_0^2 + \theta_2} = \frac{n}{R_2^n - R_1^n} \int_{R_1}^{R_2} r^{n-1} \rho_1(r) dr = 1 - \frac{nc^2}{n-1} \frac{R_2^{n-1} - R_1^{n-1}}{R_2^n - R_1^n}, \\
&\frac{\theta_3}{\theta_0^3 + \theta_3} = \frac{n}{R_3^n - R_2^n} \int_{R_2}^{R_3} r^{n-1} \rho_2(r) dr = 1 - \frac{nc^3}{n-1} \frac{R_3^{n-1} - R_2^{n-1}}{R_3^n - R_2^n}.
\end{aligned}$$

Noticing that $\theta_1 + \theta_0^2 + \theta_2 + \theta_0^3 + \theta_3 = 1$, inserting (3.68) and (3.70) into above equation, we have

$$\begin{cases}
\theta_2 = \left((\frac{R_2}{R_3})^n - (\frac{R_1}{R_3})^n\right) - \frac{\triangle c_1^L - \triangle c_2^L}{1+\triangle c_1^L}\left(\frac{R_1}{R_3}(\frac{R_2}{R_3})^{n-1} - (\frac{R_1}{R_3})^n\right), \\
\theta_0^2 = \frac{\triangle c_1^L - \triangle c_2^L}{1+\triangle c_1^L}\left(\frac{R_1}{R_3}(\frac{R_2}{R_3})^{n-1} - (\frac{R_1}{R_3})^n\right), \\
\theta_3 = \left(1 - (\frac{R_2}{R_3})^n\right) - \frac{\triangle c_2^L - \triangle c_3^L}{1+\triangle c_2^L}\left(\frac{R_2}{R_3} - (\frac{R_2}{R_3})^n\right) - \frac{(1+\triangle c_3^L)(\triangle c_1^L - \triangle c_2^L)}{(1+\triangle c_2^L)(1+\triangle c_1^L)}\left(\frac{R_1}{R_3} - \frac{R_1}{R_3}(\frac{R_2}{R_3})^{n-1}\right), \\
\theta_0^3 = \frac{\triangle c_2^L - \triangle c_3^L}{1+\triangle c_2^L}\left(\frac{R_2}{R_3} - (\frac{R_2}{R_3})^n\right) + \frac{(1+\triangle c_3^L)(\triangle c_1^L - \triangle c_2^L)}{(1+\triangle c_2^L)(1+\triangle c_1^L)}\left(\frac{R_1}{R_3} - \frac{R_1}{R_3}(\frac{R_2}{R_3})^{n-1}\right).
\end{cases} \tag{3.71}$$

Below we calculate the conductivity of the ambient medium such that the coated sphere is a neutral inclusion [66]. First, the average electric field on the coated sphere $\{r < R_3\}$ is given by

$$\fint_{\{r<R_3\}} \nabla \mathbf{v} = \fint_{\{r<R_3\}} \nabla \nabla u = \frac{\mathbf{I}}{n} \fint_{\{r<R_3\}} \Delta u = \frac{\mathbf{I}}{\omega_n R_3^n} \int_{\{r=R_3\}} u',$$

where the last equality follows from the divergence theorem, ω_n is the surface area of the unit sphere in $\mathbb{R}^n$, and hence $\omega_n R_3^n / n$ is the volume of the sphere $\{r < R_3\}$. Inserting (3.65) into the above equation, we obtain

$$\fint_{\{r<R_3\}} \nabla \mathbf{v} = \bar{a}\mathbf{I}, \quad \bar{a} = \frac{u'}{r}|_{r=R_3} = a_3[1 + \frac{c^3 n}{(n-1)\triangle c_3^L R_3}]. \tag{3.72}$$

Setting

$$u(r) = \frac{1}{2}\bar{a}r^2 + d_3 \qquad \text{if } r > R_3, \tag{3.73}$$

(d_3 is an irrelevant constant such that $u(r)$ is continuous at $r = R_3$) we verify the continuity of $\mathbf{v} = \nabla u$ and the continuity of normal current at the interface $\{r = R_3\}$ that

$$\begin{cases}
u'(R_3-) = \bar{a}R_3, \\
k_\nu(R_3-)u''(R_3-) = k_e^L \bar{a}.
\end{cases}$$

Finally, we have k_e^L in the following form

$$\frac{k_e^L}{k_0} = \frac{\triangle c_3^L + n - \frac{nc^3}{R_3}}{\triangle c_3^L + \frac{nc^3}{(n-1)R_3}}.$$

Further, by (3.70) and (3.48), we have

$$\begin{aligned} \triangle c_e^L :=& \frac{nk_0}{k_e^L - k_0} \\ =& \frac{\triangle c_3^L + \frac{\triangle c_2^L - \triangle c_3^L}{1+\triangle c_2^L}(\theta_1+\theta_0^2+\theta_2)^{1/n} + \frac{(1+\triangle c_3^L)(\triangle c_1^L - \triangle c_2^L)}{(1+\triangle c_2^L)(1+\triangle c_1^L)}(\theta_1)^{1/n}}{1 - \frac{\triangle c_2^L - \triangle c_3^L}{1+\triangle c_2^L}(\theta_1+\theta_0^2+\theta_2)^{1/n} - \frac{(1+\triangle c_3^L)(\triangle c_1^L - \triangle c_2^L)}{(1+\triangle c_2^L)(1+\triangle c_1^L)}(\theta_1)^{1/n}}. \end{aligned} \tag{3.74}$$

By straightforward algebraic calculations, we verify that the effective conductivity given by (3.74) attains the lower HS bound $\triangle c_e^L = \triangle c_{HS}^L$, if the volume fraction (3.71) is satisfied with $R_3 \geq R_2 \geq R_1 \geq 0$, that is,

$$\begin{cases} \theta_1 = (\frac{R_1}{R_3})^n, \\ \theta_2 = \big((\frac{R_2}{R_3})^n - (\frac{R_1}{R_3})^n\big) - \frac{\triangle c_1^L - \triangle c_2^L}{1+\triangle c_1^L}\big(\frac{R_1}{R_3}(\frac{R_2}{R_3})^{n-1} - (\frac{R_1}{R_3})^n\big), \\ \theta_0^2 = \frac{\triangle c_1^L - \triangle c_2^L}{1+\triangle c_1^L}\big(\frac{R_1}{R_3}(\frac{R_2}{R_3})^{n-1} - (\frac{R_1}{R_3})^n\big), \\ \theta_3 = \big(1 - (\frac{R_2}{R_3})^n\big) - \frac{\triangle c_2^L - \triangle c_3^L}{1+\triangle c_2^L}\big(\frac{R_2}{R_3} - (\frac{R_2}{R_3})^n\big) - \frac{(1+\triangle c_3^L)(\triangle c_1^L - \triangle c_2^L)}{(1+\triangle c_2^L)(1+\triangle c_1^L)}\big(\frac{R_1}{R_3} - \frac{R_1}{R_3}(\frac{R_2}{R_3})^{n-1}\big), \\ \theta_0^3 = \frac{\triangle c_2^L - \triangle c_3^L}{1+\triangle c_2^L}\big(\frac{R_2}{R_3} - (\frac{R_2}{R_3})^n\big) + \frac{(1+\triangle c_3^L)(\triangle c_1^L - \triangle c_2^L)}{(1+\triangle c_2^L)(1+\triangle c_1^L)}\big(\frac{R_1}{R_3} - \frac{R_1}{R_3}(\frac{R_2}{R_3})^{n-1}\big), \end{cases} \tag{3.75}$$

which is a sufficient condition for the lower HS bounds $\triangle c_e^L = \triangle c_{HS}^L$ to be attainable.

Construction of four-phase coated spheres attaining upper HS bounds

We construct a microstructure of four-phase coated sphere to attain the upper HS bounds. Again, we denote by k_0, k_1, k_2, k_3 ($k_0 < k_1 < k_2 < k_3$) the conductivities of the four phases, and for future convenience, we introduce notation

$$\triangle c_0^U = \frac{nk_3}{k_0 - k_3}, \qquad \triangle c_1^U = \frac{nk_3}{k_1 - k_3}, \qquad \triangle c_2^U = \frac{nk_3}{k_2 - k_3}. \tag{3.76}$$

As shown in Fig 3.3, we constructed a four-phase coated sphere to attain the upper HS bounds. We assume that the coated sphere has an inner radius R_1, the first outer layer of

radius R_2, and the second outer layer of radius R_3. The core sphere is occupied by the 2-phase, the external coating is occupied by two layers of composites, the first layer of external coating($R_1 < r < R_2$) is occupied by 3-phase as matrix and 1-phase as inclusions, and the second layer of external coating($R_2 < r < R_3$) is occupied by 3-phase as matrix and 0-phase as inclusions. The corresponding volume fractions $\theta_2, \theta_3^1, \theta_1, \theta_3^0, \theta_0$ within the

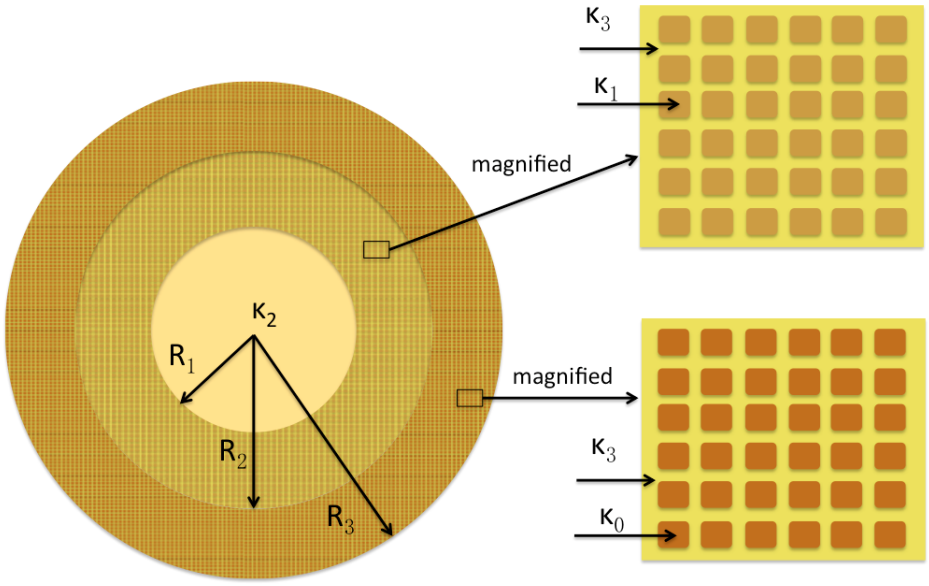

Figure 3.3: The microstructure of a four-phase coated sphere to attain upper HS bounds: the core sphere is occupied by phase-2; the external coating is occupied by two layers of composites, the microstructure of the composite is a periodic E-inclusion with local shape matrix $\mathbf{Q}(\mathbf{x})$ and local volume fraction $\rho(r)$, the first layer of external coating is occupied by $1,3$-phase(the inclusions are occupied by the 1-phase, the matrix is occupied by the 3-phase), and the second layer of external coating is occupied by $0,3$-phase(the inclusions are occupied by the 0-phase, the matrix is occupied by the 3-phase)

coated sphere are given by

$$\begin{aligned} &\theta_2 = (\frac{R_1}{R_3})^n, \qquad \theta_2 + \theta_3^1 + \theta_1 = (\frac{R_2}{R_3})^n, \\ &\theta_2 + \theta_3^1 + \theta_1 + \theta_3^0 + \theta_0 = 1, \qquad \theta_3 = \theta_3^1 + \theta_3^0. \end{aligned} \tag{3.77}$$

where θ_3^1 and θ_3^0 are the volume fraction of matrix in the first and second layers of external coating respectively. The microstructure of the external coating is locally a periodic E-inclusion corresponding to the symmetric matrix $\mathbf{Q}_(\mathbf{x})$ and volume fraction $\rho_(\mathbf{x})$. The

dependence of $\mathbf{Q}(\mathbf{x})$ and $\rho(\mathbf{x})$ on position $\mathbf{x}$ is assumed to be of the following form:

$$\mathbf{Q}(\mathbf{x}) = q_\nu(r)\mathbf{e}_r \otimes \mathbf{e}_r + q_\tau(r)[\mathbf{I} - \mathbf{e}_r \otimes \mathbf{e}_r], \quad \rho(\mathbf{x}) = \rho(r), \quad \text{if } r \in (R_1, R_3), \tag{3.78}$$

where the subscript $\nu(\tau)$ represents the radian(tangential) direction, $r = |\mathbf{x}|$, $\mathbf{e}_r = \mathbf{x}/r$, and $q_\nu(r), q_\tau(r)$ satisfy

$$q_\nu,\ q_\tau \geq 0, \qquad q_\nu + (n-1)q_\tau = \mathrm{Tr}(\mathbf{Q}(\mathbf{x})) = 1. \tag{3.79}$$

More precisely, let $\mathbf{A}(\mathbf{x})$ describes the conductivity tensor of the coated sphere and the ambient homogeneous medium of conductivity k^e, $a^e\mathbf{I}$ ($a^e \in \mathbb{R}$) be the applied electric fields, $\mathbf{v} : \mathbb{R}^n \to \mathbb{R}^n$ be the potential fields whose i-th component is the electric potential corresponding to an applied electric field given by the i-th row vector of the matrix $a^e\mathbf{I}$. Then the solution to

$$\begin{cases} \mathrm{div}(\mathbf{A}(\mathbf{x})\nabla\mathbf{v}) = 0 & \text{on } \mathbb{R}^n, \\ \nabla\mathbf{v} \to a^e\mathbf{I} & \text{as } |\mathbf{x}| \to +\infty, \end{cases} \tag{3.80}$$

satisfies

$$\nabla\mathbf{v} = a^e\mathbf{I} \qquad \text{outside the coated sphere.} \tag{3.81}$$

That is, the presence of the inhomogeneous coated sphere does not perturb the electric fields in the ambient medium. For the overall medium including the core, the external coating, and the surrounding medium, the conductivity tensors are given by

$$\mathbf{A}(\mathbf{x}) = \begin{cases} k_2\mathbf{I} & \text{if } r < R_1, \\ k_\nu(r)\mathbf{e}_r \otimes \mathbf{e}_r + k_\tau(r)(\mathbf{I} - \mathbf{e}_r \otimes \mathbf{e}_r) & \text{if } R_1 < r < R_3, \\ k^e\mathbf{I} & \text{if } r > R_3, \end{cases} \tag{3.82}$$

Inserting (3.78) into (3.54), we can find the effective conductivity tensors on the external coating by

$$\begin{aligned} \frac{k_\nu(r)}{k_3} &= 1 + \frac{n\rho(r)}{n(1-\rho(r))q_\nu(r) + \triangle c_\gamma(r)}, \\ \frac{k_\tau(r)}{k_3} &= 1 + \frac{n\rho(r)}{n(1-\rho(r))q_\tau(r) + \triangle c_\gamma(r)}, \end{aligned} \tag{3.83}$$

where

$$\triangle c_\gamma(r) = \begin{cases} \triangle c_1^U & \text{if } r \in (R_1, R_2), \\ \triangle c_0^U & \text{if } r \in (R_2, R_3). \end{cases}$$

By symmetry, we observe that the solution to (3.80) is given by

$$\mathbf{v} = \nabla u, \qquad u = u(r) \qquad \text{if } r \le R_3. \tag{3.84}$$

Then the gradient field is given by

$$\nabla \mathbf{v} = \nabla \nabla u = u'' \mathbf{e}_r \otimes \mathbf{e}_r + \frac{u'}{r}(\mathbf{I} - \mathbf{e}_r \otimes \mathbf{e}_r), \tag{3.85}$$

and hence the current on the shell $\{R_1 < r < R_3\}$ is given by

$$\mathbf{A}(\mathbf{x})\nabla \mathbf{v} = k_\nu(r) u''(r) \mathbf{e}_r \otimes \mathbf{e}_r + k_\tau(r) \frac{u'}{r}(\mathbf{I} - \mathbf{e}_r \otimes \mathbf{e}_r). \tag{3.86}$$

Therefore, the first of (3.80) can be written as

$$(k_\nu(r) u'')' + \frac{n-1}{r}[k_\nu(r) u'' - \frac{k_\tau(r)}{r} u'] = 0. \tag{3.87}$$

Further, the field on the periodic E-inclusions can be calculated as follows. For a fixed point in the external coating, the local field is given by $\nabla \mathbf{v} = \nabla \nabla u$, which is the average applied field for the underlying composite. Since the microstructures are periodic E-inclusions corresponding to symmetric matrix $\mathbf{Q}(\mathbf{x})$ and volume fraction $\rho(r)$ (cf., (3.78)), from (3.53) we find the microscopic field on the periodic E-inclusions is given by

$$[\mathbf{I} - (\mathbf{I} + \frac{k_0}{(1-\rho)(k_\gamma - k_0)} \mathbf{Q}^{-1})^{-1}] \nabla \nabla u =$$
$$\frac{u'' \triangle c_\gamma}{\triangle c_\gamma + n(1-\rho) q_\nu} \mathbf{e}_r \otimes \mathbf{e}_r + \frac{\triangle c_\gamma u'/r}{\triangle c_\gamma + n(1-\rho) q_\tau} [\mathbf{I} - \mathbf{e}_r \otimes \mathbf{e}_r].$$

from the attainment condition we shall require that

$$\frac{u'' \triangle c_\gamma}{\triangle c_\gamma + n(1-\rho) q_\nu} = \frac{\triangle c_\gamma u'/r}{\triangle c_\gamma + n(1-\rho) q_\tau} = a(r), \tag{3.88}$$

where

$$a(r) = \begin{cases} a_1 & \text{if } r \in (R_1, R_2), \\ a_0 & \text{if } r \in (R_2, R_3), \end{cases}$$

where $a_1, a_0 \in \mathbb{R}$ are to be determined. Inserting (3.83) and (3.88) into (3.87), we obtain

$$[(1-\rho)q_v + \rho]' + \frac{(n-1)(1-\rho)}{r}(q_v - q_\tau) = 0 \qquad \text{if } r \in (R_1, R_3). \tag{3.89}$$

Eliminating q_v in (3.89), by (3.79) we are left with

$$-\rho' q_\tau r + (1-\rho) r q_\tau' - (1-\rho)(1-q_\tau n) = 0 \qquad \text{if } r \in (R_1, R_3). \tag{3.90}$$

Thus, the three ordinary differential equations (ODE) in (3.88) and (3.89) imply only one ODE (3.90) for q_τ, ρ. Though equations (3.90) admit infinitely many different solutions, we focus on a simple solution as discussed in In Section 3.4.1. By assuming q_τ is constant in region of $r \in (R_1, R_3)$, the first simple solution to (3.90) is given by

$$q_\tau = \frac{1}{n-1} \qquad \text{if } r \in (R_1, R_3), \qquad \rho(r) = \begin{cases} 1 - c^1 r^{-1} & \text{if } r \in (R_1, R_2), \\ 1 - c^0 r^{-1} & \text{if } r \in (R_2, R_3), \end{cases} \tag{3.91}$$

where $q_v = 1 - (n-1)q_\tau = 0$ (cf., (3.79)) and $c^1, c^0 \in \mathbb{R}$ are integration constants to be determined. Inserting the above equation into (3.88), and by integrating we find

$$u(r) = \begin{cases} \frac{1}{2} a_1 r^2 + \frac{c^1 n a_1}{(n-1)\triangle c_1^U} r + d_1 & \text{if } r \in (R_1, R_2), \\ \frac{1}{2} a_0 r^2 + \frac{c^0 n a_0}{(n-1)\triangle c_0^U} r + d_2 & \text{if } r \in (R_2, R_3), \end{cases} \tag{3.92}$$

where d_1, d_2 are irrelevant constant such that u is continuous at $r = R_1, r = R_2$, respectively. To show the coated sphere is a neutral inclusion [66] for an appropriate ambient medium, we need to solve (3.88) for u. Again, from symmetry we infer the interior solution to (3.80) is given by (3.84) and we have

$$u(r) = \frac{1}{2} a_2 r^2 \qquad \text{if} \quad r < R_1, \tag{3.93}$$

where $a_2 \in \mathbb{R}$ is to be determined. Then the continuity of $\mathbf{v} = \nabla u$ and the continuity of normal current at the interface $\{r = R_1\}$ imply

$$\begin{cases} a_2 R_1 = u'(R_1+), \\ k_2 a_2 = k_v(R_1+) u''(R_1+). \end{cases} \tag{3.94}$$

Inserting (3.88) and (3.91) into (3.94) we obtain

$$\begin{cases} \frac{a_2}{a_1} = 1 + \frac{c^1 n}{(n-1)\triangle c_1^U R_1}, \\ \frac{k_2 a_2}{k_3 a_1} = 1 + \frac{n}{\triangle c_1^U} - \frac{c^1 n}{\triangle c_1^U R_1}. \end{cases}$$

Solving the above equation, we get

$$\frac{a_2}{a_1} = \frac{1+1/\triangle c_1^U}{1+1/\triangle c_2^U}, \qquad c^1 = \frac{(n-1)R_1}{n}\frac{\triangle c_2^U - \triangle c_1^U}{1+\triangle c_2^U}. \tag{3.95}$$

Further the continuity of $\mathbf{v} = \nabla u$ and the continuity of normal current at the interface $\{r = R_2\}$ imply

$$\begin{cases} u'(R_2-) = u'(R_2+), \\ k_v(R_2-)u''(R_2-) = k_v(R_2+)u''(R_2+). \end{cases} \tag{3.96}$$

Inserting (3.88) and (3.91) into (3.96) we obtain

$$\begin{cases} \frac{a_1}{a_0} = \frac{\triangle c_1^U((n-1)\triangle c_0^U R_2 + nc^0)}{\triangle c_0^U((n-1)\triangle c_1^U R_2 + nc^1)}, \\ \frac{a_1}{a_0} = \frac{\triangle c_1^U(\triangle c_0^U R_2 + nR_2 - nc^0)}{\triangle c_0^U(\triangle c_1^U R_2 + nR_2 - nc^1)}. \end{cases}$$

Solving the above equation, we get

$$\begin{aligned} &\frac{a_1}{a_0} = \frac{1+1/\triangle c_0^U}{1+1/\triangle c_1^U}, \\ &c^0 = -\frac{R_2(n-1)}{n}\frac{\triangle c_0^U - \triangle c_1^U}{1+\triangle c_1^U} + \frac{R_1(n-1)}{n}\frac{(1+\triangle c_0^U)(\triangle c_2^U - \triangle c_1^U)}{(1+\triangle c_1^U)(1+\triangle c_2^U)}. \end{aligned} \tag{3.97}$$

Additionally, by (3.77), we have the volume fractions $\theta_2, \theta_3^1, \theta_1, \theta_3^0, \theta_0$ satisfy that

$$\begin{aligned} &\theta_2 = \left(\frac{R_1}{R_3}\right)^n, \qquad \theta_2 + \theta_3^1 + \theta_1 = \left(\frac{R_2}{R_3}\right)^n, \\ &\frac{\theta_1}{\theta_3^1 + \theta_1} = \frac{n}{R_2^n - R_1^n}\int_{R_1}^{R_2} r^{n-1}\rho_1(r)dr = 1 - \frac{nc^1}{n-1}\frac{R_2^{n-1} - R_1^{n-1}}{R_2^n - R_1^n}, \\ &\frac{\theta_0}{\theta_3^0 + \theta_0} = \frac{n}{R_3^n - R_2^n}\int_{R_2}^{R_3} r^{n-1}\rho_2(r)dr = 1 - \frac{nc^0}{n-1}\frac{R_3^{n-1} - R_2^{n-1}}{R_3^n - R_2^n}. \end{aligned}$$

Noticing that $\theta_2+\theta_3^1+\theta_1+\theta_3^0+\theta_0=1$, inserting (3.95) and (3.97) into above equation, we have

$$\begin{cases}\theta_1=\big((\frac{R_2}{R_3})^n-(\frac{R_1}{R_3})^n\big)-\frac{\triangle c_2^U-\triangle c_1^U}{1+\triangle c_2^U}\big(\frac{R_1}{R_3}(\frac{R_2}{R_3})^{n-1}-(\frac{R_1}{R_3})^n\big),\\ \theta_3^1=\frac{\triangle c_2^U-\triangle c_1^U}{1+\triangle c_2^U}\big(\frac{R_1}{R_3}(\frac{R_2}{R_3})^{n-1}-(\frac{R_1}{R_3})^n\big),\\ \theta_0=\big(1-(\frac{R_2}{R_3})^n\big)+\frac{\triangle c_0^U-\triangle c_1^U}{1+\triangle c_1^U}\big(\frac{R_2}{R_3}-(\frac{R_2}{R_3})^n\big)-\frac{(1+\triangle c_0^U)(\triangle c_2^U-\triangle c_1^U)}{(1+\triangle c_1^U)(1+\triangle c_2^U)}\big(\frac{R_1}{R_3}-\frac{R_1}{R_3}(\frac{R_2}{R_3})^{n-1}\big),\\ \theta_3^0=-\frac{\triangle c_0^U-\triangle c_1^U}{1+\triangle c_1^U}\big(\frac{R_2}{R_3}-(\frac{R_2}{R_3})^n\big)+\frac{(1+\triangle c_0^U)(\triangle c_2^U-\triangle c_1^U)}{(1+\triangle c_1^U)(1+\triangle c_2^U)}\big(\frac{R_1}{R_3}-\frac{R_1}{R_3}(\frac{R_2}{R_3})^{n-1}\big).\end{cases}\tag{3.98}$$

Below we calculate the conductivity of the ambient medium such that the coated sphere is a neutral inclusion [66]. First, the average electric field on the coated sphere $\{r<R_3\}$ is given by

$$\fint_{\{r<R_3\}}\nabla\mathbf{v}=\fint_{\{r<R_3\}}\nabla\nabla u=\frac{\mathbf{I}}{n}\fint_{\{r<R_3\}}\Delta u=\frac{\mathbf{I}}{\omega_n R_3^n}\int_{\{r=R_3\}}u',$$

where the last equality follows from the divergence theorem, ω_n is the surface area of the unit sphere in $\mathbb{R}^n$, and hence $\omega_n R_3^n/n$ is the volume of the sphere $\{r<R_3\}$. Inserting (3.92) into the above equation, we obtain

$$\fint_{\{r<R_3\}}\nabla\mathbf{v}=\bar{a}\mathbf{I},\quad \bar{a}=\frac{u'}{r}|_{r=R_3}=a_0[1+\frac{c^0 n}{(n-1)\triangle c_0^U R_3}].\tag{3.99}$$

Setting

$$u(r)=\frac{1}{2}\bar{a}r^2+d_3\qquad\text{if } r>R_3,\tag{3.100}$$

(d_3 is an irrelevant constant such that $u(r)$ is continuous at $r=R_3$) we verify the continuity of $\mathbf{v}=\nabla u$ and the continuity of normal current at the interface $\{r=R_3\}$ that

$$\begin{cases}u'(R_3-)=\bar{a}R_3,\\ k_\nu(R_3-)u''(R_3-)=k_e^U\bar{a}.\end{cases}$$

Finally, we have k_e^U in the following form

$$\frac{k_e^U}{k_3}=\frac{\triangle c_0^U+n-\frac{nc^0}{R_3}}{\triangle c_0^U+\frac{nc^0}{(n-1)R_3}}.$$

Further, by (3.97) and (3.77), we have

$$\begin{aligned}\triangle c_e^U :&= \frac{nk_3}{k_e^U - k_3} \\ &= \frac{\triangle c_0^U + \frac{\triangle c_1^U - \triangle c_0^U}{1+\triangle c_1^U}(\theta_2+\theta_3^1+\theta_1)^{1/n} + \frac{(1+\triangle c_0^U)(\triangle c_2^U - \triangle c_1^U)}{(1+\triangle c_1^U)(1+\triangle c_2^U)}(\theta_2)^{1/n}}{1 - \frac{\triangle c_1^U - \triangle c_0^U}{1+\triangle c_1^U}(\theta_2+\theta_3^1+\theta_1)^{1/n} - \frac{(1+\triangle c_0^U)(\triangle c_2^U - \triangle c_1^U)}{(1+\triangle c_1^U)(1+\triangle c_2^U)}(\theta_2)^{1/n}}\end{aligned} \tag{3.101}$$

By straightforward algebraic calculations, we verify that the effective conductivity given by (3.101) attains the upper HS bound $\triangle c_e^U = \triangle c_{HS}^U$, if the volume fraction (3.98) is satisfied with $R_3 \geq R_2 \geq R_1 \geq 0$, that is,

$$\begin{cases} \theta_2 = (\frac{R_1}{R_3})^n, \\ \theta_1 = \big((\frac{R_2}{R_3})^n - (\frac{R_1}{R_3})^n\big) - \frac{\triangle c_2^U - \triangle c_1^U}{1+\triangle c_2^U}\big(\frac{R_1}{R_3}(\frac{R_2}{R_3})^{n-1} - (\frac{R_1}{R_3})^n\big), \\ \theta_3^1 = \frac{\triangle c_2^U - \triangle c_1^U}{1+\triangle c_2^U}\big(\frac{R_1}{R_3}(\frac{R_2}{R_3})^{n-1} - (\frac{R_1}{R_3})^n\big), \\ \theta_0 = \big(1 - (\frac{R_2}{R_3})^n\big) + \frac{\triangle c_0^U - \triangle c_1^U}{1+\triangle c_1^U}\big(\frac{R_2}{R_3} - (\frac{R_2}{R_3})^n\big) - \frac{(1+\triangle c_0^U)(\triangle c_2^U - \triangle c_1^U)}{(1+\triangle c_1^U)(1+\triangle c_2^U)}\big(\frac{R_1}{R_3} - \frac{R_1}{R_3}(\frac{R_2}{R_3})^{n-1}\big), \\ \theta_3^0 = -\frac{\triangle c_0^U - \triangle c_1^U}{1+\triangle c_1^U}\big(\frac{R_2}{R_3} - (\frac{R_2}{R_3})^n\big) + \frac{(1+\triangle c_0^U)(\triangle c_2^U - \triangle c_1^U)}{(1+\triangle c_1^U)(1+\triangle c_2^U)}\big(\frac{R_1}{R_3} - \frac{R_1}{R_3}(\frac{R_2}{R_3})^{n-1}\big), \end{cases} \tag{3.102}$$

which is a sufficient condition for the upper HS bounds $\triangle c_e^U = \triangle c_{HS}^U$ to be attainable.

3.4.3 Generalization of the optimal N-phase coated spheres

In this section, we summarize the generalization of the optimal N-phase coated sphere.

For the N-phase coated spheres attaining lower HS bounds, The microstructure is constructed as shown in Fig 3.4(a), We assume that the coated sphere has an inner radius R_1, and the external coating are occupied by layers of radius R_2 to R_N in ascending order. The effective conductivity is given by

$$\triangle c_e^L := \frac{\triangle c_N^L + \sum_{j=1}^{N-1} \frac{(1+\triangle c_N^L)(\triangle c_{N-j}^L - \triangle c_{N-j+1}^L)}{(1+\triangle c_{N-j+1}^L)(1+\triangle c_{N-j}^L)}\big(\frac{R_{N-j}}{R_N}\big)}{1 - \sum_{j=1}^{N-1} \frac{(1+\triangle c_N^L)(\triangle c_{N-j}^L - \triangle c_{N-j+1}^L)}{(1+\triangle c_{N-j+1}^L)(1+\triangle c_{N-j}^L)}\big(\frac{R_{N-j}}{R_N}\big)}, \tag{3.103}$$

where $\triangle c_i^L = \frac{nk_0}{k_i - k_0}$, and $\frac{R_i}{R_N} = \big(\theta_1 + \sum_{j=2}^{i-1}(\theta_j + \theta_0^j)\big)^{\frac{1}{n}}$. The effective conductivity given by (3.103) attains the lower HS bound $\triangle c_e^L = \triangle c_{HS}^L$, if the volume fractions are satisfied in the

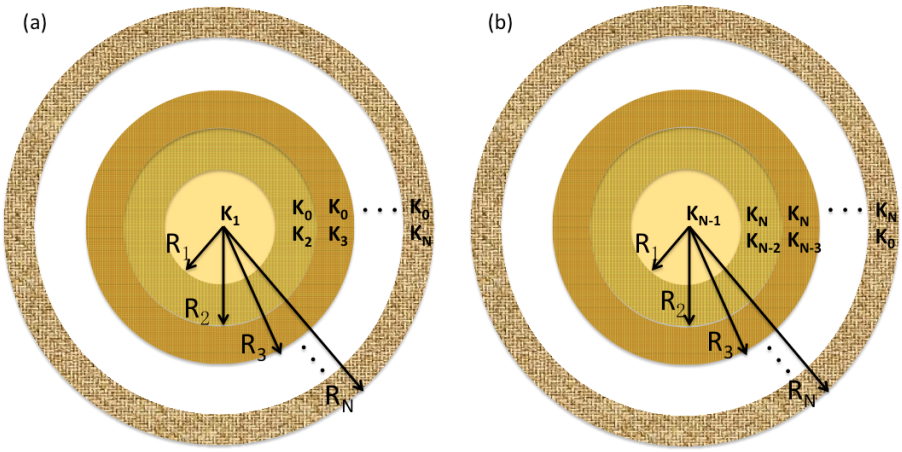

Figure 3.4: (a)The microstructure of a N-phase coated sphere to attain lower HS bounds: the core sphere is occupied by phase-1; the external coating is occupied by two-phase periodic E-inclusion: the matrix occupied by the 0-phase and the inclusion occupied by i-phase($i = 2,3,...,N$) in ascending order. (b)The microstructure of a N-phase coated sphere to attain upper HS bounds: the core sphere is occupied by phase-$N-1$; the external coating is occupied by two-phase periodic E-inclusion: the matrix occupied by the N-phase and the inclusion occupied by i-phase($i = N-2, N-3, ..., 1, 0$) in descending order.

following form

$$\begin{cases} \theta_i = (\frac{R_i}{R_N})^n - (\frac{R_{i-1}}{R_N})^n - \sum_{j=1}^{i-1} \frac{(1+\triangle c_N^L)(\triangle c_{N-j}^L - \triangle c_{N-j+1}^L)}{(1+\triangle c_{N-j+1}^L)(1+\triangle c_{N-j}^L)} (\frac{R_{i-j}}{R_N})((\frac{R_i}{R_N})^{n-1} - (\frac{R_{i-1}}{R_N})^{n-1}), \\ \theta_1 = (\frac{R_1}{R_N})^n, \\ \theta_0^i = (\frac{R_i}{R_N})^n - (\frac{R_{i-1}}{R_N})^n - \theta_i \qquad\qquad i = 2,...,N. \end{cases} \tag{3.104}$$

The above equation (3.104) is a sufficient condition for the lower HS bounds to be attainable.

For the N-phase coated spheres attaining upper HS bounds, The microstructure is constructed as shown in Fig 3.4(b). The effective conductivity is given by

$$\triangle c_e^U := \frac{\triangle c_0^U + \sum_{j=1}^{N-1} \frac{(1+\triangle c_0^U)(\triangle c_j^U - \triangle c_{j-1}^U)}{(1+\triangle c_{j-1}^U)(1+\triangle c_j^U)} (\frac{R_{N-j}}{R_N})}{1 - \sum_{j=1}^{N-1} \frac{(1+\triangle c_0^U)(\triangle c_j^U - \triangle c_{j-1}^U)}{(1+\triangle c_{j-1}^U)(1+\triangle c_j^U)} (\frac{R_{N-j}}{R_N})}, \tag{3.105}$$

where $\triangle c_i^U = \frac{nk_N}{k_i - k_N}$, and $\frac{R_i}{R_N} = \left(\theta_{N-1} + \sum_{j=N-i}^{N-2} (\theta_j + \theta_N^j)\right)^{\frac{1}{n}}$. The effective conductivity given by (3.105) attains the upper HS bound $\triangle c_e^U = \triangle c_{HS}^U$, if the volume fractions are satisfied in

the following form

$$\begin{cases} \theta_i = (\frac{R_{N-i}}{R_N})^n - (\frac{R_{N-i-1}}{R_N})^n - \sum\limits_{j=1}^{N-i-1} \frac{(1+\triangle c_0^U)(\triangle c_j^U - \triangle c_{j-1}^U)}{(1+\triangle c_{j-1}^U)(1+\triangle c_j^U)} (\frac{R_{N-i-j}}{R_N})((\frac{R_{N-i}}{R_N})^{n-1} - (\frac{R_{N-i-1}}{R_N})^{n-1}), \\ \theta_{N-1} = (\frac{R_1}{R_N})^n, \\ \theta_N^i = (\frac{R_{N-i}}{R_N})^n - (\frac{R_{N-i-1}}{R_N})^n - \theta_i \qquad\qquad i = N-2, ..., 1, 0. \end{cases} \tag{3.106}$$

The above equation (3.106) is a sufficient condition for the upper HS bounds to be attainable.

3.5 Attainment of the Hashin-Shtrikman bounds

In this section, we construct a new optimal microstructures of multiphase composites to derive the sufficient condition of Hashin-Shtrikman bounds attainment. The building blocks of our new optimal microstructures consist of three-phase coated spheres and two-phase periodic E-inclusions [60]. Assuming the bound is optimal by setting $\triangle c_e = \triangle c_{HS}$ in each constituent part, we systematically derive the sufficient condition for the attainability of HS bounds in the constraint of volume fractions of the constituent phases. Specified to four-phase cases, we compare the new optimal microstructures with four-phase coated sphere.

3.5.1 Brief description of the optimal microstructures

We summarize the properties of optimal three-phase coated sphere of the first type. By straightforward algebraic calculations, we verify that the effective conductivity given by (3.40) attains the HS lower bounds if $k_\gamma > k_\alpha$ and the HS upper bounds if $k_\gamma < k_\alpha$, i.e. $\triangle c_e = \triangle c_{\mathrm{HS}}$, the function $\triangle c_e(\theta_\beta; \triangle c_\beta, \triangle c_\gamma)$ is given by (3.40) as

$$\triangle c_e(\theta_\beta; \triangle c_\beta, \triangle c_\gamma) := \frac{\triangle c_\gamma + \theta_\beta^{1/n}[\frac{\triangle c_\beta - \triangle c_\gamma}{1+\triangle c_\beta}]}{1 - \theta_\beta^{1/n}[\frac{\triangle c_\beta - \triangle c_\gamma}{1+\triangle c_\beta}]}. \tag{3.107}$$

For future convenience, we notice that if $k_\gamma > k_\alpha$, the function $\theta_\beta \mapsto \triangle c_e(\theta_\beta; \triangle c_\beta, \triangle c_\gamma)$ given by (3.107) increases strictly from $\triangle c_\gamma$ to $\triangle c_\beta$ when θ_β increases from 0 to 1; if

$k_\gamma < k_\alpha$, $\theta_\beta \mapsto \triangle c_e(\theta_\beta; \triangle c_\beta, \triangle c_\gamma)$ decreases strictly from $\triangle c_\gamma$ to $\triangle c_\beta$ when θ_β increases from 0 to 1. We write the inverse function as

$$\tilde{\theta}_\beta = \tilde{\theta}_\beta(\triangle c_e; \triangle c_\beta, \triangle c_\gamma) := \left[1 - \frac{(\triangle c_\beta - \triangle c_e)(1+\triangle c_\gamma)}{(1+\triangle c_\beta)(\triangle c_\gamma - \triangle c_e)}\right]^n. \tag{3.108}$$

and, by (3.37), we rewrite the volume fraction of α and γ-phase as

$$\begin{cases} \tilde{\theta}_\alpha(\triangle c_e; \triangle c_\beta, \triangle c_\gamma) := \triangle c_\gamma[\frac{1+1/\triangle c_\gamma}{1+1/\triangle c_\beta} - 1](\tilde{\theta}_\beta^{1/n} - \tilde{\theta}_\beta), \\ \tilde{\theta}_\gamma(\triangle c_e; \triangle c_\beta, \triangle c_\gamma) := 1 - \frac{\triangle c_\beta - \triangle c_\gamma}{1+\triangle c_\beta}\tilde{\theta}_\beta^{1/n} - \frac{1+\triangle c_\gamma}{1+\triangle c_\beta}\tilde{\theta}_\beta. \end{cases} \tag{3.109}$$

Subsequently, for brevity we sometimes write the functions given by (3.107), (3.108), (3.109) simply as $\triangle c_e$, $\tilde{\theta}_\beta$, $\tilde{\theta}_\alpha$, $\tilde{\theta}_\gamma$ if the omissions do not cause confusion. Next we summarize the properties of a two-phase conductive composite with microstructure being periodic E-inclusions with symmetric matrix $\mathbf{Q}$. The theory of (periodic) E-inclusions has been developed in [61]. Note that the symmetric matrix $\mathbf{Q}$ is positive semi-definite with $\mathrm{Tr}(\mathbf{Q}) = 1$. To avoid confusion, we denote by k_a (k_b) the conductivity of the matrix phase (the inclusion phase), and by θ_a, θ_b their corresponding volume fractions. Consider the conductivity problem for an average applied field $\mathbf{F} \in \mathbb{R}^{n\times n}$,

$$\begin{cases} \mathrm{div}[(k_a(1-\chi_E) + k_b\chi_E)(\nabla \mathbf{w} + \mathbf{F})] = 0 & \text{on } Y, \\ \text{periodic boundary conditions} & \text{on } \partial Y, \end{cases}$$

where Y is the unit cell of the periodicity, e.g., $(0,1)^n$, χ_E is the characteristic function of the periodic E-inclusion in the unit cell Y, and $\mathbf{w} : Y \to \mathbb{R}^n$ are the electric potentials. Then the field on the periodic E-inclusion is uniform and given by

$$\nabla \mathbf{w} + \mathbf{F} = [\mathbf{I} - (\mathbf{I} + \frac{\triangle c_b}{(1-\theta_b)n}\mathbf{Q}^{-1})^{-1}]\mathbf{F}, \tag{3.110}$$

and the effective conductivity tensor is given by

$$\mathbf{A}^e/k_a = \mathbf{I} + \frac{n\theta_b}{\triangle c_b}\mathbf{I} - \theta_a\theta_b\mathbf{Q}[\frac{\theta_a \triangle c_b}{n}\mathbf{Q} + \frac{\triangle c_b^2}{n^2}\mathbf{I}]^{-1}. \tag{3.111}$$

In particular, if $\mathbf{Q} = \mathbf{I}/n$, $\mathbf{A}^e = k^e\mathbf{I}$, we have

$$k^e = k_a(1 + \frac{n}{\triangle c_e}), \;\; \triangle c_e = \triangle c_{\mathrm{HS}} = \frac{1 - \theta_b + \triangle c_b}{\theta_b}. \tag{3.112}$$

Noticing if $k_a < k_b$, the function $\theta_b \mapsto \triangle c_e = \frac{1-\theta_b+\triangle c_b}{\theta_b}$ decreases from $+\infty$ to $\triangle c_b$ as θ_b increases from 0 to 1; if $k_a > k_b$, $\theta_b \mapsto \triangle c_e = \frac{1-\theta_b+\triangle c_b}{\theta_b}$ increases from $-\infty$ to $\triangle c_b$ as θ_b increases from 0 to 1, we write the inverse function as

$$\tilde{\theta}_b = \tilde{\theta}_b(\triangle c_e; \triangle c_b) = \frac{1+\triangle c_b}{1+\triangle c_e}. \tag{3.113}$$

3.5.2 Attainment of the lower Hashin-Shtrikman bounds

We propose an optimal microstructure attaining the lower HS bounds for (N +1)-phase composites by combining three-phase coated spheres and two-phase E-inclusion. By (3.3), we observe that $0 < \triangle c_N^L < \triangle c_{HS}^L < \triangle c_0^L$, that is, $\triangle c_{HS}^L \in [\triangle c_{m+1}^L, \triangle c_m^L)$ for some $m \in \{N-1, ..., 1, 0\}$, $(\triangle c_m^L = +\infty$ if $m = 0)$ and $\triangle c_{HS}^L = \frac{1}{\Gamma^L} - 1$ with $\Gamma^L = \sum_{i=0}^{N} \frac{\theta_i}{1+\triangle c_i^L}$, thus we have

$$\frac{1}{1+\triangle c_m^L} < \Gamma^L \leq \frac{1}{1+\triangle c_{m+1}^L}. \tag{3.114}$$

The optimal (N +1)-phase composites is constructed by N-parts: (0, i , N)-phase coated spheres and (0, j)-phase periodic E-inclusion, the volume fraction of each part is denoted by θ_k'(k =1, ..., N) with $\theta_k' > 0$. To attain the lower HS bounds, it is required that $\triangle c_e^L \leq \triangle c_{HS}^L$ for each part of the composite. For (0, i, N)-phase coated sphere, by (3.107) we have $\triangle c_e^L \in (\triangle c_N^L, \triangle c_i^L)$. To guarantee $\triangle c_e^L \leq \triangle c_{HS}^L \in [\triangle c_{m+1}^L, \triangle c_m^L)$, the i-phase can only be chosen between $(1, ..., m)$-phase as shown in Fig. 3.5 *i*th-part. Again for (0, j)-phase E-inclusion, by (3.112) we have $\triangle c_e^L > \triangle c_j^L$. To guarantee $\triangle c_e^L \leq \triangle c_{HS}^L \in [\triangle c_{m+1}^L, \triangle c_m^L)$, the j-phase can only be chosen between $(m+1, ..., N)$-phase as shown in Fig. 3.5 *j*th-part. Therefore, we construct the microstructure as shown in Fig. 3.5, the ith-part(i =1, ..., m) consists of the three-phase coated spheres with the core occupied by i-th phase and the external coating occupied by 0 and N-phase(0-phase as matrix and N-phase as inclusions); the jth-part(j = m+1, ..., N) consists of two-phase E-inclusion with the matrix occupied by 0 phase and the inclusion occupied by j-th phase. For the overall composite, we know the volume fraction of each material phase as $\theta_i (i = 0, 1, ..., N)$. By (3.108), we can get

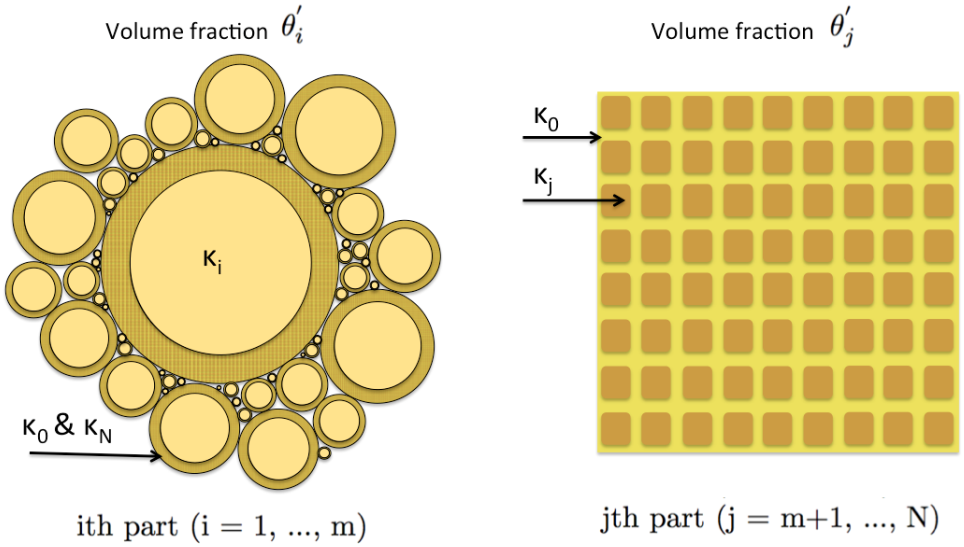

Figure 3.5: The optimal microstructure of the overall composites: the ith-part($i = 1,...,m$) consists of the(0, i , N)-phase coated spheres; the jth-part($j = m+1,...,N$) consists of 0, j-phases periodic E-inclusion with the shape matrix $\mathbf{Q} = \mathbf{I}/n$. The volume fraction of each part of the composite is denoted by θ_k'(k =1, ..., N) with $\theta_k' > 0$ and the total volume fraction of the composite is $\sum_{k=1}^{N} \theta_k' = 1$.

the volume fraction of i-phase($i = 1,...,m$) in terms of $(0,i,N)$-phase coated sphere by replacing β with i, γ with N, and replacing $\triangle c_e^L$ with $\triangle c_{HS}^L$

$$\theta_i^{\beta} = [\frac{1-(1+\triangle c_N^L)\sum_{i=0}^{N}\frac{\theta_i}{1+\triangle c_i^L}}{\frac{\triangle c_i^L - \triangle c_N^L}{1+\triangle c_i^L}}]^n \qquad i = 1,...,m. \tag{3.115}$$

By (3.109) and (3.115), we can get the volume fraction of N-phase in terms of $(0,i,N)$-phase coated sphere by replacing γ with N, θ_β with θ_i^{β}, and $\triangle c_e^L$ with $\triangle c_{HS}^L$ as

$$\theta_i^{\gamma} = (1+\triangle c_N^L)\sum_{i=0}^{N}\frac{\theta_i}{1+\triangle c_i^L} - \frac{1+\triangle c_N^L}{1+\triangle c_i^L}\theta_i^{\beta} \qquad i = 1,...,m. \tag{3.116}$$

By (3.113) we can get the volume fraction of j-phase($j = m+1,...,N$) in terms of $(0,j)$-phase E-inclusion by replacing b with j and $\triangle c_e^L$ with $\triangle c_{HS}^L$ as

$$\theta_j^b = (1+\triangle c_j^L)\sum_{i=0}^{N}\frac{\theta_i}{1+\triangle c_i^L} \qquad j = m+1,...,N. \tag{3.117}$$

Further, we have the volume fraction of each part θ_k' $(k = 1, ..., N)$ of the composite by

$$\begin{aligned}
\theta_i^{'} &= \frac{\theta_i}{\theta_i^{\beta}} && \text{if } i = 1, ..., m, \\
\theta_j^{'} &= \frac{\theta_j}{\theta_j^{b}} && \text{if } j = m+1, ..., N-1, \\
\theta_N^{'} &= \frac{1}{\theta_N^{b}}[\theta_N - \sum_{i=1}^{m} \theta_i^{\gamma}\theta_i^{'}],
\end{aligned} \tag{3.118}$$

where $\theta_i^{'}$(i = 1, ..., m) is the volume fraction of (0, i, N)-phase coated sphere, $\theta_j^{'}$(j = m+1, ..., N-1) is the volume fraction of (0, j)-phase E-inclusion, and $\theta_N^{'}$ is the volume fraction of (0, N)-phase E-inclusion. We know the total volume fraction of the composite $\sum_{k=1}^{N} \theta_k^{'} = 1$ with $\theta_k' \geq 0$(k =1, ..., N). Specified by $\triangle c_e^L = \triangle c_{HS}^L$, the conductivity of the constructed composite achieves the lower HS bounds since each part is optimal. Inserting (3.115), (3.116), and (3.117) into (3.118), by direct calculations we obtain that

$$\sum_{k=1}^{N} \theta_k^{'} = \sum_{j=m+1}^{N-1} \frac{\theta_j}{\theta_j^{b}} + \frac{1}{\theta_N^{b}}[\theta_N + \sum_{i=1}^{m} \frac{\theta_i}{\theta_i^{\beta}}(\theta_N^{b} - \theta_i^{\gamma})] = 1.$$

with $\theta_k' \geq 0 \; \forall \; k = 1, ..., N$, We have $\theta_N' = 1 - \theta_1' - \theta_2' - ... - \theta_{N-1}' \geq 0$, which gives rise to the following equation

$$\begin{aligned}
&[\theta_0 + \sum_{i=1}^{N-1} \theta_i \frac{\triangle c_i^L - \triangle c_N^L}{1 + \triangle c_i^L}]^{-n} \sum_{i=1}^{m} \theta_i [\frac{\triangle c_i^L - \triangle c_N^L}{1 + \triangle c_i^L}]^{n} + \\
&[\sum_{i=1}^{N} \frac{\theta_i}{1 + \triangle c_i^L}]^{-1} \sum_{j=m+1}^{N-1} \frac{\theta_j}{1 + \triangle c_j^L} \leq 1.
\end{aligned} \tag{3.119}$$

which, together with (3.114), forms a sufficient condition such that the lower HS bounds $\triangle c_e^L \leq \triangle c_{HS}^L$ is attainable (by the constructed composite). The necessary condition (3.10) and the sufficient condition (3.114), (3.119) are explicit in terms of conductivities and volume fractions of the constituent phases. We remark that (3.119) is trivially satisfied if $m = 0$, the lower HS bounds is attainable when $\triangle c_{HS}^L \geq \triangle c_1^L$, which consists with result shown in [72, 64]. For three-phase composites(N = 2), we find the necessary condition (3.10) guarantees (3.114), (3.119) for some $m \in \{N-1, ..., 0\}$, and hence is sufficient as well. For $N > 2$, the attainability of the lower HS bounds can be easily studied for specified conductivities and volume fractions in three dimensions. In particular, for four-phase

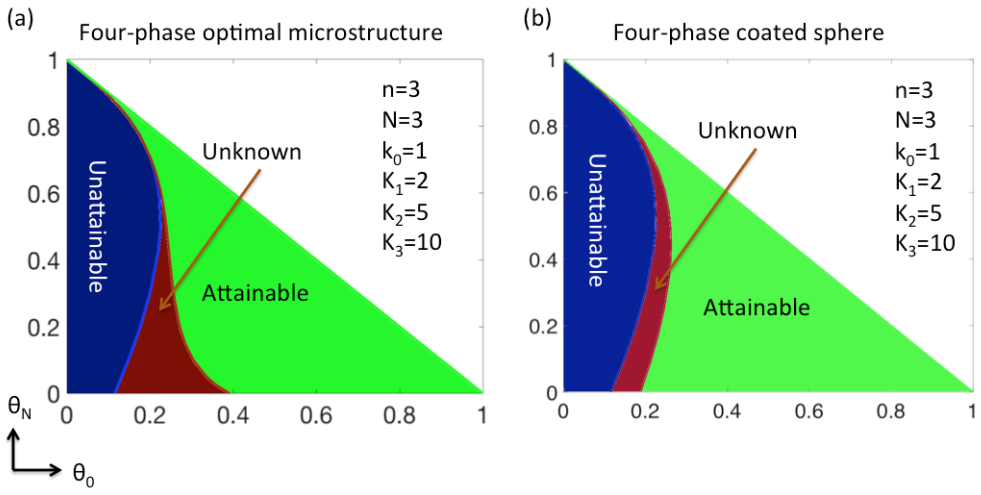

Figure 3.6: The attainability of lower HS bounds for four-phase composite in three dimensions in terms of θ_0 and θ_N(assuming the intermediate phases have equal volume fraction): (a) Four-phase optimal microstructure constructed by three-phase coated sphere and two-phase E-inclusion, material properties given on the top-right of the panel. The region necessary condition violated is labeled as Unattainable, sufficient condition satisfied is labeled as Attainable, and the gap between the necessary and sufficient condition is labeled as Unknown. (b) Four-phase coated sphere with material properties given on the top-right of the panel. The region necessary condition violated is labeled as Unattainable, sufficient condition satisfied is labeled as Attainable, and the gap between the necessary and sufficient condition is labeled as Unknown.

composites (N = 3), we present the sufficient condition of the lower HS bounds attainability of the four-phase optimal microstructure in Fig. 3.6(a), and further compare with the sufficient condition of four-phase coated sphere in Fig. 3.6(b). We assign specific conductivities k_0, k_1, k_2, k_3 and corresponding volume fractions $\theta_0, \theta_1, \theta_2, \theta_3$ (with equal volume fraction of intermediate phases i.e. $\theta_1 = \theta_2$). Varying (θ_0, θ_3), we have the region of attainability of the lower HS bounds. In Fig. 3.6(a), the region where the necessary condition (3.10) violated implies that the lower HS bound is unattainable and is labeled as "Unattainable", while the region where the sufficient condition (3.114) and (3.119) satisfied for some $m \in \{0, ..., N-1\}$ means that the lower HS bounds is attainable and is labeled as "Attainable". The attainability of the lower HS bounds is unknown for the remaining region, labeled as "Unknown". In Fig. 3.6 (b), The region where the necessary condition (3.10) violated implies that the lower HS bound is unattainable and is labeled as "Unattainable",

while the region where the sufficient condition (3.75) satisfied means that the lower HS bound is attainable and is labeled as "Attainable". The attainability of the lower HS bound is unknown for the remaining region, labeled as "Unknown". Compare the two figures we observe that when $\theta_3 \in (0.45, 1)$, The four-phase optimal microstructure have more attainable region, whereas when $\theta_3 \in (0, 0.45)$, the four-phase coated sphere have more attainable region.

3.5.3 Attainment of the upper Hashin-Shtrikman bounds

We propose an optimal microstructure attaining the upper HS bounds for (N +1)-phase composites by combining three-phase coated spheres with two-phase E-inclusions. By (3.3), we observe that $\triangle c_N^U < \triangle c_{HS}^U < \triangle c_0^U < 0$, that is, $\triangle c_{HS}^U \in (\triangle c_{m+1}^U, \triangle c_m^U]$ for some $m \in \{N-1, ..., 1, 0\}$, ($\triangle c_{m+1}^U = -\infty$ if $m = N-1$) and $\triangle c_{HS}^U = \frac{1}{\Gamma^U} - 1$ with $\Gamma^U = \sum_{i=0}^{N} \frac{\theta_i}{1+\triangle c_i^U}$, thus we have

$$\frac{1}{1+\triangle c_m^U} \leq \Gamma^U < \frac{1}{1+\triangle c_{m+1}^U}. \tag{3.120}$$

The optimal (N +1)-phase composite is constructed by N-parts: (N, i , 0)-phase coated spheres and (N, j)-phase E-inclusions, the volume fraction of each part is denoted by θ_k'(k =0, ..., N-1) with $\theta_k' > 0$. To attain the upper HS bounds, it is required that $\triangle c_e^U \leq \triangle c_{HS}^U$ for each part of the composite. For (N, i, 0)-phase coated spheres, by (3.107) we have $\triangle c_e^U \in (\triangle c_i^U, \triangle c_0^U)$. To guarantee $\triangle c_e^U \leq \triangle c_{HS}^U \in [\triangle c_{m+1}^U, \triangle c_m^U)$, the i-phase can only be chosen between $(m+1, ..., N-1)$-phase as shown in Fig. 3.7 *i*th-part. Again for (N, j)-phase E-inclusion, by (3.112) we have $\triangle c_e^U < \triangle c_j^U$. To guarantee $\triangle c_e^U \leq \triangle c_{HS}^U \in [\triangle c_{m+1}^U, \triangle c_m^U)$, the j-phase can only be chosen between $(0, ..., m)$-phase as shown in Fig. 3.7 *j*th-part. Therefore, we construct the microstructure as shown in Fig. 3.7, the ith-part(i =m+1, ..., N-1) consists of the three-phase coated spheres with the core occupied by i-th phase and the external coating occupied by N and 0-phase(N-phase as matrix and 0-phase as inclusions); the jth-part(j = 0, 1, ..., m) consists of two-phase E-inclusion with the matrix occupied by N-phase and the inclusions occupied by j-th phase. For the overall composite, we know

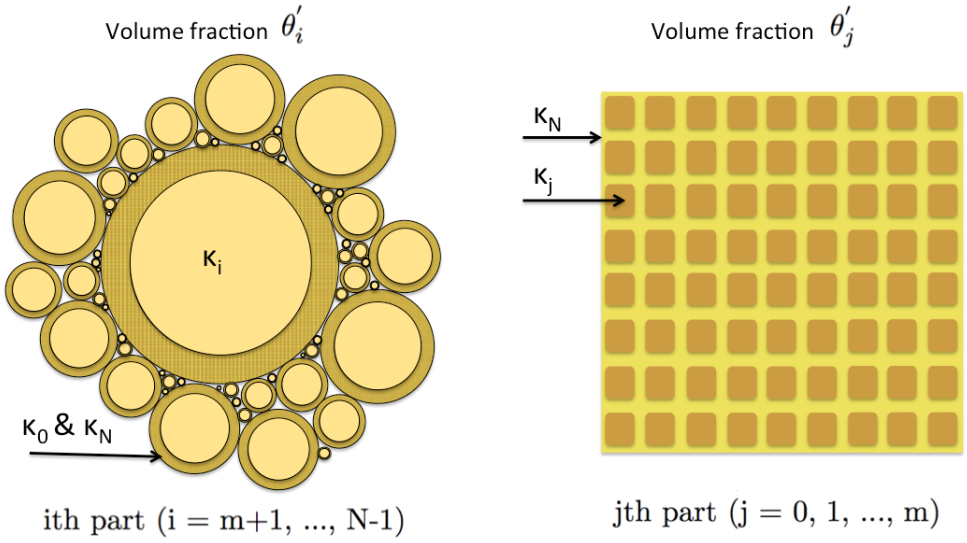

Figure 3.7: The microstructure of the overall composite: the ith-part(i =m+1, ..., N-1) consists of (N, i, 0)-phases coated spheres ; the jth-part(j = 0, 1, ..., m) consists of (N, j)-phases periodic E-inclusion with the shape matrix $\mathbf{Q} = \mathbf{I}/n$. The volume fraction of the each constituent part is denoted by θ_k'(k =0, ..., N-1) with $\theta_k' > 0$ and $\sum_{k=0}^{N-1} \theta_k' = 1$.

the volume fraction of each material phase as $\theta_i (i = 0, 1, ..., N)$. By (3.108), we can get the volume fraction of i-phase$(i = m+1, ..., N-1)$ in terms of $(N, i, 0)$-phases coated sphere by replacing β with i, γ with 0, and replacing $\triangle c_e^U$ with $\triangle c_{HS}^U$

$$\theta_i^\beta = [\frac{1 - (1 + \triangle c_0^U) \sum_{i=0}^{N} \frac{\theta_i}{1+\triangle c_i^U}}{\frac{\triangle c_i^U - \triangle c_0^U}{1+\triangle c_i^U}}]^n \qquad i = m+1, ..., N-1. \tag{3.121}$$

By (3.109) and (3.121), we can get the volume fraction of 0-phase in terms of $(N, i, 0)$-phases coated sphere by replacing γ with 0, θ_β with θ_i^β, and $\triangle c_e^U$ with $\triangle c_{HS}^U$ as

$$\theta_i^\gamma = (1 + \triangle c_0^U) \sum_{i=0}^{N} \frac{\theta_i}{1+\triangle c_i^U} - \frac{1+\triangle c_0^U}{1+\triangle c_i^U} \theta_i^\beta \qquad i = m+1, ..., N-1. \tag{3.122}$$

By (3.113) we can get the volume fraction of j-phase$(j = 0, ..., m)$ in terms of (N, j)-phase E-inclusion by replacing b with j and $\triangle c_e^U$ with $\triangle c_{HS}^U$ as

$$\theta_j^b = (1 + \triangle c_j^U) \sum_{i=0}^{N} \frac{\theta_i}{1 + \triangle c_i^U} \qquad j = 0, ..., m. \tag{3.123}$$

Further, we have the volume fraction of each part θ_k' $(k = 0, ..., N-1)$ by

$$\begin{aligned} \theta_i' &= \frac{\theta_i}{\theta_i^\beta} && \text{if } i = m+1, ..., N-1, \\ \theta_j' &= \frac{\theta_j}{\theta_j^b} && \text{if } j = 1, ..., m, \\ \theta_0' &= \frac{1}{\theta_0^b}[\theta_0 - \sum_{i=1}^{m} \theta_i^\gamma \theta_i'], \end{aligned} \tag{3.124}$$

where θ_i'(i = m+1, ..., N-1) is the volume fraction of (N, i, 0)-phase coated sphere, θ_j'(j = 1, ..., m) is the volume fraction of (N, j)-phase E-inclusion, and θ_0' is the volume fraction of (N, 0)-phase E-inclusion. We know the total volume fraction of the composite $\sum_{k=1}^{N} \theta_k' = 1$ with $\theta_k' \geq 0 (k = 0, ..., N-1)$. Specified by $\triangle c_e^U = \triangle c_{HS}^U$, the conductivity of the constructed composite achieves the upper HS bound since each part is optimal. Inserting (3.121), (3.122), and (3.123) into (3.124), by direct calculations we obtain that

$$\sum_{i=0}^{N-1} \theta_i' = \sum_{j=1}^{m} \frac{\theta_j}{\theta_j^b} + \frac{1}{\theta_0^b}[\theta_0 + \sum_{i=m+1}^{N-1} \frac{\theta_i}{\theta_i^\beta}(\theta_0^b - \theta_i^\gamma)] = 1.$$

with $\theta_i' \geq 0 \; \forall \; i = 0, ..., N-1$, We have $\theta_0' = 1 - \theta_1' - \theta_2' - ... - \theta_{N-1}' \geq 0$, which gives rise to

$$\begin{aligned} &[\theta_N + \sum_{i=1}^{N-1} \theta_i \frac{\triangle c_i^U - \triangle c_0^U}{1 + \triangle c_i^U}]^{-n} \sum_{i=m+1}^{N-1} \theta_i [\frac{\triangle c_i^U - \triangle c_0^U}{1 + \triangle c_i^U}]^n + \\ &[\sum_{i=0}^{N-1} \frac{\theta_i}{1 + \triangle c_i^U}]^{-1} \sum_{j=1}^{m} \frac{\theta_j}{1 + \triangle c_j^U} \leq 1. \end{aligned} \tag{3.125}$$

which, together with (3.120), forms a sufficient condition such that upper HS bounds $\triangle c_e^U = \triangle c_{HS}^U$ is attainable (by the constructed composite). The necessary condition (3.14) and the sufficient condition (3.120), (3.125) are explicit in terms of conductivities and volume fractions of the constituent phases. We remark that (3.125) is trivially satisfied if $m = N-1$, the upper HS bounds is attainable when $\triangle c_{HS}^U \leq \triangle c_{N-1}^U$, which consists with result shown in [72, 64]. For three-phase composites (N = 2), we find the necessary condition (3.14) guarantees (3.120), (3.125) for some $m \in \{N-1, ..., 0\}$, and hence is sufficient as well. In particular, for four-phase composites (N = 3), we present the sufficient condition of the upper HS bounds attainability of four-phase optimal microstructure in Fig. 3.8(a), and

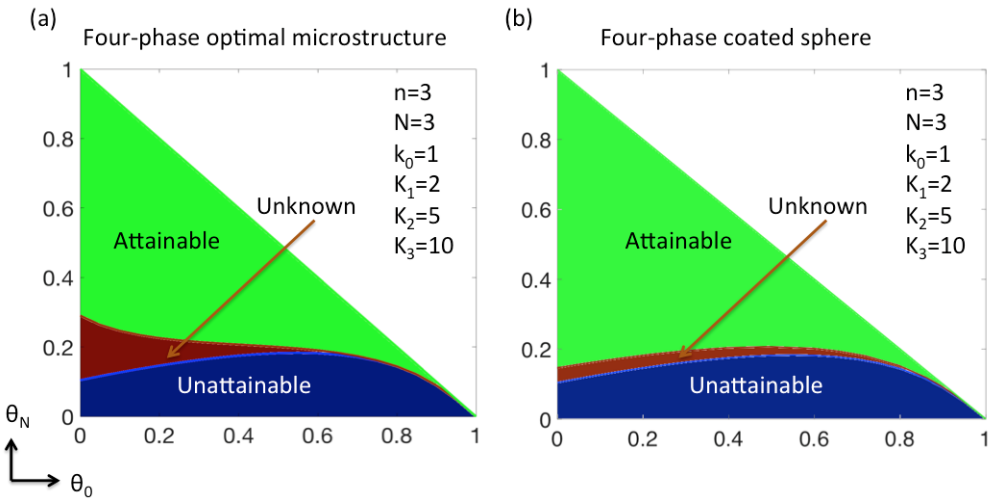

Figure 3.8: The attainability of upper HS bounds for four-phase composites in three dimensions in terms of θ_0 and θ_N (assuming the intermediate phases have the same volume fraction): (a) Four-phase optimal microstructure constructed by three-phase coated spheres and two-phase E-inclusions, material properties given on the top-right of the panel. The region necessary condition violated is labeled as Unattainable, sufficient condition satisfied is labeled as Attainable, and the gap between the necessary and sufficient condition is labeled as Unknown. (b) Four-phase coated sphere with material properties given on the top-right of the panel. The region necessary condition violated is labeled as Unattainable, sufficient condition satisfied is labeled as Attainable, and the gap between the necessary and sufficient condition is labeled as Unknown.

further compare with the sufficient condition of four-phase coated sphere in Fig. 3.8(b). We assign specific conductivities k_0, k_1, k_2, k_3 and corresponding volume fractions $\theta_0, \theta_1, \theta_2, \theta_3$ (with equal volume fraction of intermediate phases i.e. $\theta_1 = \theta_2$). Varying (θ_0, θ_3), we get the region of attainability of the upper HS bounds. In Fig. 3.8(a), the region where the necessary condition (3.14) violated implies that the upper HS bounds is unattainable and is labeled as "Unattainable", while the region where the sufficient condition (3.120) and (3.125) satisfied for some $m \in \{0, ..., N-1\}$ means that the upper HS bounds is attainable and is labeled as "Attainable". The attainability of the upper HS bounds is unknown for the remaining region, labeled as "Unknown". In Fig. 3.8(b), the region where the necessary condition (3.14) violated implies that the upper HS bounds is unattainable and is labeled as "Unattainable", while the region where the sufficient condition (3.102) satisfied means that the upper HS bounds is attainable and is labeled as "Attainable". The attainability of the

upper HS bounds is unknown for the remaining region, labeled as "Unknown". Compare the two figures we observe that when $\theta_0 \in (0.42, 1)$, The four-phase optimal microstructure have more attainable region, whereas when $\theta_0 \in (0, 0.42)$, the four-phase coated sphere have more attainable region.

3.6 The G_Θ-closure of multiphase conductive composites

Followed by attainment condition of both lower and upper HS bounds, we summarize the G_Θ-closure of multiphase conductive composites. G-closure is a set of tensors, which characterize the effective properties of composite material. Specifically, G_Θ-closure problems are those placing a constraint on the volume fraction Θ to find optimal design of composite. Lurie et al. solved the G-closure problem for two isotropic components using translation method by finite rank laminates [63, 70]. Grabovsky extended the G-closure problem for mixtures of two well-ordered possibly anisotropic conductors [32]. Further, Milton and Cherkaev demonstrated the whole G-closure with infinitely rigid and infinitely soft constituents [71]. In this section, we focus on the G-closure of multiphase conductive composites. We demonstrate the necessary condition for the lower HS bounds by (3.10) as

$$\left[\theta_0 + \sum_{i=1}^{N-1} \theta_i \frac{\triangle c_i^L - \triangle c_N^L}{1 + \triangle c_i^L}\right]^{-n} \sum_{i=1}^{N-1} \theta_i \left[\frac{\triangle c_i^L - \triangle c_N^L}{1 + \triangle c_i^L}\right]^n \leq 1. \tag{3.126}$$

and also the sufficient condition for the lower bounds by constructing optimal composite combining three-phase coated spheres and two-phase E-inclusions, by (3.114) and (3.119) we have the sufficient condition given by

$$\frac{1}{1 + \triangle c_m^L} < \Gamma^L \leq \frac{1}{1 + \triangle c_{m+1}^L}, \qquad \Gamma^L = \sum_{i=0}^{N} \frac{\theta_i}{1 + \triangle c_i^L}, \tag{3.127}$$

$$\begin{aligned} &[\theta_0 + \sum_{i=1}^{N-1} \theta_i \frac{\triangle c_i^L - \triangle c_N^L}{1 + \triangle c_i^L}]^{-n} \sum_{i=1}^{m} \theta_i [\frac{\triangle c_i^L - \triangle c_N^L}{1 + \triangle c_i^L}]^n + \\ &[\sum_{i=1}^{N} \frac{\theta_i}{1 + \triangle c_i^L}]^{-1} \sum_{j=m+1}^{N-1} \frac{\theta_j}{1 + \triangle c_j^L} \leq 1. \end{aligned} \tag{3.128}$$

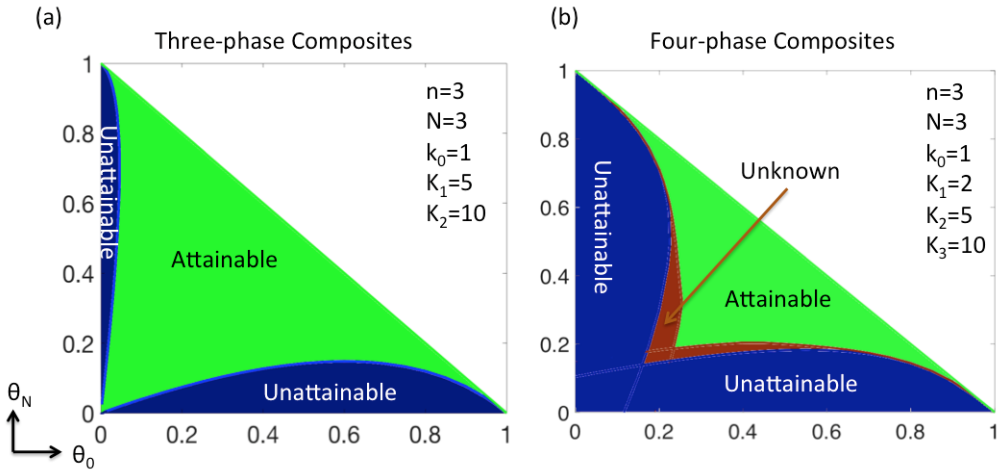

Figure 3.9: The G_Θ-closure in three dimensions in terms of θ_0 and θ_N (the intermediate phases have the same volume fraction): (a) Three-phase composites with material properties given on the top-right of the panel, the G_Θ-closure is presented in the green region labeled as "Attainable", where the sufficient condition(necessary condition) for attainability of HS bounds are satisfied. (b) Four-phase composites with material properties given on the top-right of the panel, the G_Θ-closure is presented in the green region labeled as "Attainable", where the sufficient condition for attainability of HS bounds are satisfied.

In particular, we present four-phase coated sphere as an alternative four -phase optimal microstructure to attain the lower HS bounds. The sufficient condition of lower HS bounds attainment is given by (3.75), that is

$$\begin{cases} \theta_1 = (\frac{R_1}{R_3})^n, \\ \theta_2 = \big((\frac{R_2}{R_3})^n - (\frac{R_1}{R_3})^n\big) - \frac{\triangle c_1^L - \triangle c_2^L}{1+\triangle c_1^L}\big(\frac{R_1}{R_3}(\frac{R_2}{R_3})^{n-1} - (\frac{R_1}{R_3})^n\big), \\ \theta_0^2 = \frac{\triangle c_1^L - \triangle c_2^L}{1+\triangle c_1^L}\big(\frac{R_1}{R_3}(\frac{R_2}{R_3})^{n-1} - (\frac{R_1}{R_3})^n\big), \\ \theta_3 = \big(1 - (\frac{R_2}{R_3})^n\big) - \frac{\triangle c_2^L - \triangle c_3^L}{1+\triangle c_2^L}\big(\frac{R_2}{R_3} - (\frac{R_2}{R_3})^n\big) - \frac{(1+\triangle c_3^L)(\triangle c_1^L - \triangle c_2^L)}{(1+\triangle c_2^L)(1+\triangle c_1^L)}\big(\frac{R_1}{R_3} - \frac{R_1}{R_3}(\frac{R_2}{R_3})^{n-1}\big), \\ \theta_0^3 = \frac{\triangle c_2^L - \triangle c_3^L}{1+\triangle c_2^L}\big(\frac{R_2}{R_3} - (\frac{R_2}{R_3})^n\big) + \frac{(1+\triangle c_3^L)(\triangle c_1^L - \triangle c_2^L)}{(1+\triangle c_2^L)(1+\triangle c_1^L)}\big(\frac{R_1}{R_3} - \frac{R_1}{R_3}(\frac{R_2}{R_3})^{n-1}\big). \end{cases} \tag{3.129}$$

where the total volume fraction of 0-phase is given by $\theta_0 = \theta_0^2 + \theta_0^3$.

Further, we demonstrate the necessary condition for the upper HS bounds by (3.14) as

$$\left[\theta_N + \sum_{i=0}^{N-1} \theta_i \frac{\triangle c_i^U - \triangle c_0^U}{1+\triangle c_i^U}\right]^{-n} \sum_{i=0}^{N-1} \theta_i \left[\frac{\triangle c_i^U - \triangle c_0^U}{1+\triangle c_i^U}\right]^n \leq 1. \tag{3.130}$$

and also the sufficient condition for the upper bounds by constructing optimal composite combining three-phase coated spheres and two-phase E-inclusions by (3.120) and (3.125)

we have the sufficient condition given by

$$\frac{1}{1+\triangle c_m^U} \leq \Gamma^U < \frac{1}{1+\triangle c_{m+1}^U}, \qquad \Gamma^U = \sum_{i=0}^{N} \frac{\theta_i}{1+\triangle c_i^U}, \tag{3.131}$$

$$\begin{aligned} &[\theta_N + \sum_{i=1}^{N-1} \theta_i \frac{\triangle c_i^U - \triangle c_0^U}{1+\triangle c_i^U}]^{-n} \sum_{i=m+1}^{N-1} \theta_i [\frac{\triangle c_i^U - \triangle c_0^U}{1+\triangle c_i^U}]^n + \\ &[\sum_{i=0}^{N-1} \frac{\theta_i}{1+\triangle c_i^U}]^{-1} \sum_{j=1}^{m} \frac{\theta_j}{1+\triangle c_j^U} \leq 1. \end{aligned} \tag{3.132}$$

In particular, we present four-phase coated sphere as an alternative four -phase optimal microstructure to attain the upper HS bounds. The sufficient condition of upper HS bounds attainment is given by (3.102) , that is

$$\begin{cases} \theta_2 = (\frac{R_1}{R_3})^n, \\ \theta_1 = \big((\frac{R_2}{R_3})^n - (\frac{R_1}{R_3})^n\big) - \frac{\triangle c_2^U - \triangle c_1^U}{1+\triangle c_2^U}\big(\frac{R_1}{R_3}(\frac{R_2}{R_3})^{n-1} - (\frac{R_1}{R_3})^n\big), \\ \theta_3^1 = \frac{\triangle c_2^U - \triangle c_1^U}{1+\triangle c_2^U}\big(\frac{R_1}{R_3}(\frac{R_2}{R_3})^{n-1} - (\frac{R_1}{R_3})^n\big), \\ \theta_0 = \big(1 - (\frac{R_2}{R_3})^n\big) + \frac{\triangle c_0^U - \triangle c_1^U}{1+\triangle c_1^U}\big(\frac{R_2}{R_3} - (\frac{R_2}{R_3})^n\big) - \frac{(1+\triangle c_0^U)(\triangle c_2^U - \triangle c_1^U)}{(1+\triangle c_1^U)(1+\triangle c_2^U)}\big(\frac{R_1}{R_3} - \frac{R_1}{R_3}(\frac{R_2}{R_3})^{n-1}\big), \\ \theta_3^0 = -\frac{\triangle c_0^U - \triangle c_1^U}{1+\triangle c_1^U}\big(\frac{R_2}{R_3} - (\frac{R_2}{R_3})^n\big) + \frac{(1+\triangle c_0^U)(\triangle c_2^U - \triangle c_1^U)}{(1+\triangle c_1^U)(1+\triangle c_2^U)}\big(\frac{R_1}{R_3} - \frac{R_1}{R_3}(\frac{R_2}{R_3})^{n-1}\big). \end{cases} \tag{3.133}$$

where the total volume fraction of 3-phase is given by $\theta_3 = \theta_3^1 + \theta_3^0$. Combining the necessary and sufficient attainment conditions of the lower and upper HS bound in terms of θ, we get the G_Θ-closure of multiphase conductive composites. As shown in Fig. 3.9, we present G_Θ-closure of three-phase and four-phase conductive composites in terms of θ_0, θ_N. For three-phase conductive composites, The G_Θ-closure is presented in the green region labeled as "Attainable", which is satisfied by the sufficient condition of new optimal microstructure (3.127),(3.128),(3.131),(3.132), and the necessary condition guarantees the sufficient condition in this region; For the four-phase conductive composites, The G_Θ-closure is presented in the green region labeled as "Attainable", which is satisfied by the sufficient condition of new optimal microstructure (3.127),(3.128),(3.131),(3.132) and the four-phase coated sphere (3.129)(3.133). there is an unknown region presented in brown region, where we expect to construct more optimal microstructures to further expand the G_Θ-closure.

3.7 Summary and discussion

We have achieved the set of optimal effective properties of multiphase composites by HS bounds, and we have established the HS bounds attainability of multiphase composites by the necessary conditions and sufficient conditions in the constraint of volume fractions of the constituent phases. By constructing a new three-phase coated sphere and four-phase coated sphere, we demonstrate that optimal conductivity is attainable and generalize the coated sphere to a larger phase. Further, we propose new optimal microstructures comprised of three-phase coated spheres and two-phase E-inclusions, and systematically derive the sufficient condition for the attainability of HS bounds in terms of conductivities and volume fractions of the constituent phases. For three-phase composites, the necessary condition guarantees the sufficient condition; whereas, for four-phase composite, there is a gap between sufficient condition and necessary condition when θ_N is small, we apply both four-phase coated sphere and four-phase optimal microstructure to minimize the gap. Combining the necessary and sufficient condition of HS bounds attainability, we can precisely characterize the G-closure and describe effective properties of multiphase conductive materials for a broader range, which are anticipated to have applications in actuators, phase transitions, smart materials, and graded materials. Finally, the G-closure can be generalized to other problems such as bulk modulus to of elastic material and permittivity of dielectric materials.

Chapter 4

Phase transitions of 3D printed artificial shape memory crystals

4.1 Introduction

A lattice structure consisting of repeating structure elements, as called unit cells, can be tessellated along any axis with no gaps between cells [40]. The versatility of additive manufacturing allows for the fabrication of more creative and complicate lattice structures [88, 21, 43, 44, 10, 65, 106], which can be applied to mimic some unique properties observed in shape memory alloys. Shape memory alloys (SMAs) are a group of metallic alloys that can recover to their original shape when subjected to a stimulus such as thermomechanical or magnetic variations. The transformation phenomenon between austenite (one homogeneous phase) and martensite (other phases) is known as the shape memory effect [99, 15, 83, 84], which makes SMAs have applications in numerous commercial fields [73], such as in structures and composites [29], automotive and aerospace [98, 35, 14], microactuators and robotics [53, 97], and biomedical [67, 74]. As shown in the aforementioned works, most applications are limited to NiTi-based SMAs. However, NiTi-based SMAs have two major limitations: high materials cost and the narrow temperature range. Though the cost of iron-based and copper-based SMAs are low, their applications are limited due to instability, impracticability, and poor thermo-mechanic performance. Therefore, it is important to stabilize and improve the shape-memory effect in known materials and develop new materials.

To understand the phase transformation process between austenite and martensite and shape memory effect, James theoretically approached these fine phase mixtures based on

free energy minimization. The energetic interpretation of these configurations (phases) was in terms of minimizing sequences rather than minimizers. By studying the minimizers and minimizing sequences, they predicted that the microstructure is both a twinned martensite interface and an austenite/finely twinned martensite interface [48, 49]. According to the energy minimization, Bhattacharya further illustrated that when the lattice parameters satisfying some significant restrictions, energy minimization with many variants (phases) naturally results in the microstructure. For polycrystals, the greater the change in symmetry during transformation, the greater the recoverable strain, their study suggested that the microstructure and macroscopic properties depended very delicately on the lattice parameters [13, 12]. Remarkable progress in mathematically understanding the relationship between the microstructure formation and lattice parameters of SMAs boosts the design of new materials, advances in the understanding of the relation between microscopic and macroscopic deformation also play a key role [50]. However, designing such new material is challenging because compatibility conditions must be considered when multi phases coexist at martensite.

To mimic the shape memory effect, we propose a two-dimensional (2D) lattice with simple stress-induced phase transitions [103, 96]. Based on a one-dimensional (1D) elastic bar model, we investigate the free energy density before and after buckling by free energy minimization and extend to a two-dimensional lattice structure under compressive load. The microstructure of the lattice structure may easily buckle by design, while the macrostructure of the lattice structure is in compression. The structural behavior of the entire lattice structure can be represented by the unit cell when a set of periodic boundary conditions is applied. By the Cauchy-Born rule, we adopt the continuum model of the 2D unit cell and assume that the bulk-free energy density depends on the local change in shape measured by the deformation gradient. Minimizing the total free energy based on the geometrically linear theory, we get four distinct stable configurations corresponding to four stable phases, the transitions between these phases of the unit cell are regarded as phase transformations of the lattice structure. Applying the Hadamard compatibility condition,

we found that when the lattice satisfies significant restrictions on the parameters, the microstructure forms as the lattice tends to keep in the bottom of the energy wells. Further, we conduct numerical simulation to validate theoretical predictions. we observe the buckling phenomenon of the 1D beam and 2D unit cell, and extend the analysis to 50 by 50 lattice structures.

The paper is organized as follows. First, in Section 4.2.1 we present the general scheme of deriving the free energy density before and after buckling of the 1D elastic bar. In Section 4.2.2 we extend to a 2D unit cell model with general deformation gradients and get four distinct stable configurations. We discuss the compatibility condition of the borderline where multi phases coexist and discuss the microstructure formed by two different types of load. In section 4.3 we study the buckling phenomenon of unit cell and lattice structure under biaxial loading numerically and compare the results with theoretical predictions. Finally, we summarize and present an outlook of possible applications in Section 4.4.

4.2 Material models

4.2.1 1D elastic bar deformation

In this section, we construct a one-dimensional (1D) elastic bar model to investigate free energy density under compression, and we obtain free energy density before and after buckling by the minimization of the total free energy. Let u be the displacement and $\varepsilon = u_{,x}$ be the strain. Under the application of an external force (or stress) σ^e [25], the total free energy of the system is identified as

$$F_{tot}(u) = \int_0^1 [W(u_{,x}) - \sigma^e u_{,x}]dx, \tag{4.1}$$

where $W(\varepsilon)$ is the free energy density of the elastic bar placed in the soft loading device, that is, one end of the elastic bar is firmly fixed, the other end subjects to a given dead load, and the boundary condition is $u(0) = u'(0) = u'(L) = 0$ and $u(L)$ is determined by external force σ^e. For a stress-induced phase transition model in the elastic bar, we describe the

free energy density in the following form

$$W(\varepsilon) = \min\{W_1(\varepsilon), W_2(\varepsilon)\}, \qquad \begin{cases} W_1(\varepsilon) = \frac{1}{2}E_1\varepsilon^2 & \text{in compression,} \\ W_2(\varepsilon) = \frac{1}{2}E_2\varepsilon^2 + c_1 & \text{in buckling,} \end{cases} \tag{4.2}$$

where E_1, E_2 are Young's modulus with $E_2 < E_1$, and c_1 is a constant value to be determined. The free energy density of the two states are equal at the critical strain, and the critical strain is derived as $\varepsilon_{cr} = -\frac{1}{\gamma+1}$ with dimensionless parameter $\gamma = \frac{AL^2}{8\pi^2 I}$ by (4.60) (see Section 4.5 for detailed calculations). Combining the above free energy density equations (4.2), we can express c_1 in terms of E_1, E_2 as

$$c_1 = \frac{1}{2}(E_1 - E_2)(\frac{1}{\gamma+1})^2. \tag{4.3}$$

According to the energy criterion, the equilibrium configurations satisfy the Euler-Lagrange equations $\frac{\partial W}{\partial \varepsilon} = \sigma^e$, we describe the minimum total free energy in the following form

$$F_{tot}^{min}(\varepsilon) = \begin{cases} -\frac{(\sigma^e)^2}{2E_1} & \text{if } \sigma^e > \sigma_{cr}, \\ -\frac{(\sigma^e)^2}{2E_1} = -\frac{(\sigma^e)^2}{2E_2} + \frac{1}{2}(E_1 - E_2)(\frac{1}{\gamma+1})^2 & \text{if } \sigma^e = \sigma_{cr}, \\ -\frac{(\sigma^e)^2}{2E_2} + \frac{1}{2}(E_1 - E_2)(\frac{1}{\gamma+1})^2 & \text{if } \sigma^e < \sigma_{cr}, \end{cases} \tag{4.4}$$

where $\sigma_{cr} = \frac{E_1}{2\gamma}$ is the critical stress, which has been calculated by (4.49). Inserting the critical stress into above equation, we get E_2 in terms of E_1 as

$$E_2 = \frac{(\gamma+1)^2}{4\gamma^2}E_1. \tag{4.5}$$

Inserting (4.3) and (4.5) back to (4.2), we have the free energy density of 1D elastic bar as

$$W(\varepsilon) = \begin{cases} W_1(\varepsilon) = \frac{1}{2}E_1\varepsilon^2 & \text{if } \varepsilon > \varepsilon_{cr}, \\ W_2(\varepsilon) = \frac{(\gamma+1)^2}{8\gamma^2}E_1\varepsilon^2 + E_1(\frac{1}{2(\gamma+1)^2} - \frac{1}{8\gamma^2}) & \text{if } \varepsilon \le \varepsilon_{cr}, \end{cases} \tag{4.6}$$

where the critical strain $\varepsilon_{cr} = -\frac{1}{\gamma+1}$ with $\gamma = \frac{AL^2}{8\pi^2 I}$. We remark that since the system is under compressive load, both the external load and the strain are negative values. Therefore, when $\varepsilon > \varepsilon_{cr}$ the system is in compression and when $\varepsilon \le \varepsilon_{cr}$ the system is in buckling, and this clarification applies to all the following sections.

4.2.2 2D lattice with general deformation gradient

2D unit cell model

In this section, we construct a two-dimensional (2D) unit cell under the compressive load to investigate the stress-induced phase transitions. A lattice structure consists of repeating unit cells, when a set of periodic boundary conditions is applied to the representative unit cell, its response represents the structural behavior of the entire lattice structure. Therefore, based on the selection of the smallest repeatable unit of the geometry, we generalize the unit cell to the generic of the lattice structure. The undeformed unit cell is constructed as shown in Fig. 4.1(a) in e_a-e_b coordinate, the unit cell consist of four frame beams and two diagonal beams with one diagonal beam along e_a direction and the other one along e_b direction. Applying load $\mathbf{P}$ in the following form

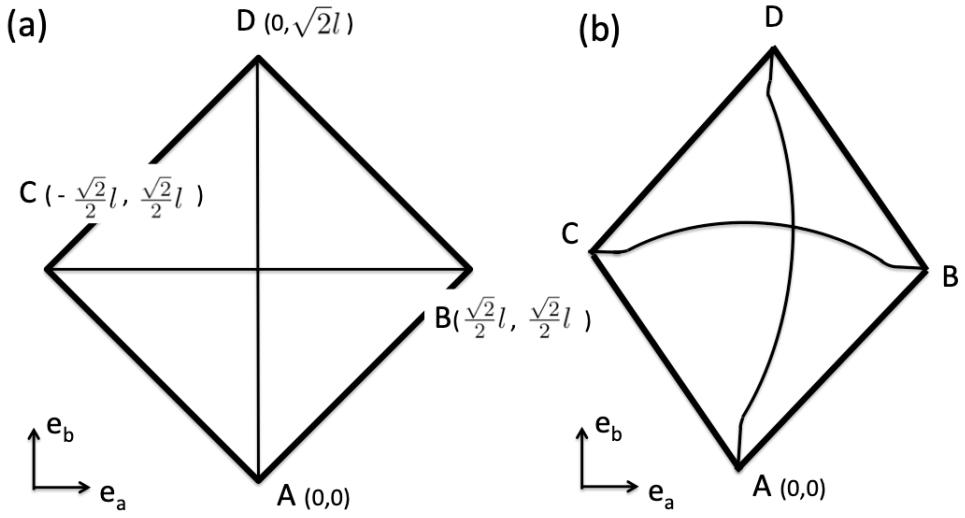

Figure 4.1: Unit cell in e_a-e_b coordinate (a) undeformed (b) deformed

$$\mathbf{P} = \begin{bmatrix} P_{aa} & P_{ab} \\ P_{ab} & P_{bb} \end{bmatrix}, \tag{4.7}$$

the unit cell deforms as illustrated in Fig. 4.1(b). The configuration of the deformed unit cell can be described by a deformation gradient $\mathbf{F} \in \mathbb{R}^{2\times 2}$ relative to the reference square. In other words, corresponding to the deformation gradient $\mathbf{F}$, the vertices of the unit cell is

given by

$$\mathbf{y} = \mathbf{F}\mathbf{x}, \qquad \mathbf{x} \in \mathscr{V}_0, \tag{4.8}$$

where $\mathscr{V}_0 = \{(x,y) : x,y \in \{0, \pm\frac{\sqrt{2}}{2}l, \sqrt{2}l\}\}$ denotes the set of vertices of the square of side length l. In this study, we adopt a geometric linear theory [11], which uses transformation strains instead of transformation matrices to characterize different configurations. Therefore, for prescribed vertices positions of the deformed unit cell, we can describe the deformation gradient $\mathbf{F}$ as

$$\mathbf{F} = \mathbf{I} + \mathbf{E} = \begin{bmatrix} 1+\varepsilon_{aa} & \varepsilon_{ab} \\ \varepsilon_{ab} & 1+\varepsilon_{bb} \end{bmatrix}, \tag{4.9}$$

where the Green-Lagrange Strain $\mathbf{E}$ is given in the following form

$$\mathbf{E} = \frac{1}{2}(\mathbf{F}^T + \mathbf{F}) - \mathbf{I} = \begin{bmatrix} \varepsilon_{aa} & \varepsilon_{ab} \\ \varepsilon_{ab} & \varepsilon_{bb} \end{bmatrix}. \tag{4.10}$$

The strain of the deformed diagonal beams are given by (4.10), and we get the linearized strain of the deformed frame beams along $\mathbf{e}_1$ and $\mathbf{e}_2$ direction as ε_{11}, ε_{22}, respectively,

$$\begin{cases} \varepsilon_{11} = \mathbf{e}_1 \cdot \mathbf{E}\mathbf{e}_1 = \frac{1}{2}(\varepsilon_{aa} - 2\varepsilon_{ab} + \varepsilon_{bb}), \\ \varepsilon_{22} = \mathbf{e}_2 \cdot \mathbf{E}\mathbf{e}_2 = \frac{1}{2}(\varepsilon_{aa} + 2\varepsilon_{ab} + \varepsilon_{bb}), \end{cases} \tag{4.11}$$

where $\mathbf{e}_1 = [\frac{\sqrt{2}}{2}, \frac{\sqrt{2}}{2}]^T$, $\mathbf{e}_2 = [-\frac{\sqrt{2}}{2}, \frac{\sqrt{2}}{2}]^T$ are unit vector in 45° and 135°, respectively.
Recall that the free energy density of 1D elastic bar has already been demonstrated by (4.6), by integrating along the whole beam, we get elastic energy of a beam in the following form

$$W(\varepsilon) = \begin{cases} W_1(\varepsilon) = \frac{1}{2}E_1AL\varepsilon^2 & \text{if } \varepsilon > \varepsilon_{cr}, \\ W_2(\varepsilon) = \frac{(\gamma+1)^2}{8\gamma^2}E_1AL\varepsilon^2 + E_1AL(\frac{1}{2(\gamma+1)^2} - \frac{1}{8\gamma^2}) & \text{if } \varepsilon \le \varepsilon_{cr}, \end{cases} \tag{4.12}$$

where E_1 is the Yong's Modulus and A, L is the cross section area and length of the beam, respectively, and $\varepsilon_{cr} = -\frac{1}{1+\gamma}$ is the critical strain with $\gamma = \frac{AL^2}{8\pi^2 I}$. When $\varepsilon > \varepsilon_{cr}$, the beam is in compression and the elastic energy is given by $W_1(\varepsilon)$; when $\varepsilon < \varepsilon_{cr}$, the beam is buckled

and the elastic energy is given by $W_2(\varepsilon)$. We design the 2D unit cell as follows, the four frame beams are strong enough when the load is applied, they are only in compression with the deformation strains given by (4.11). While the two diagonal beams may easily buckle with the deformation strains given by (4.10). Consequently, the total elastic energy may have four distinct cases: the first case is both diagonal beams in compression; the second case is the only diagonal beam in $\mathbf{e_a}$ direction buckled; the third case is the only diagonal beam in $\mathbf{e_b}$ direction buckled; the fourth case is both diagonal beams buckled. Therefore, we describe the total elastic energy of the 2D unit cell by the summation of four frame beams and two diagonal beams as

$$
\begin{aligned}
W^*(\mathbf{E}) &= \sum_{i=1}^{6} W^i(\mathbf{E}) \\
&= \begin{cases}
E_1A_1L_1\left(\frac{1}{4}(\varepsilon_{aa}-2\varepsilon_{ab}+\varepsilon_{bb})^2+\frac{1}{4}(\varepsilon_{aa}+2\varepsilon_{ab}+\varepsilon_{bb})^2\right) & \\
+\frac{1}{2}E_1A_2L_2\varepsilon_{aa}^2+\frac{1}{2}E_1A_2L_2\varepsilon_{bb}^2 & \text{if } \varepsilon_{aa}>\varepsilon_{cr}, \varepsilon_{bb}>\varepsilon_{cr}, \\
E_1A_1L_1\left(\frac{1}{4}(\varepsilon_{aa}-2\varepsilon_{ab}+\varepsilon_{bb})^2+\frac{1}{4}(\varepsilon_{aa}+2\varepsilon_{ab}+\varepsilon_{bb})^2\right) & \\
+\frac{(\gamma_2+1)^2}{8\gamma_2^2}E_1A_2L_2\varepsilon_{aa}^2+\frac{1}{2}E_1A_2L_2\zeta+\frac{1}{2}E_1A_2L_2\varepsilon_{bb}^2 & \text{if } \varepsilon_{aa}\le\varepsilon_{cr}, \varepsilon_{bb}>\varepsilon_{cr}, \\
E_1A_1L_1\left(\frac{1}{4}(\varepsilon_{aa}-2\varepsilon_{ab}+\varepsilon_{bb})^2+\frac{1}{4}(\varepsilon_{aa}+2\varepsilon_{ab}+\varepsilon_{bb})^2\right) & \\
+\frac{1}{2}E_1A_2L_2\varepsilon_{aa}^2+\frac{(\gamma_2+1)^2}{8\gamma_2^2}E_1A_2L_2\varepsilon_{bb}^2+\frac{1}{2}E_1A_2L_2\zeta & \text{if } \varepsilon_{aa}>\varepsilon_{cr}, \varepsilon_{bb}\le\varepsilon_{cr}, \\
E_1A_1L_1\left(\frac{1}{4}(\varepsilon_{aa}-2\varepsilon_{ab}+\varepsilon_{bb})^2+\frac{1}{4}(\varepsilon_{aa}+2\varepsilon_{ab}+\varepsilon_{bb})^2\right) & \\
+\frac{(\gamma_2+1)^2}{8\gamma_2^2}E_1A_2L_2\varepsilon_{aa}^2+\frac{(\gamma_2+1)^2}{8\gamma_2^2}E_1A_2L_2\varepsilon_{bb}^2+E_1A_2L_2\zeta & \text{if } \varepsilon_{aa}<\varepsilon_{cr}, \varepsilon_{bb}<\varepsilon_{cr},
\end{cases}
\end{aligned}
\tag{4.13}
$$

where A_1, A_2 are the cross section of the frame beams and diagonal beams respectively, and L_1, L_2 are the length of frame beams and diagonal beams respectively, I_2 is the Area Moment of Inertia of diagonal beam, and dimensionless parameter $\gamma_2 = \frac{A_2L_2^2}{8\pi^2I_2}$ and $\zeta = (\frac{1}{(\gamma_2+1)^2}-\frac{1}{4\gamma_2^2})$. Further we introduce a new dimensionless parameter $\eta = \frac{A_1L_1}{A_2L_2}$, and rewrite

the above equation in vector form, we have

$$W^*(\mathbf{E}) = \begin{cases} \frac{1}{2}E_1A_2L_2\hat{\phi}\cdot\mathbf{K}_I\hat{\phi} & \text{if } \varepsilon_{aa} > \varepsilon_{cr}, \varepsilon_{bb} > \varepsilon_{cr}, \\ \frac{1}{2}E_1A_2L_2\hat{\phi}\cdot\mathbf{K}_{II}\hat{\phi} + \frac{1}{2}E_1A_2L_2\zeta & \text{if } \varepsilon_{aa} \leq \varepsilon_{cr}, \varepsilon_{bb} > \varepsilon_{cr}, \\ \frac{1}{2}E_1A_2L_2\hat{\phi}\cdot\mathbf{K}_{III}\hat{\phi} + \frac{1}{2}E_1A_2L_2\zeta & \text{if } \varepsilon_{aa} > \varepsilon_{cr}, \varepsilon_{bb} \leq \varepsilon_{cr}, \\ \frac{1}{2}E_1A_2L_2\hat{\phi}\cdot\mathbf{K}_{IV}\hat{\phi} + E_1A_2L_2\zeta & \text{if } \varepsilon_{aa} < \varepsilon_{cr}, \varepsilon_{bb} < \varepsilon_{cr}, \end{cases} \tag{4.14}$$

where we introduce a strain vector $\hat{\phi}$ as

$$\hat{\phi} = \begin{bmatrix} \varepsilon_{aa} \\ \varepsilon_{bb} \\ \varepsilon_{ab} \end{bmatrix}, \tag{4.15}$$

and the coefficient matrix of four phases as

$$\begin{aligned} \mathbf{K}_I &= \begin{bmatrix} \eta+1 & \eta & 0 \\ \eta & \eta+1 & 0 \\ 0 & 0 & 4\eta \end{bmatrix}, \qquad \mathbf{K}_{II} = \begin{bmatrix} \eta+\frac{(\gamma_2+1)^2}{4\gamma_2^2} & \eta & 0 \\ \eta & \eta+1 & 0 \\ 0 & 0 & 4\eta \end{bmatrix}, \\ \mathbf{K}_{III} &= \begin{bmatrix} \eta+1 & \eta & 0 \\ \eta & \eta+\frac{(\gamma_2+1)^2}{4\gamma_2^2} & 0 \\ 0 & 0 & 4\eta \end{bmatrix}, \quad \mathbf{K}_{IV} = \begin{bmatrix} \eta+\frac{(\gamma_2+1)^2}{4\gamma_2^2} & \eta & 0 \\ \eta & \eta+\frac{(\gamma_2+1)^2}{4\gamma_2^2} & 0 \\ 0 & 0 & 4\eta \end{bmatrix}. \end{aligned} \tag{4.16}$$

We plot the second derivative of total elastic energy of the 2D unit cell with specific values of parameter $\gamma = 380$, $\eta = 7.73$, and the critical strain in percent $\varepsilon_{cr} = -\frac{1}{\gamma+1} = -0.26\%$. From Fig. 4.2 it can be see that the second derivative of total elastic energy are divided into four region: region I is all the beams are in compression with $\varepsilon_{aa} > \varepsilon_{cr}, \varepsilon_{bb} > \varepsilon_{cr}$; region II is the diagonal beam in $\mathbf{e_a}$ direction buckled with $\varepsilon_{aa} \leq \varepsilon_{cr}, \varepsilon_{bb} > \varepsilon_{cr}$; region III is the diagonal beam in $\mathbf{e_b}$ direction buckled with $\varepsilon_{aa} > \varepsilon_{cr}, \varepsilon_{bb} \leq \varepsilon_{cr}$; and region IV is both diagonal beam buckled with $\varepsilon_{aa} < \varepsilon_{cr}, \varepsilon_{bb} < \varepsilon_{cr}$. Given an applied load by (4.7), the corresponding deformation strain and elastic energy are given by (4.10) and (4.14), so we

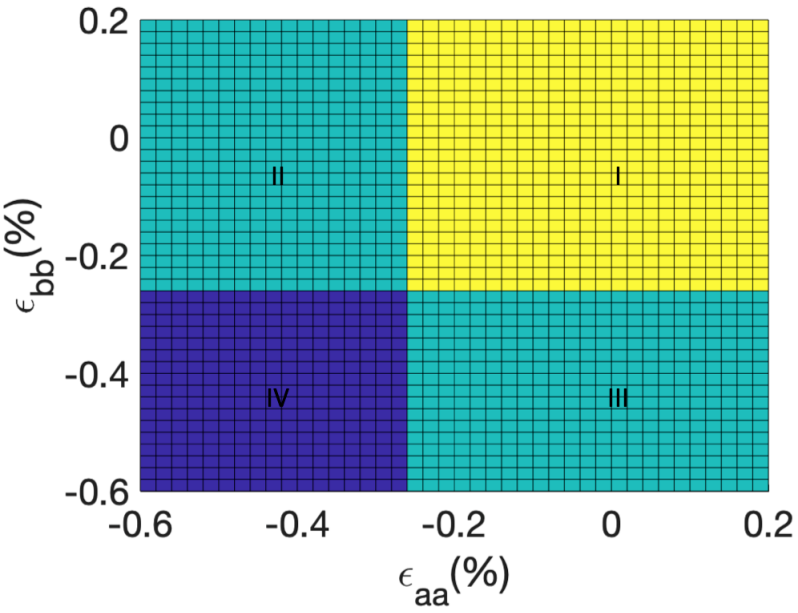

Figure 4.2: The second derivative of total elastic energy of 2D unit cell.

can characterize the total free energy as

$$
\begin{aligned}
F_{tot} &= \sum_{i=1}^{6} W^i(\mathbf{E}) - \int \mathbf{P}\cdot\mathbf{E}dx \\
&= \begin{cases}
E_1A_2L_2\left(\frac{1}{2}\hat{\phi}\cdot\mathbf{K}_I\hat{\phi}\right) - L_2\hat{\phi}\cdot\hat{P} & \text{if } \varepsilon_{aa} > \varepsilon_{cr}, \varepsilon_{bb} > \varepsilon_{cr}, \\
E_1A_2L_2\left(\frac{1}{2}\hat{\phi}\cdot\mathbf{K}_{II}\hat{\phi} + \frac{1}{2}\zeta\right) - L_2\hat{\phi}\cdot\hat{P} & \text{if } \varepsilon_{aa} \le \varepsilon_{cr}, \varepsilon_{bb} > \varepsilon_{cr}, \\
E_1A_2L_2\left(\frac{1}{2}\hat{\phi}\cdot\mathbf{K}_{III}\hat{\phi} + \frac{1}{2}\zeta\right) - L_2\hat{\phi}\cdot\hat{P} & \text{if } \varepsilon_{aa} > \varepsilon_{cr}, \varepsilon_{bb} \le \varepsilon_{cr}, \\
E_1A_2L_2\left(\frac{1}{2}\hat{\phi}\cdot\mathbf{K}_{IV}\hat{\phi} + \zeta\right) - L_2\hat{\phi}\cdot\hat{P} & \text{if } \varepsilon_{aa} < \varepsilon_{cr}, \varepsilon_{bb} < \varepsilon_{cr},
\end{cases}
\end{aligned}
\tag{4.17}
$$

where we introduce a vector form of load as

$$
\hat{P} = \begin{bmatrix} P_{aa} \\ P_{bb} \\ 2P_{ab} \end{bmatrix}.
$$

Assuming that the unit cell will occupy the state that minimizes the total energy, by the principle of minimum free energy, the equilibrium configuration is given by

$$
\frac{\partial F_{tot}}{\partial \hat{\phi}} = 0,
$$

which gives us

$$\begin{cases} \mathbf{K}_I\hat{\phi} = \frac{\hat{P}}{E_1A_2} & \text{if } \varepsilon_{aa} > \varepsilon_{cr}, \varepsilon_{bb} > \varepsilon_{cr}, \\ \mathbf{K}_{II}\hat{\phi} = \frac{\hat{P}}{E_1A_2} & \text{if } \varepsilon_{aa} \leq \varepsilon_{cr}, \varepsilon_{bb} > \varepsilon_{cr}, \\ \mathbf{K}_{III}\hat{\phi} = \frac{\hat{P}}{E_1A_2} & \text{if } \varepsilon_{aa} > \varepsilon_{cr}, \varepsilon_{bb} \leq \varepsilon_{cr}, \\ \mathbf{K}_{IV}\hat{\phi} = \frac{\hat{P}}{E_1A_2} & \text{if } \varepsilon_{aa} < \varepsilon_{cr}, \varepsilon_{bb} < \varepsilon_{cr}. \end{cases} \tag{4.18}$$

By direct calculation, we can describe the strain vector $\hat{\phi}$ in terms of the load vector $\hat{P}$ as

$$\begin{cases} \hat{\phi} = \mathbf{K}_I^{-1}\frac{\hat{P}}{E_1A_2} & \text{if } \varepsilon_{aa} > \varepsilon_{cr}, \varepsilon_{bb} > \varepsilon_{cr}, \\ \hat{\phi} = \mathbf{K}_{II}^{-1}\frac{\hat{P}}{E_1A_2} & \text{if } \varepsilon_{aa} \leq \varepsilon_{cr}, \varepsilon_{bb} > \varepsilon_{cr}, \\ \hat{\phi} = \mathbf{K}_{III}^{-1}\frac{\hat{P}}{E_1A_2} & \text{if } \varepsilon_{aa} > \varepsilon_{cr}, \varepsilon_{bb} \leq \varepsilon_{cr}, \\ \hat{\phi} = \mathbf{K}_{IV}^{-1}\frac{\hat{P}}{E_1A_2} & \text{if } \varepsilon_{aa} < \varepsilon_{cr}, \varepsilon_{bb} < \varepsilon_{cr}, \end{cases} \tag{4.19}$$

where the inverse of coefficient matrix of four phases $\mathbf{K}_I^{-1}$, $\mathbf{K}_{II}^{-1}$, $\mathbf{K}_{III}^{-1}$ and $\mathbf{K}_{IV}^{-1}$ have the following form,

$$\begin{aligned} \mathbf{K}_I^{-1} &= \begin{bmatrix} a & b & 0 \\ b & a & 0 \\ 0 & 0 & \frac{1}{4\eta} \end{bmatrix} = \begin{bmatrix} \frac{\eta+1}{2\eta+1} & \frac{-\eta}{2\eta+1} & 0 \\ \frac{-\eta}{2\eta+1} & \frac{\eta+1}{2\eta+1} & 0 \\ 0 & 0 & \frac{1}{4\eta} \end{bmatrix}, \\ \mathbf{K}_{II}^{-1} &= \begin{bmatrix} c & d & 0 \\ d & e & 0 \\ 0 & 0 & \frac{1}{4\eta} \end{bmatrix} = \begin{bmatrix} \frac{4\gamma_2^2(\eta+1)}{4\eta\gamma_2^2+(\eta+1)(\gamma_2+1)^2} & \frac{-4\eta\gamma_2^2}{4\eta\gamma_2^2+(\eta+1)(\gamma_2+1)^2} & 0 \\ \frac{-4\eta\gamma_2^2}{4\eta\gamma_2^2+(\eta+1)(\gamma_2+1)^2} & \frac{4\eta\gamma_2^2+(\gamma_2+1)^2}{4\eta\gamma_2^2+(\eta+1)(\gamma_2+1)^2} & 0 \\ 0 & 0 & \frac{1}{4\eta} \end{bmatrix}, \\ \mathbf{K}_{III}^{-1} &= \begin{bmatrix} e & d & 0 \\ d & c & 0 \\ 0 & 0 & \frac{1}{4\eta} \end{bmatrix} = \begin{bmatrix} \frac{4\eta\gamma_2^2+(\gamma_2+1)^2}{4\eta\gamma_2^2+(\eta+1)(\gamma_2+1)^2} & \frac{-4\eta\gamma_2^2}{4\eta\gamma_2^2+(\eta+1)(\gamma_2+1)^2} & 0 \\ \frac{-4\eta\gamma_2^2}{4\eta\gamma_2^2+(\eta+1)(\gamma_2+1)^2} & \frac{4\gamma_2^2(\eta+1)}{4\eta\gamma_2^2+(\eta+1)(\gamma_2+1)^2} & 0 \\ 0 & 0 & \frac{1}{4\eta} \end{bmatrix}, \\ \mathbf{K}_{IV}^{-1} &= \begin{bmatrix} f & g & 0 \\ g & f & 0 \\ 0 & 0 & \frac{1}{4\eta} \end{bmatrix} = \begin{bmatrix} \frac{4\gamma_2^2(4\eta\gamma_2^2+(\gamma_2+1)^2)}{(\gamma_2+1)^2(8\eta\gamma_2^2+(\gamma_2+1)^2)} & \frac{-16\eta\gamma_2^4}{(\gamma_2+1)^2(8\eta\gamma_2^2+(\gamma_2+1)^2)} & 0 \\ \frac{-16\eta\gamma_2^4}{(\gamma_2+1)^2(8\eta\gamma_2^2+(\gamma_2+1)^2)} & \frac{4\gamma_2^2(4\eta\gamma_2^2+(\gamma_2+1)^2)}{(\gamma_2+1)^2(8\eta\gamma_2^2+(\gamma_2+1)^2)} & 0 \\ 0 & 0 & \frac{1}{4\eta} \end{bmatrix}. \end{aligned} \tag{4.20}$$

Here and subsequently, we will apply the parameters a, b, c, d, e to simplify the expression. Inserting (4.19) into (4.17) , we have the minimum total free energy of the 2D unit cell as

$$F_{tot}^{min} = \begin{cases} -\frac{L_2}{2E_1A_2}\hat{P}\cdot\mathbf{K}_I^{-1}\hat{P} & \text{if } \varepsilon_{aa} > \varepsilon_{cr}, \varepsilon_{bb} > \varepsilon_{cr}, \\ -\frac{L_2}{2E_1A_2}\hat{P}\cdot\mathbf{K}_{II}^{-1}\hat{P} + \frac{1}{2}E_1A_2L_2\zeta & \text{if } \varepsilon_{aa} \leq \varepsilon_{cr}, \varepsilon_{bb} > \varepsilon_{cr}, \\ -\frac{L_2}{2E_1A_2}\hat{P}\cdot\mathbf{K}_{III}^{-1}\hat{P} + \frac{1}{2}E_1A_2L_2\zeta & \text{if } \varepsilon_{aa} > \varepsilon_{cr}, \varepsilon_{bb} \leq \varepsilon_{cr}, \\ -\frac{L_2}{2E_1A_2}\hat{P}\cdot\mathbf{K}_{IV}^{-1}\hat{P} + E_1A_2L_2\zeta & \text{if } \varepsilon_{aa} < \varepsilon_{cr}, \varepsilon_{bb} < \varepsilon_{cr}. \end{cases} \tag{4.21}$$

We observe from Fig. 4.3 that in terms of dimensionless form of P_{aa} and P_{bb}, the minimum total free energy has four distinct configurations corresponding to four phases: phase I all the beams in compression (blue region); phase II the diagonal beam in $\mathbf{e_a}$ direction buckled (red region); phase III the diagonal beam in $\mathbf{e_b}$ direction buckled (green region); phase IV both diagonal beams buckled (magenta region). When two-phases (or three-phases) coexist, the overlap region forms a borderline which is illustrated in the dark line, we will discuss in detail the compatibility of the borderline in the following sections.

4.2.3 Compatibility of the borderline

In this section, we will check the compatibility of the borderline where multi-phase coexist based on the continuum theory. We rewrite the minimum total free energy (4.21) into dimensionless form in terms of $\tilde{P} = \frac{\hat{P}}{E_1A_2}$ as

$$\frac{F_{tot}^{min}}{E_1A_2L_2} = \begin{cases} -\frac{1}{2}\tilde{P}\cdot\mathbf{K}_I^{-1}\tilde{P} & \text{if } \varepsilon_{aa} > \varepsilon_{cr}, \varepsilon_{bb} > \varepsilon_{cr}, \\ -\frac{1}{2}\tilde{P}\cdot\mathbf{K}_{II}^{-1}\tilde{P} + \frac{1}{2}\zeta & \text{if } \varepsilon_{aa} \leq \varepsilon_{cr}, \varepsilon_{bb} > \varepsilon_{cr}, \\ -\frac{1}{2}\tilde{P}\cdot\mathbf{K}_{III}^{-1}\tilde{P} + \frac{1}{2}\zeta & \text{if } \varepsilon_{aa} > \varepsilon_{cr}, \varepsilon_{bb} \leq \varepsilon_{cr}, \\ -\frac{1}{2}\tilde{P}\cdot\mathbf{K}_{IV}^{-1}\tilde{P} + \zeta & \text{if } \varepsilon_{aa} < \varepsilon_{cr}, \varepsilon_{bb} < \varepsilon_{cr}. \end{cases} \tag{4.22}$$

where the dimensionless parameter $\zeta = (\frac{1}{(\gamma_2+1)^2} - \frac{1}{4\gamma_2^2})$ as previous definition. Applying load $\tilde{P}$, the corresponding strain matrices of three phases $\mathbf{E}_1$, $\mathbf{E}_2$ and $\mathbf{E}_3$ are given by (4.10)

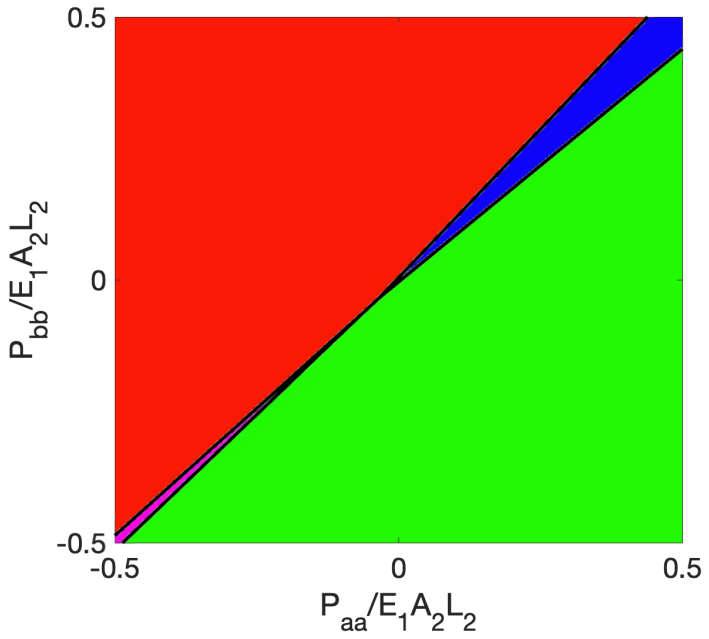

Figure 4.3: Minimum total free energy with specific values of parameter $\gamma = 380$, $\eta = 7.73$. Phase I (Blue region) with $\varepsilon_{aa} > \varepsilon_{cr}, \varepsilon_{bb} > \varepsilon_{cr}$, Phase II (Red region) with $\varepsilon_{aa} \leq \varepsilon_{cr}, \varepsilon_{bb} > \varepsilon_{cr}$, Phase III (Green region) with $\varepsilon_{aa} > \varepsilon_{cr}, \varepsilon_{bb} \leq \varepsilon_{cr}$, Phase IV (Magenta region) with $\varepsilon_{aa} < \varepsilon_{cr}, \varepsilon_{bb} < \varepsilon_{cr}$.

and (4.19) as,

$$\mathbf{E}_1 = \begin{bmatrix} (a+b)\tilde{P}_{aa} & 0 \\ 0 & (b+a)\tilde{P}_{bb} \end{bmatrix}, \tag{4.23}$$

$$\mathbf{E}_2 = \begin{bmatrix} (c+d)\tilde{P}_{aa} & 0 \\ 0 & (d+e)\tilde{P}_{bb} \end{bmatrix}, \tag{4.24}$$

$$\mathbf{E}_3 = \begin{bmatrix} (e+d)\tilde{P}_{aa} & 0 \\ 0 & (c+d)\tilde{P}_{bb} \end{bmatrix}. \tag{4.25}$$

We will discuss the compatibility of borderline by three cases.

Case I: borderline of phase I and phase II coexist

When phase I and phase II coexist, the overlap region forms a borderline. As shown in Fig. 4.3, we find that the borderline is a straight line (black line between blue and red region), which is determined when minimum total free energy of phase I and phase II are

equal, that is

$$-\frac{1}{2}\tilde{P}\cdot\mathbf{K}_I^{-1}\tilde{P}=-\frac{1}{2}\tilde{P}\cdot\mathbf{K}_{II}^{-1}\tilde{P}+\frac{1}{2}\zeta. \tag{4.26}$$

Simplify the above equation, by (4.20) we can get the borderline equation in terms of parameters a,b,c,d,e as

$$\frac{(c-a)}{\zeta}\tilde{P}_{aa}^2+\frac{2(d-b)}{\zeta}\tilde{P}_{aa}\tilde{P}_{bb}+\frac{(e-a)}{\zeta}\tilde{P}_{bb}^2=1 \quad \text{if } \tilde{P}_{aa},\tilde{P}_{bb}>\tilde{P}_{cr}. \tag{4.27}$$

where $\zeta=(\frac{1}{(\gamma_2+1)^2}-\frac{1}{4\gamma_2^2})$, and $\tilde{P}_{cr}$ is the intersection point calculated by setting $\tilde{P}_{aa}=\tilde{P}_{bb}$, that is

$$\tilde{P}_{cr}=-\sqrt{\frac{\zeta}{c+e+2d-2a-2b}}. \tag{4.28}$$

Since the deformation is continuous, the kinematic compatibility condition of two phase for some vectors $\mathbf{a},\hat{\mathbf{n}}$ is given by [48, 49, 12]

$$\mathbf{E}_1-\mathbf{E}_2=\frac{1}{2}(\mathbf{a}\otimes\hat{\mathbf{n}}+\hat{\mathbf{n}}\otimes\mathbf{a}), \tag{4.29}$$

where $\mathbf{E}_1,\mathbf{E}_2$ are strain of phase I and phase II respectively, which is given by (4.23). With straightforward calculation we get

$$\begin{bmatrix}\Delta\varepsilon_{aa} & 0\\ 0 & \Delta\varepsilon_{bb}\end{bmatrix}=\begin{bmatrix}a_1n_1 & \frac{1}{2}(a_1n_2+a_2n_1)\\ \frac{1}{2}(a_1n_2+a_2n_1) & a_2n_2\end{bmatrix},$$

where $\Delta\varepsilon_{aa}=(a+b-c-d)\tilde{P}_{aa}$ and $\Delta\varepsilon_{bb}=(a+b-d-e)\tilde{P}_{bb}$ are the strain difference of phase I and phase II. The above equation give us the compatibility equation as

$$\frac{\Delta\varepsilon_{aa}}{\Delta\varepsilon_{bb}}=-(\frac{n_1}{n_2})^2\le 0,$$

which can be rewritten as

$$\Delta\varepsilon_{aa}\Delta\varepsilon_{bb}\le 0. \tag{4.30}$$

Inserting the specific values of $\Delta\varepsilon_{aa},\Delta\varepsilon_{bb}$ into above equation, we can get the compatibility condition as

$$(a-c)(b-d)\tilde{P}_{aa}^2+\big((b-d)^2+(a-c)(a-e)\big)\tilde{P}_{aa}\tilde{P}_{bb}+(b-d)(a-e)\tilde{P}_{bb}^2\le 0. \tag{4.31}$$

Inserting the borderline equation (4.27) into the compatibility condition (4.31), we find the whole borderline of phase I and phase II coexist is compatible.

Case II: borderline of phase I and phase III coexist

When phase I and phase III coexist, the overlap region forms a borderline. As shown in Fig. 4.3, we find that the borderline is a straight line (black line between blue and green region), which is determined when the minimum total free energy of phase I and phase III are equal, that is

$$-\frac{1}{2}\tilde{P}\cdot\mathbf{K}_I\tilde{P} = -\frac{1}{2}\tilde{P}\cdot\mathbf{K}_{III}\tilde{P} + \frac{1}{2}\zeta. \tag{4.32}$$

Simplify the above equation, by (4.20) we can get the borderline equation in terms of parameters a,b,c,d,e as

$$\frac{(e-a)}{\zeta}\tilde{P}_{aa}^2 + \frac{2(d-b)}{\zeta}\tilde{P}_{aa}\tilde{P}_{bb} + \frac{(c-a)}{\zeta}\tilde{P}_{bb}^2 = 1 \quad \text{if } \tilde{P}_{aa},\tilde{P}_{bb} > \tilde{P}_{cr}. \tag{4.33}$$

where $\zeta = (\frac{1}{(\gamma_2+1)^2} - \frac{1}{4\gamma_2^2})$ and $\tilde{P}_{cr} = -\sqrt{\frac{\zeta}{c+e+2d-2a-2b}}$ by (4.28). Since the deformation is continuous, the kinematic compatibility condition of two phase for some vectors $\mathbf{a},\hat{\mathbf{n}}$ is given by [48, 49, 12]

$$\mathbf{E}_1 - \mathbf{E}_3 = \frac{1}{2}(\mathbf{a}\otimes\hat{\mathbf{n}} + \hat{\mathbf{n}}\otimes\mathbf{a}), \tag{4.34}$$

where $\mathbf{E}_1,\mathbf{E}_3$ are strain of phase I and phase III respectively, which is given by (4.23). With straightforward calculation we get

$$\begin{bmatrix} \Delta\varepsilon_{aa} & 0 \\ 0 & \Delta\varepsilon_{bb} \end{bmatrix} = \begin{bmatrix} a_1n_1 & \frac{1}{2}(a_1n_2+a_2n_1) \\ \frac{1}{2}(a_1n_2+a_2n_1) & a_2n_2 \end{bmatrix},$$

where $\Delta\varepsilon_{aa} = (a+b-d-e)\tilde{P}_{aa}$ and $\Delta\varepsilon_{bb} = (a+b-c-d)\tilde{P}_{bb}$ are the strain difference of phase I and phase III. The above equation give us the compatibility equation as

$$\frac{\Delta\varepsilon_{aa}}{\Delta\varepsilon_{bb}} = -(\frac{n_1}{n_2})^2 \le 0,$$

which can be rewritten as

$$\Delta\varepsilon_{aa}\Delta\varepsilon_{bb} \le 0. \tag{4.35}$$

Inserting the specific values of $\Delta\varepsilon_{aa}$, $\Delta\varepsilon_{bb}$ into above equation, we can get the compatibility condition as

$$(a-e)(b-d)\tilde{P}_{aa}^2+\big((b-d)^2+(a-e)(a-c)\big)\tilde{P}_{aa}\tilde{P}_{bb}+(b-d)(a-c)\tilde{P}_{bb}^2\leq 0. \quad (4.36)$$

Inserting the borderline equation (4.33) into the compatibility condition (4.36), we find the whole borderline of phase I and phase III coexist is compatible.

Case III: borderline of phase II and phase III coexist

When phase II and phase III coexist, the overlap region forms a borderline. As shown in Fig. 4.3, we find that the borderline is a straight line (black line between red and green region). We can express the borderline of phase II and phase III coexist as

$$-\frac{1}{2}\tilde{P}\cdot\mathbf{K}_{II}\tilde{P}+\frac{1}{2}\zeta=-\frac{1}{2}\tilde{P}\cdot\mathbf{K}_{III}\tilde{P}+\frac{1}{2}\zeta. \quad (4.37)$$

Simplify the above equation, by (4.20) we can get the borderline equation in terms of parameters a,b,c,d,e as

$$\tilde{P}_{aa}-\tilde{P}_{bb}=0 \quad \text{if } -\sqrt{\tfrac{\zeta}{2f+2g-c-e-2d}}\leq\tilde{P}_{aa},\tilde{P}_{bb}\leq-\sqrt{\tfrac{\zeta}{c+e+2d-2a-2b}}. \quad (4.38)$$

Since the deformation is continuous, the kinematic compatibility condition of two phase for some vectors $\mathbf{a},\hat{\mathbf{n}}$ is given by [48, 49, 12]

$$\mathbf{E}_2-\mathbf{E}_3=\frac{1}{2}(\mathbf{a}\otimes\hat{\mathbf{n}}+\hat{\mathbf{n}}\otimes\mathbf{a}), \quad (4.39)$$

where $\mathbf{E}_2,\mathbf{E}_3$ are strain of phase II and phase III respectively, which is given by (4.23). With straightforward calculation we get

$$\begin{bmatrix}\Delta\varepsilon_{aa} & 0\\ 0 & \Delta\varepsilon_{bb}\end{bmatrix}=\begin{bmatrix}a_1n_1 & \frac{1}{2}(a_1n_2+a_2n_1)\\ \frac{1}{2}(a_1n_2+a_2n_1) & a_2n_2\end{bmatrix},$$

where $\Delta\varepsilon_{aa}=(c-e)\tilde{P}_{aa}$ and $\Delta\varepsilon_{bb}=(e-c)\tilde{P}_{bb}$ are the strain difference of phase II and phase III. The above equation give us the compatibility equation as

$$\frac{\Delta\varepsilon_{aa}}{\Delta\varepsilon_{bb}}=-(\frac{n_1}{n_2})^2\leq 0,$$

which can be rewritten as

$$\Delta\varepsilon_{aa}\Delta\varepsilon_{bb} = -(c-e)^2\tilde{P}_{aa}\tilde{P}_{bb} \leq 0. \tag{4.40}$$

Inserting (4.38) into (4.40), we get the compatibility condition for phase II and phase III borderline

$$-(c-e)^2\tilde{P}_{aa}^2 \leq 0. \tag{4.41}$$

which means that the whole borderline of phase II and phase III coexist is compatible.

4.2.4 Microstructure formation

From the previous section, we find that the borderline is compatible when multi-phase coexist, minimizing the total free energy based on the geometrically linear theory of the 2D unit cell, we get four distinct stable configurations corresponding to four stable phases, and the transitions between these phases of the 2D unit cell can be regarded as phase transformations of the lattice structure. In the transformation, the corresponding strain is the only input, the microstructure arises as a consequence of energy minimization, which can predict various aspects of microstructure and macrostructure properties of the lattice structure. In this section, we discuss when applying two different loads, what kind of microstructure it will form. The microstructure forms as a consequence of the multi-phase (multi-well) structure of the total free energy minimization. For a unit cell subjected to a boundary condition, it tends to keep at the bottom of the energy wells and satisfy the imposed boundary conditions [11]. If the boundary condition corresponds to one of the energy wells, then the lattice can easily accommodate it. If on the other hand, the applied boundary condition corresponds to multi-energy wells, then the lattice can satisfy boundary condition by making a mixture of different energy wells. However, the mixture cannot be arbitrary due to the requirement of kinematic compatibility or coherent deformation. It is found that fine mixing of the unit cells will greatly enhance the ability of lattice to meet the kinematic compatibility restrictions. Therefore, the lattice structure typically contains microstructure,

and the microstructure is reversible and macroscopically coherent. We will demonstrate the microstructure formation by two cases.

Case I

The first case is when we apply load in the form as

$$\mathbf{P} = \sigma \begin{bmatrix} 1 & 0 \\ 0 & 1 \end{bmatrix},$$

where σ is the stress under compression. Based on continuum theory, the deformation is continuous, so the jump in strain across the surface must be a rank-one matrix, the well-known Hadamard jump condition or compatibility condition ensures that the interface is coherent [11]. Given the applied load, we get the constant strain matrices of three phases $\mathbf{E}_1$, $\mathbf{E}_2$ and $\mathbf{E}_3$ by (4.10) and (4.19) respectively, it is possible to choose constant vectors $\mathbf{a}$, $\mathbf{b}$, $\mathbf{d}$, $\hat{\mathbf{n}}$, $\hat{\mathbf{m}}$ and $\hat{\mathbf{q}}$ for some vectors $\mathbf{a}$, $\mathbf{b}$ and $\mathbf{d}$, the interface is necessarily a plane with normal $\hat{\mathbf{n}}$, $\hat{\mathbf{m}}$ and $\hat{\mathbf{q}}$. The strain of three phases are given by

$$\mathbf{E}_1 = \begin{bmatrix} (a+b)\sigma & 0 \\ 0 & (b+a)\sigma \end{bmatrix},$$
$$\mathbf{E}_2 = \begin{bmatrix} (c+d)\sigma & 0 \\ 0 & (d+e)\sigma \end{bmatrix},$$
$$\mathbf{E}_3 = \begin{bmatrix} (e+d)\sigma & 0 \\ 0 & (c+d)\sigma \end{bmatrix}.$$

By (4.28), $\sigma_{cr} = \tilde{P}_{cr} = -\sqrt{\frac{\zeta}{c+e+2d-2a-2b}}$ is the critical load at the intersection point where the three phase (phase I, phase II and phase III) coexist, the kinematic compatibility equations to form an interface are given by

$$\mathbf{E}_1 - \mathbf{E}_2 = \frac{1}{2}(\mathbf{a} \otimes \hat{\mathbf{n}} + \hat{\mathbf{n}} \otimes \mathbf{a}),$$
$$\mathbf{E}_1 - \mathbf{E}_3 = \frac{1}{2}(\mathbf{b} \otimes \hat{\mathbf{m}} + \hat{\mathbf{m}} \otimes \mathbf{b}),$$
$$\mathbf{E}_2 - \mathbf{E}_3 = \frac{1}{2}(\mathbf{d} \otimes \hat{\mathbf{q}} + \hat{\mathbf{q}} \otimes \mathbf{d}).$$

By direct calculation, we get the two solutions of the interface as

$$\mathbf{a} = \begin{bmatrix} \sqrt{(c-e)[(c+d)-(a+b)]}\sigma \\ \sqrt{(c-e)[(a+b)-(d+e)]}\sigma \end{bmatrix}, \qquad \hat{\mathbf{n}} = \begin{bmatrix} -\sqrt{\frac{(c+d)-(a+b)}{c-e}} \\ \sqrt{\frac{(a+b)-(d+e)}{c-e}} \end{bmatrix},$$

$$\mathbf{b} = \begin{bmatrix} \sqrt{(c-e)[(a+b)-(d+e)]}\sigma \\ \sqrt{(c-e)[(c+d)-(a+b)]}\sigma \end{bmatrix}, \qquad \hat{\mathbf{m}} = \begin{bmatrix} \sqrt{\frac{(a+b)-(d+e)}{c-e}} \\ -\sqrt{\frac{(c+d)-(a+b)}{c-e}} \end{bmatrix},$$

$$\mathbf{d} = \begin{bmatrix} \sqrt{2}(c-e)\sigma \\ \sqrt{2}(c-e)\sigma \end{bmatrix}, \qquad \hat{\mathbf{q}} = \begin{bmatrix} \frac{\sqrt{2}}{2} \\ -\frac{\sqrt{2}}{2} \end{bmatrix}.$$

We illustrate the microstructure of three phases coexist in Fig. 4.4, we find that phase I (blue unit cell) and phase II (red unit cell) coexist with interface normal vector $\hat{\mathbf{n}}$, phase I (blue unit cell) and phase III (green unit cell) coexist with interface normal vector $\hat{\mathbf{m}}$ and phase II (red unit cell) and phase III (green unit cell) coexist with interface normal vector $\hat{\mathbf{q}}$. On the interface, the unit cells of the two phases are coherent based on the compatibility condition. The unit cells in phase I (blue unit cell) keep the square shape under critical loading σ_{cr}, whereas the unit cells in phase II (red unit cell) are deformed to parallelogram under critical loading and the diagonal beam in $\mathbf{e_a}$ direction buckled, and the unit cells in phase III (green unit cell) are deformed to parallelogram and the diagonal beam in $\mathbf{e_b}$ direction buckled.

Case II

The second case is when critical loading applied in the following form with $\sigma_a \neq \sigma_b$,

$$\mathbf{P} = \begin{bmatrix} \sigma_a & 0 \\ 0 & \sigma_b \end{bmatrix}.$$

When σ_a, σ_b satisfy the borderline equation (4.27) where phase I and phase II coexist, that is

$$(c-a)\sigma_a^2 + 2(d-b)\sigma_a\sigma_b + (e-a)\sigma_b^2 = \zeta, \tag{4.42}$$

where $\zeta = \frac{1}{(\gamma_2+1)^2} - \frac{1}{4\gamma_2^2}$. The corresponding strain of phase I and phase II can be determined

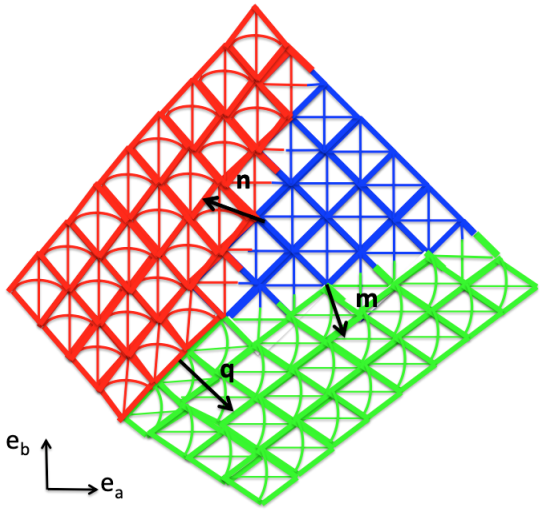

Figure 4.4: Microstructure of three phase coexist with specific values of parameter $\gamma = 380$, $\eta = 7.73$ and $\sigma = \sigma_{cr} = -0.0336$: phase I (blue unit cell), phase II (red unit cell) and phase III (green unit cell). Phase I and phase II coexist with interface normal vector $\hat{\mathbf{n}}$, phase I and phase III coexist with interface normal vector $\hat{\mathbf{m}}$, and phase II and phase III coexist with interface normal vector $\hat{\mathbf{q}}$.

by (4.10) and (4.19) respectively,

$$\mathbf{E}_1 = \begin{bmatrix} (a+b)\sigma_a & 0 \\ 0 & (b+a)\sigma_b \end{bmatrix}, \qquad \mathbf{E}_2 = \begin{bmatrix} (c+d)\sigma_a & 0 \\ 0 & (d+e)\sigma_b \end{bmatrix}.$$

The interface of phase I and Phase II forms as the strain satisfy the kinematic compatibility condition

$$\mathbf{E}_1 - \mathbf{E}_2 = \frac{1}{2}(\mathbf{a} \otimes \hat{\mathbf{n}} + \hat{\mathbf{n}} \otimes \mathbf{a}).$$

By direct calculation, we get the two solutions of the interface as

$$\mathbf{a} = \begin{bmatrix} \sqrt{[(c+d)-(a+b)]\sigma_a\big([(a+b)-(d+e)]\sigma_b - [(a+b)-(c+d)]\sigma_a\big)} \\ \sqrt{[(a+b)-(d+e)]\sigma_b\big([(a+b)-(d+e)]\sigma_b - [(a+b)-(c+d)]\sigma_a\big)} \end{bmatrix},$$

$$\hat{\mathbf{n}} = \begin{bmatrix} -\sqrt{\frac{[(c+d)-(a+b)]\sigma_a}{[(a+b)-(d+e)]\sigma_b - [(a+b)-(c+d)]\sigma_a}} \\ \sqrt{\frac{[(a+b)-(d+e)]\sigma_b}{[(a+b)-(d+e)]\sigma_b - [(a+b)-(c+d)]\sigma_a}} \end{bmatrix}.$$

We illustrate the microstructure of phase I and phase II coexist with interface normal

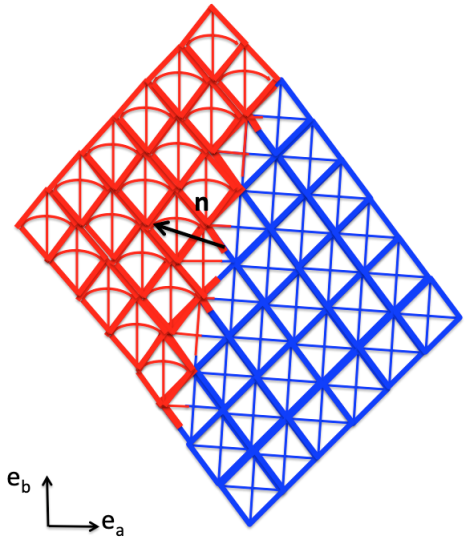

Figure 4.5: Microstructure of phase I and phase II coexist with specific values of parameter $\gamma = 380$, $\eta = 7.73$, $\sigma_a = -0.02$ and $\sigma_b = -0.0182$. The blue unit cells are in phase I, the red unit cells are in phase II, the interface normal vector is $\hat{\mathbf{n}}$.

vector $\hat{\mathbf{n}}$ in Fig. 4.5, on the interface the unit cells of two phases are coherent based on the compatibility condition, and the unit cells in phase I (blue unit cell) are deformed to parallelogram under compressive loading with all beams in compression, whereas the unit cells in phase II (red unit cell) are deformed to parallelogram with the diagonal beam in $\mathbf{e_a}$ direction buckled. When σ_a, σ_b satisfy the borderline equation (4.33) where phase I and Phase III coexist, that is

$$(e-a)\sigma_a^2 + 2(d-b)\sigma_a\sigma_b + (c-a)\sigma_b^2 = \zeta. \tag{4.43}$$

Where in this case, the corresponding strain of phase I and phase III can be determined by (4.10) and (4.19) respectively,

$$\mathbf{E}_1 = \begin{bmatrix} (a+b)\sigma_a & 0 \\ 0 & (b+a)\sigma_b \end{bmatrix}, \qquad \mathbf{E}_3 = \begin{bmatrix} (d+e)\sigma_a & 0 \\ 0 & (c+d)\sigma_b \end{bmatrix},$$

the interface of phase I and phase III forms as the strain satisfy the kinematic compatibility condition

$$\mathbf{E}_1 - \mathbf{E}_3 = \frac{1}{2}(\mathbf{b} \otimes \hat{\mathbf{m}} + \hat{\mathbf{m}} \otimes \mathbf{b}).$$

By direct calculation, we get the two solutions of the interface as

$$\mathbf{b} = \begin{bmatrix} \sqrt{[(a+b)-(d+e)]\sigma_a\big([(a+b)-(d+e)]\sigma_a - [(a+b)-(c+d)]\sigma_b\big)} \\ \sqrt{[(c+d)-(a+b)]\sigma_b\big([(a+b)-(d+e)]\sigma_a - [(a+b)-(c+d)]\sigma_b\big)} \end{bmatrix},$$

$$\hat{\mathbf{m}} = \begin{bmatrix} \sqrt{\frac{[(a+b)-(d+e)]\sigma_a}{[(a+b)-(d+e)]\sigma_a - [(a+b)-(c+d)]\sigma_b}} \\ -\sqrt{\frac{[(c+d)-(a+b)]\sigma_b}{[(a+b)-(d+e)]\sigma_a - [(a+b)-(c+d)]\sigma_b}} \end{bmatrix}.$$

We illustrate the microstructure of phase I and phase III coexist with interface normal vec-

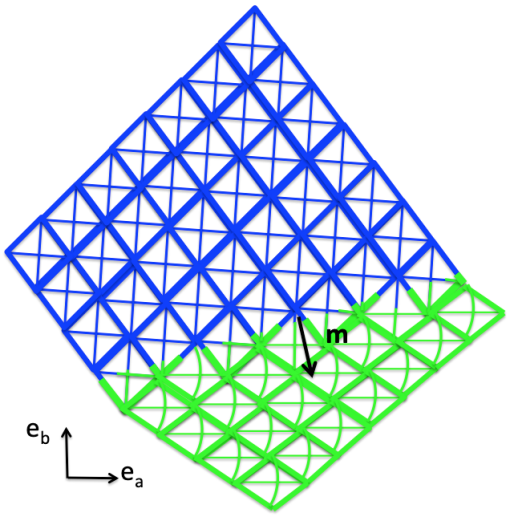

Figure 4.6: Microstructure of phase I and phase III coexist with specific values of parameter $\gamma = 380$, $\eta = 7.73$, $\sigma_a = -0.0182$ and $\sigma_b = -0.02$. The blue unit cells are in phase I, the green unit cells are in phase III, the interface normal vector is $\hat{\mathbf{m}}$.

tor $\hat{\mathbf{m}}$ in Fig. 4.6, on the interface the unit cells of two phases are coherent based on the compatibility condition. The unit cells in phase I (blue unit cell) are deformed to parallelogram under compressive loading with all beams in compression, whereas the unit cells in phase III (green unit cell) are deformed to parallelogram with the diagonal beam in $\mathbf{e_b}$ direction buckled.

4.3 Numerical validation

To validate the developed analytical methodology, a numerical approach based on the finite element (FE) method is applied. To this end, we perform a numerical simulation with the

commercial FE package ABAQUS Standard to demonstrate the phase transformation of the 2D lattice structure under compression. In the simulation, the 2D lattice composed of 50 by 50 unit cells and made of acrylonitrile butadiene styrene (ABS) with Young's Modulus $E = 1.8\ GPa$ and Poisson's ratio $\nu = 0.35$. An implicit time integration method is applied and geometric nonlinearity is considered to represent the large deformation of the structure. The simulation is force controlled, for 2D unit cell and lattice structure, we apply concentrated loads to vertex points on the right and top edges along the horizontal and vertical direction, respectively, a small force in z-direction was introduced to the center of the diagonal beam to trigger out of plane buckling. For the boundary condition, the left and bottom edges are fixed in the horizontal and vertical direction, respectively, and we restrict the displacement in z-direction of the frame beam to avoid out of plane buckling. All models are generated by beam elements (ABAQUS type B32 for diagonal beam and B31 for the frame beam), and a mesh refinement study is conducted to ensure the accuracy. In the following section, we show the buckling phenomenon of 1D beam and 2D unit cell under compressive load with different design parameters. Further, we observe the phase transformation of the lattice structure under compressive load based on the investigation of the unit cell.

4.3.1 Buckling of 1D beam

In this section, we investigate the buckling phenomenon of one-dimensional (1D) beam under compressive load numerically. We have theoretically derived the critical load with clamped boundary condition by (4.48). In the numerical simulation, we apply a concentrated load to one end and introduce a small force to the center of the beam to trigger buckling. We apply the clamped boundary condition, and generate all models by beam elements (ABAQUS type B32). The beam of length l has a rectangular cross section with a constant width $= 1.4\ mm$ and height h. We analyze the buckling phenomenon of the beam with varying length l and height h under compressive load, and divide the results by the critical load (4.48) to compare with the theoretical value. From Fig. 4.7 it can be seen that

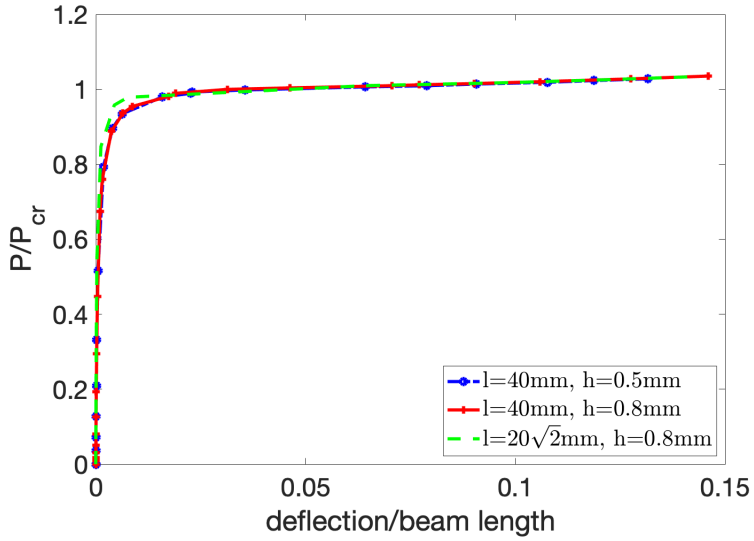

Figure 4.7: Buckling of 1D beam under compressive loading.

although varying the length l and the height h of the beam, the numerical results show an excellent agreement with the theoretical predictions, the beam buckled when the applied load is greater than the critical load in all cases.

4.3.2 Buckling of 2D unit cell

In this section, we investigate the buckling phenomenon of two-dimensional (2D) unit cell under compressive load numerically. We have theoretically derived the critical load when three phase coexist under compressive load, and the critical load is represented in (4.28). The dimension of the unit cell is l by l, the frame beams have square cross section with height a and the diagonal beams have rectangular cross section with width w and height h. For better observation of the buckling phenomenon, we describe the critical load in terms of diagonal beam. Since the frame beams only in compression under compressive load, by (4.28), (4.23) and (4.11) and direct calculation, the critical load of diagonal beam P_{cr}^{diag} is given as

$$P_{cr}^{diag} = \tilde{P}_{cr} EA_2 - \frac{\sqrt{2}}{2}\tilde{P}_{cr}(c+2d+e)EA_1, \tag{4.44}$$

where the two terms on the right are the critical load of the 2D unit cell and the corresponding load of frame beam. The result of (4.44) is illustrated in Fig. 4.8, we plot the critical

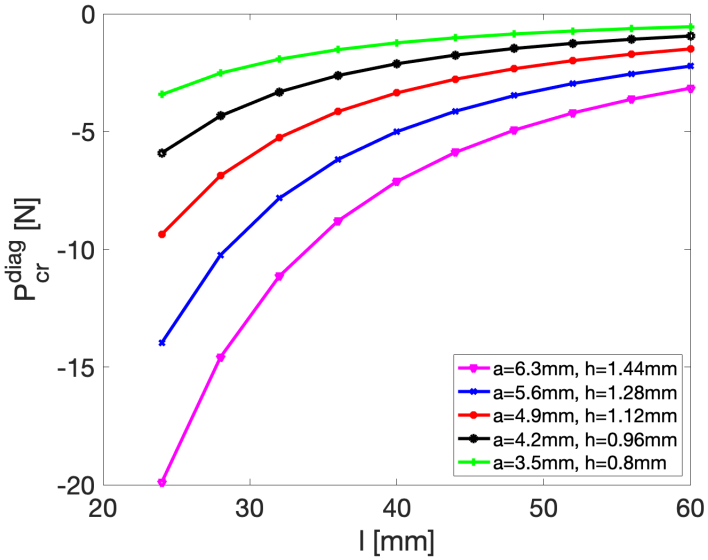

Figure 4.8: Theoretically derived critical buckling load of the diagonal beam in terms of different unit cell parameters.

load of the diagonal beam versus the beam length l with different height of the frame beam a and diagonal beam h. We observe that the critical buckling loads of diagonal beam decrease as the length of the unit cell increase, and the critical buckling load of diagonal beam increase as the height of the frame and diagonal beam increase. For specific length of the unit cell, we will compare the corresponding critical buckling load with numerical simulation. In the numerical simulation, we adopt the same geometry as the theoretical unit cell with constant length $l = 40\ mm$ and constant width of diagonal beam $w = 2\ mm$, and we analysis the critical load with varying design parameters: height of the frame beam a and height of the diagonal beam h. In the Fig. 4.9, we present the critical load of diagonal beam versus the deflection of the center point, we represent x axis as deflection of the center point of diagonal beam and y axis as the point loading of diagonal beam divided by critical load in theoretical prediction (4.44). We illustrate only the point load of diagonal beam in e_a direction considering the point load of diagonal beam in e_b direction has the same results. Since the frame beams deform only in compression, the point load of the

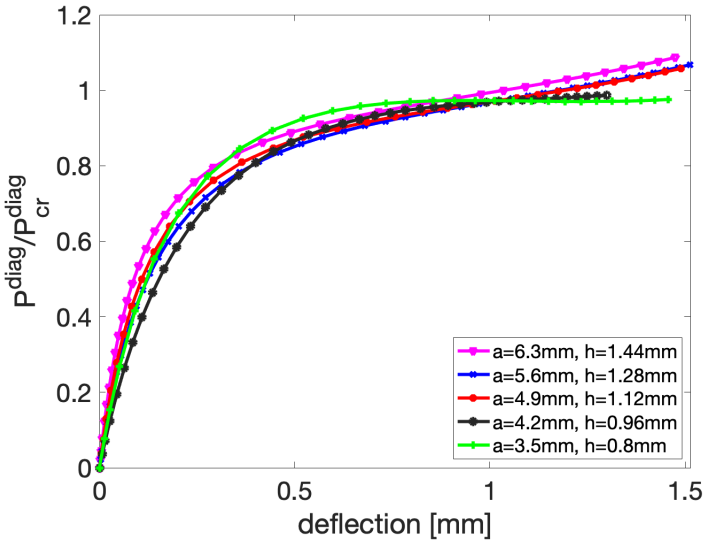

Figure 4.9: Numerically derived point load of the diagonal beam in terms of different unit cell Parameters.

diagonal beam is estimated by subtracting the load of the frame beam from the point load of the unit cell. We find that the numerical result coincident with the theoretical prediction with different parameters: frame width a and diagonal beam width h, and we observe that the diagonal beam buckled when the applied load is greater than the critical load. However, as the height of frame beam and diagonal beam increase, the buckling phenomenon of the diagonal beam becomes difficult to observe.

4.3.3 Phase transformation of lattice structure

In this section, we investigate the phase transformation of lattice structure under biaxial compressive load by numerical simulation. We present the critical load of the diagonal beam to observe the buckling phenomenon of the unit cell by (4.44) in previous section. For a lattice model, if we apply the boundary condition corresponding to the stable phases (stable configurations) of the unit cell, then the lattice can easily accommodate it, and the transitions between these phases of the 2D unit cell can be regarded as phase transformations of the lattice structure. Therefore, we adopt the critical load of the unit cell to observe the phase transformation phenomenon of the lattice structure in the numerical simulation.

The lattice model consist of 50 by 50 repeated unit cells, the dimension of the unit cell is l by l, the frame beams have square cross section with height a and the diagonal beam have rectangular cross section with width w and height h. As mentioned previously, we focus on the point load of the diagonal beam to better observe the buckling phenomenon. As shown in Fig. 4.10, we plot the average point load of diagonal beam of the lattice structure versus the average deflection of the diagonal beam. We represent the x axis as average

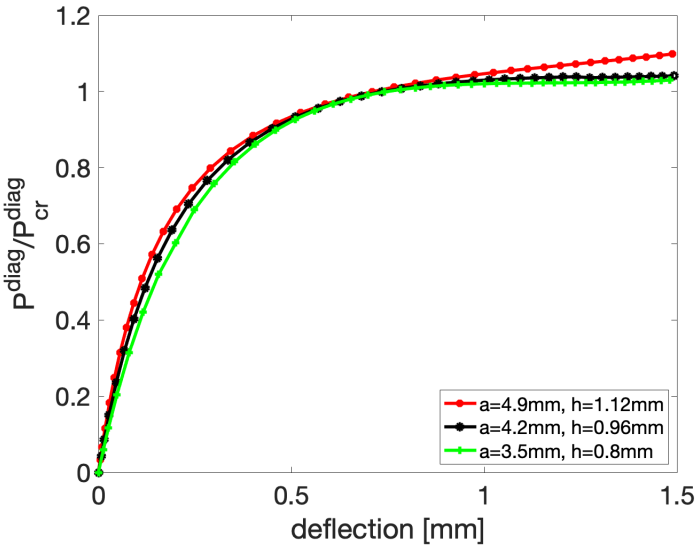

Figure 4.10: Numerically derived point load in terms of lattice Parameters.

deflection of diagonal beam and the y axis as the average point load of diagonal beam divided by critical load of diagonal beam, the point load of diagonal beam is obtained by subtracting the average load of the frame beam from the average point load of the lattice structure. we observe the buckling phenomenon at critical load with different parameters (height of frame beam a and height of diagonal beam h), and we find that the numerical results are consistent with the theoretical predictions, which means that the diagonal beam of lattice structure buckled when applied load is greater than critical load predicted by the unit cell, while the macrostructure of the lattice structure is in compression. Therefore, the transitions between phases of the 2D unit cell can be regarded as phase transformation of the lattice structure.

4.4 Conclusion

We have designed and characterized a two-dimensional (2D) crystal formed by a lattice structure consisting of unit cells to mimic the Austenite-Martensite phase transition in shape memory alloys (SMAs). We report a theoretical study on the behavior of stress-induced phase transition of the unit cells by the continuum model. Based on the minimization of the total free energy of unit cells, we observe four distinct stable configurations corresponding to four stable phases, and consider the transitions between these phases as phase transformations of the lattice structure. Extending the unit cell scheme to 2D lattice structure, we found that when the lattice satisfies significant restrictions on the parameters, the microstructure forms as the lattice tends to keep in the bottom of the energy wells and holds the imposed boundary condition. Further, the properties of the lattice structure are also studied by numerical simulations in 2D biaxial stress system. We conduct the buckling analysis of a 1D beam and 2D unit cell with different design parameters, and we extend the analysis to a 50 by 50 lattice structure and observe the phase transformation at critical load by theoretical predictions. Such lattice structures can undergo "phase transitions" mimicking the Austenite-Martensite phase transition in shape memory alloys (SMAs) and may realize the proposed applications of SMAs as transducers, actuators, and sensors. More importantly, they offer directly observable material models that can shed light on the fundamental mechanisms of the first-order non-diffusive phase transitions and shape memory effects, their interactions with defects, and the physical origins of hysteresis.

4.5 Appendix

In the appendix, we investigate the elastic energy of a beam before and after buckling, and determine the corresponding critical strain by imposing equilibrium conditions. For a beam subjects to a compressive load P with clamped boundary condition, the original length of the beam is L, after deformation the length becomes l. We have the elastic energy before

buckling as

$$W^1(\varepsilon) = \int_0^L \frac{1}{2} E_1 A \varepsilon^2 = \frac{1}{2} E_1 A L \varepsilon^2. \tag{4.45}$$

After buckling, we have Euler–Bernoulli equation as

$$E_1 I \frac{d^4 v}{dx^4} + P_{cr} \frac{d^2 v}{dx^2} = 0,$$

where v is the deflection, E_1 is the Young's Modulus, I is the Area Moment of Inertia. Solving the above equation, we get the general form of deflection $v(x)$ as

$$v(x) = \bar{A}\cos(kx) + \bar{B}\sin(kx) + \bar{C}x + \bar{D}. \tag{4.46}$$

With the clamped boundary condition, we have $v(0) = v(l) = v'(0) = v'(l) = 0$. Applying the boundary condition into (4.46), we can get the expression of the deflection as

$$v(x) = \bar{A}\big(\cos(\frac{2n\pi}{l}x) - 1\big) \qquad n = 1, 2, ... \tag{4.47}$$

where $\bar{A}$ is the amplitude of deflection to be determined. We have the critical loading and critical stress as

$$P_{cr} = \frac{4n^2\pi^2 E_1 I}{l^2}, \quad \sigma_{cr} = \frac{4n^2\pi^2 E_1 I}{Al^2} \qquad n = 1, 2, ... \tag{4.48}$$

by introducing a dimensionless parameter $\gamma = \frac{AL^2}{8\pi^2 I}$, with $n = 1$ the second term of above equation can be described as

$$\sigma_{cr} = \frac{E_1}{2\gamma}. \tag{4.49}$$

Further, We can obtain the amplitude of deflection based on the condition that the length of the beam unchanged after buckling [101]. By assuming the beam is inextensible after buckling, the length can be written as

$$L = \int_0^l \sqrt{1 + v'^2}\, dx. \tag{4.50}$$

Inserting the expression of the deflection (4.47) with $n = 1$ into above equation (4.50), we have

$$L = \int_0^l \sqrt{1 + \bar{A}^2 \frac{4\pi^2}{L^2} \sin^2(\frac{2\pi}{l}x)}\, dx. \tag{4.51}$$

Substituting $\theta = \frac{2\pi}{l}x$, we can rewrite the above integral with respect to θ as:

$$L = \frac{l}{2\pi}\int_0^{2\pi}\sqrt{1+\bar{A}^2\frac{4\pi^2}{L^2}\sin^2(\theta)}d\theta. \tag{4.52}$$

Further introducing $\phi = \frac{\pi}{2} - \theta$ and $m = \bar{A}^2\frac{4\pi^2}{L^2}$, we rewrite the above equation as

$$\begin{aligned}\frac{L}{l} &= \frac{1}{2\pi}\int_{-\frac{3\pi}{2}}^{\frac{\pi}{2}}\sqrt{1+m(1-\sin^2(\phi))}d\phi \\ &= \frac{\sqrt{1+m}}{2\pi}\int_{-\frac{3\pi}{2}}^{\frac{\pi}{2}}\sqrt{1-\frac{m}{1+m}\sin^2(\phi)}d\phi.\end{aligned} \tag{4.53}$$

The above equation (4.53) can be simplify by the incomplete elliptic integral of the second kind as:

$$\frac{L}{l} = \frac{\sqrt{1+m}}{2\pi}E(\frac{\pi}{2}|\frac{m}{1+m}) - \frac{\sqrt{1+m}}{2\pi}E(-\frac{3\pi}{2}|\frac{m}{1+m}), \tag{4.54}$$

where $E(\varphi|k^2) = \int_0^{\varphi}\sqrt{1-k^2\sin^2(\theta)}d\theta$. Further, we rewrite the above equation into the complete elliptic integral of the second kind by applying the property of the elliptic integral $E(\lambda\pi m) = 2\lambda E(m)$ for all integers λ, we have

$$\frac{L}{l} = \frac{\sqrt{1+m}}{2\pi}E(\frac{m}{1+m}) + \frac{3\sqrt{1+m}}{2\pi}E(\frac{m}{1+m}) = \frac{2\sqrt{1+m}}{\pi}E(\frac{m}{1+m}). \tag{4.55}$$

when only considering the small amplitude (i.e. $\bar{A} \to 0$), we can apply the Taylor expansion of elliptic integral and get an approximation of above equation as

$$\frac{L}{l} \approx \sqrt{1+m}(1-\frac{m}{4(1+m)}) \approx 1+\frac{m}{4}+O(m^2). \tag{4.56}$$

Substituting $m = \bar{A}^2\frac{4\pi^2}{L^2}$ into (4.56), we get the amplitude $\bar{A}$ in terms of ε ($\varepsilon = \frac{L-l}{L}$) as

$$\bar{A} = \frac{L}{\pi}\sqrt{\frac{\varepsilon}{1-\varepsilon}}. \tag{4.57}$$

The elastic energy after buckling are given by

$$W^2(\varepsilon) = \frac{1}{2}\int_0^l EI\kappa^2 dx = \frac{1}{2}\int_0^l EI(\frac{16\pi^4}{L^4}\bar{A}^2\cos^2(\frac{2\pi}{L}x))dx = \frac{8EI\pi^4}{L^4}\bar{A}^2(\frac{l}{2}+\frac{L\sin(\frac{4\pi l}{L})}{8\pi}),$$

where the curvature $\kappa = v''(x) = \frac{4\pi^2}{L^2}\bar{A}\cos(\frac{2\pi}{L}x)$. Inserting (4.57) into the above equation, we rewrite W^2 in terms of ε as

$$W^2(\varepsilon) = \frac{8EI\pi^2}{L}\frac{\varepsilon}{1-\varepsilon}\big(\frac{1}{2}(1-\varepsilon) - \frac{1}{8\pi}\sin(4\pi\varepsilon)\big).$$

Taking taylor expansion of the above equation and keeping up to $O(\varepsilon^5)$, we have

$$W^2(\varepsilon) = \frac{4EI\pi^2}{L}(\varepsilon - \varepsilon^2 - \varepsilon^3 + (\frac{8\pi^2}{3} - 1)\varepsilon^4) + O(\varepsilon^5). \tag{4.58}$$

Combining (4.45) and (4.58), we can describe the elastic energy of 1D elastic beam before and after buckling in the following form

$$W(\varepsilon) = \begin{cases} W^1(\varepsilon) = \frac{1}{2}EAL\varepsilon^2 & \text{if } \varepsilon \leq \varepsilon_{cr} \\ W^2(\varepsilon) = \frac{4EI\pi^2}{L}(\varepsilon - \varepsilon^2 - \varepsilon^3 + (\frac{8\pi^2}{3} - 1)\varepsilon^4) & \text{if } \varepsilon > \varepsilon_{cr}. \end{cases} \tag{4.59}$$

When $W^1(\varepsilon) = W^2(\varepsilon)$, we can estimate the critical strain as

$$\varepsilon_{cr} \approx -\frac{1}{\gamma + 1}, \tag{4.60}$$

where the dimensionless parameter $\gamma = \frac{AL^2}{8\pi^2 I}$.

Chapter 5
Conclusions

In this dissertation, we have investigated three nonlinear problems in mechanics. Firstly, we describe dynamic responses of a two-dimensional lattice with harmonic, weakly nonlinear, and Hertzian interactions through the analytical and numerical approach. we have theoretically derived the continuum approximations of the discrete system in a square lattice and a hexagonal lattice. For the hexagonal lattice, we obtain some nontrivial exact longitudinal solitary wave solutions along with certain symmetric directions for systems with weakly nonlinear and Hertzian interactions. Through numerical simulations, we have explored the properties of solitary waves and obtained the scaling laws between the wave-front velocity amplitudes and propagation distance: $V_p \propto R^{-1/1.9}$ for a weakly nonlinear lattice and $V_p \propto R^{-1/2.4}$ for a Hertzian lattice. The closed-form solitary wave solutions and scaling laws are expected to have an important impact on the design of shock absorbers, acoustic lens, non-destructive structural testing devices among many others.

Secondly, we have solved the exact description of the set of effective properties of multiphase composites by deriving the necessary conditions and sufficient conditions of the Hashin Shtrikman bounds attainability. Under the constraint of volume fractions of the constituent phases, we have obtained the necessary condition by a null lagrangian, and obtained sufficient conditions by constructing two kinds of microstructures: a new three-phase and four-phase coated sphere; new optimal microstructures comprised of three-phase coated spheres and two-phase E-inclusions. For three-phase composites, the necessary condition guarantees sufficient condition. For four-phase composites, when θ_N is small, there is a gap between sufficient condition and necessary condition , which will require the construction of more optimal microstructures to fill the gap. Combining the necessary

and sufficient condition of HS bounds attainability, we can precisely characterize the G-closure to describe the set of effective properties of multiphase conductive materials for a broader range, which is anticipated to have applications in actuators, phase transitions, smart materials, and graded materials.

Finally, We have constructed a two-dimensional (2D) crystal formed by a lattice structure, which consists of repeating structure elements as called unit cells, to mimic the Austenite-Martensite phase transition in shape memory alloys (SMAs). We theoretically investigate the stress-induced phase transition of the unit cell by a continuum model. According to the geometric linear theory, we get four distinct stable configurations corresponding to four stable phases by the total free energy minimization, and the transitions between these phases are regarded as phase transformations of the lattice structure. Extending the unit cell scheme to 2D lattice structure, we found that the microstructure forms when the lattice satisfies significant restrictions on the parameters by the Hadamard compatibility condition. Further, We apply numerical simulation to study phase transition characteristics of the lattice structure in the 2D biaxial stress system. By applying biaxial loading to the 2D unit cell and 50 by 50 lattice structure with different parameters, we observe that the critical load when the phase transition occurs is consistent with the theoretical prediction. Such engineered structures may realize the proposed applications of SMAs as transducers, actuators, and sensors. More importantly, they offer directly observable material models that can shed light on the fundamental mechanisms of the first-order non-diffusive phase transitions and shape memory effects, their interactions with defects, and the physical origins of hysteresis.

Appendix A

Core codes (Matlab) for 2D hexagonal packing lattice with hertzian interactions

```
% The main code investigates the solitary wave in 2D hexagonal packing
% of steel balls. We set initial velocity for the six spheres around
% the center sphere, and employ the fourth-order Runge-Kutta method
% for the simulation.
clear all;
clc;
time_steps = 500;
dt = 5e-7;
q = 100;    % Number of balls in each row and column are 100
N = 10000; % Total number of balls are 10000
init_vel = 0.5; % Initial velocity
% Creating position, velocity and acceleration matrices.
[mass, E, R, poisson, position_x,  position_y,...
velocity_x, velocity_y,velocity, ...
overlaps_e11,overlaps_e21,overlaps_e31, A] = ...
twodrkhertz0906initialise(time_steps, N, q, init_vel);
% Iterating forward in time:
velocity(:,:,1)=sqrt(velocity_x(:,:,1).^2+velocity_y(:,:,1).^2);
position(:,:,1)= sqrt((position_x(:,:,1)-position_x(50,50,1)).^2...
             +(position_y(:,:,1)-position_y(50,50,1)).^2);
i=2;
while(i<time_steps+1)
 % We apply the 4th runge-kutta method to integrate our
```

```
 % equations forward in time:
    [velocity_x(:,:,i), velocity_y(:,:,i), position_x(:,:,i),...
    position_y(:,:,i)] = twodrkhertz0906(position_x(:,:,i-1),...
    position_y(:,:,i-1), velocity_x(:,:,i-1), velocity_y(:,:,i-1),...
    q, N, R, mass, E, poisson, i, dt, A);
    position(:,:,i)= sqrt((position_x(:,:,i)-position_x(50,50,1)).^2...
                +(position_y(:,:,i)-position_y(50,50,1)).^2);
    velocity(:,:,i)=sqrt(velocity_x(:,:,i).^2+velocity_y(:,:,i).^2);
    i=i+1;
end
% Plot the propagation of solitary wave
x=1:q;
y=1:q;
X=position_x(x,y,1);
Y=position_y(x,y,1);
Z= velocity(x,y,1);
axis equal tight ;
colormap(jet);
surf(X,Y,Z);
caxis([0,0.5]);
U = velocity_x(x,y,1);
V = velocity_y(x,y,1);
title('The velocity')
figure
contour(X,Y,Z)
hold on
quiver(X,Y,U,V,5);
hold off

% Initialization function
function [mass, E, R, poisson, position_x,  position_y,...
         velocity_x,velocity_y, velocity, overlaps_e11,...
         overlaps_e21, overlaps_e31, A] = ...
         twodrkhertz0906initialise(time_steps, N, q, init_vel)
```

```
% Parameter definitions
rho_steel = 7780; % Density of steel
E_steel = 1.93*10^11; % Young's modulus for steel
rad = 0.00476/2; % Ball radius
poisson_steel = 0.3; % Poisson ratio for steel
%Creating vectors for the material properties
mass = zeros(q,q);
E = zeros(q,q); % Young's modulus matrix
R = zeros(q,q); % Radius matrix
poisson = zeros(q,q); % Poisson ratio matrix
A = zeros(q, q); % Force coefficients matrix
% Assign values to material properties
E(1:q,1:q) = E_steel;
R(1:q,1:q) = rad;
poisson(1:q,1:q) = poisson_steel;
mass(1:q,1:q) = 0.00045;
A(1:q,1:q) = 2*E(1:q,1:q).*sqrt(R(1:q,1:q))...
             ./(1-poisson(1:q,1:q).^2);
% Creating the matrices for the positions and velocities.
position_x = zeros(q,q,time_steps);
position_y = zeros(q,q,time_steps);
velocity_x = zeros(q,q,time_steps);
velocity_y = zeros(q,q,time_steps);
velocity   = zeros(q,q,time_steps);
% overlaps_e1 represent overlap on e_1 direction;
overlaps_e1 = zeros(q,q,time_steps);
% overlaps_e2 represent overlap in e_2 direction;
overlaps_e2 = zeros(q,q,time_steps);
% overlaps_e3 represent overlap in e_3 direction;
overlaps_e3 = zeros(q,q,time_steps);
% The overlap between the 1st ball and its left neighbour:
overlaps_e11(:,:,1) = zeros(q,q);
overlaps_e21(:,:,1) = zeros(q,q);
overlaps_e31(:,:,1) = zeros(q,q);
```

```
    % Initialize the positions:
    i=1;
    while(i<q+1)
        position_x(i,:,1) = 1+(i-1)/2.0 : 1 : q+(i-1)/2.0;
        position_y(i,:,1) = ones(1,q)*i*sqrt(3)/2;
        i=i+1;
    end
    % Initialize the velocities:
    velocity_x(:,:,1) = zeros(q,q);
    velocity_x(49,51,1) = 1/2*init_vel;
    velocity_x(51,49,1)= -1/2*init_vel;
    velocity_x(49,50,1) = -1/2*init_vel;
    velocity_x(51,50,1)= 1/2*init_vel;
    velocity_x(50,49,1) = -init_vel;
    velocity_x(50,51,1)= init_vel;
    velocity_x(q,q,1)=0;
    velocity_y(:,:,1) = zeros(q,q);
    velocity_y(49,51,1) = -sqrt(3)/2*init_vel;
    velocity_y(51,49,1)= sqrt(3)/2*init_vel;
    velocity_y(49,50,1) = -sqrt(3)/2*init_vel;
    velocity_y(51,50,1)= sqrt(3)/2*init_vel;
    velocity_y(q,q,1)=0;
end

% This function update velocities and positions of
% each ball using a 4th order Runge-Kutta method.
function [u_new, v_new, x_new, y_new] =...
         twodrkhertz0906(x_old, y_old, u_old,...
         v_old, q, N, R, mass, E, poisson, i, dt, A)
    % Firstly, we create matrix for the k1, k2, k3, k4 :
    % k1,k2,k3,k4 represent position and velocity in e1 direction.
    k1_x = zeros(q,q); k1_u = zeros(q,q);
    k2_x = zeros(q,q); k2_u = zeros(q,q);
    k3_x = zeros(q,q); k3_u = zeros(q,q);
```

```
k4_x = zeros(q,q); k4_u = zeros(q,q);
k1_y = zeros(q,q);
k2_y = zeros(q,q);
k3_y = zeros(q,q);
k4_y = zeros(q,q);
% f1,f2,f3,f4 represent velocity in e2 direction.
f1_u = zeros(q,q);  f1_v = zeros(q,q);
f2_u = zeros(q,q);  f2_v = zeros(q,q);
f3_u = zeros(q,q);  f3_v = zeros(q,q);
f4_u = zeros(q,q);  f4_v = zeros(q,q);
% g1,g2,g2,g4 represent velocity in e3 direction.
g1_u = zeros(q,q); g2_u = zeros(q,q);
g3_u = zeros(q,q); g4_u = zeros(q,q);
g1_v = zeros(q,q); g2_v = zeros(q,q);
g3_v = zeros(q,q); g4_v = zeros(q,q);
% Create matrix for the overlaps:
overlaps_e11 = zeros(q, q);
overlaps_e21 = zeros(q, q);
overlaps_e31 = zeros(q, q);
overlaps_e12 = zeros(q, q);
overlaps_e22 = zeros(q, q);
overlaps_e32 = zeros(q, q);
overlaps_e13 = zeros(q, q);
overlaps_e23 = zeros(q, q);
overlaps_e33 = zeros(q, q);
overlaps_e14 = zeros(q, q);
overlaps_e24 = zeros(q, q);
overlaps_e34 = zeros(q, q);
% Create matrix for the temporary displacement and velocity:
xx1 = zeros(q, q);
yy1 = zeros(q, q);
uu1 = zeros(q, q);
vv1 = zeros(q, q);
% Calculate k1_x, k1_y:
```

```
k1_x = dt * u_old;
k1_y = dt * v_old;
% Check for contacts in e_1 direction:
overlaps_e11 = twodrkhertz0906contacts1(N, q, x_old, R);
% Calculate k1_u:
k1_u(1:q,1) = dt*(-(A(1:q,1)).*overlaps_e11(1:q,1)...
            .^(3/2)./mass(1:q,1));
k1_u(1:q,2:q)=dt*(A(1:q,1:(q-1)).*overlaps_e11(1:q,1:(q-1))...
            .^(3/2)./mass(1:q,2:q) - (A(1:q,2:q)).* ...
            overlaps_e11(1:q,2:q).^(3/2)./mass(1:q,2:q));
% Check for contacts in e_2 direction:
overlaps_e21 = twodrkhertz0906contacts2(N, q, x_old, y_old, R);
% Calculate f1_u:
f1_u(1,1:q) = dt/2*(-(A(1,1:q)).*overlaps_e21(1,1:q)...
            .^(3/2)./mass(1,1:q));
f1_u(2:q,1:q)=dt/2*(A(1:(q-1),1:q).*overlaps_e21(1:(q-1),1:q)...
            .^(3/2)./mass(2:q,1:q) - (A(2:q,1:q))...
            .*overlaps_e21(2:q,1:q).^(3/2)./mass(2:q,1:q));
% Calculate f1_v:
f1_v(1,1:q) = sqrt(3)*dt/2*(-(A(1,1:q)).*overlaps_e21(1,1:q)...
            .^(3/2)./mass(1,1:q));
f1_v(2:q,1:q)=sqrt(3)*dt/2*(A(1:(q-1),1:q)...
            .*overlaps_e21(1:(q-1),1:q)...
            .^(3/2)./mass(2:q,1:q) - (A(2:q,1:q))...
            .*overlaps_e21(2:q,1:q).^(3/2)./mass(2:q,1:q));
% Check for contacts in e_3 direction:
overlaps_e31 = twodrkhertz0906contacts3(N, q, x_old, y_old, R);
% Calculate g1_u:
g1_u(1:q,1) = dt/2*(-(A(1:q,1)).*overlaps_e31(1:q,1)...
            .^(3/2)./mass(1:q,1));
g1_u(1:(q-1),2:q)=dt/2*(A(2:q,1:(q-1)).*overlaps_e31(2:q,1:(q-1))...
            .^(3/2)./mass(2:q,1:(q-1)) - A(1:(q-1),2:q)...
        .*overlaps_e31(1:(q-1),2:q).^(3/2)./mass(1:(q-1),2:q));
g1_u(q,2:q)=dt/2*(-A(q,1:(q-1)).*overlaps_e31(q,2:q))...
```

```
            .^(3/2)./mass(q,2:q);
% Calculate g1_v:
g1_v(1:q,1) = -sqrt(3)*dt/2*(-(A(1:q,1)).*overlaps_e31(1:q,1)...
            .^(3/2)./mass(1:q,1));
g1_v(1:(q-1),2:q)=-sqrt(3)*dt/2*(A(2:q,1:(q-1))...
            .*overlaps_e31(2:q,1:(q-1))...
            .^(3/2)./mass(2:q,1:(q-1)) - A(1:(q-1),2:q)...
            .*overlaps_e31(1:(q-1),2:q).^(3/2)./mass(1:(q-1),2:q));
g1_v(q,2:q)=-sqrt(3)*dt/2*(-A(q,1:(q-1)).*overlaps_e31(q,2:q))...
            .^(3/2)./mass(q,2:q);
% Update temporary displacements and velocities:
xx1 = x_old + 0.5 * k1_x;
yy1 = y_old + 0.5 * k1_y;
uu1 = u_old + 0.5 * (k1_u + f1_u + g1_u);
vv1 = v_old + 0.5 * ( f1_v + g1_v);
% Calculate k2_x k2_y:
k2_x = dt * uu1;
k2_y = dt * vv1;
% Check for contacts between balls using the new xx1 values:
overlaps_e12 = twodrkhertz0906contacts1(N, q, xx1, R);
% Calculate k2_u:
k2_u(1:q,1) = dt*(-(A(1:q,1)).*overlaps_e12(1:q,1)...
            .^(3/2)./mass(1:q,1));
k2_u(1:q,2:q)=dt*(A(1:q,1:(q-1)).*overlaps_e12(1:q,1:(q-1))...
            .^(3/2)./mass(1:q,2:q) - (A(1:q,2:q))...
            .*overlaps_e12(1:q,2:q).^(3/2)./mass(1:q,2:q));
% Check for contacts in e_2 direction:
overlaps_e22 = twodrkhertz0906contacts2(N, q, xx1, yy1, R);
% Calculate f2_u:
f2_u(1,1:q) = dt/2*(-(A(1,1:q)).*overlaps_e22(1,1:q)...
            .^(3/2)./mass(1,1:q));
f2_u(2:q,1:q)=dt/2*(A(1:(q-1),1:q).*overlaps_e22(1:(q-1),1:q)...
            .^(3/2)./mass(2:q,1:q) - (A(2:q,1:q))...
            .*overlaps_e22(2:q,1:q).^(3/2)./mass(2:q,1:q));
```

```
% Calculate f2_v:
f2_v(1,1:q) = sqrt(3)*dt/2*(-(A(1,1:q)).*overlaps_e22(1,1:q)...
            .^(3/2)./mass(1,1:q));
f2_v(2:q,1:q)=sqrt(3)*dt/2*(A(1:(q-1),1:q)...
            .*overlaps_e22(1:(q-1),1:q)...
            .^(3/2)./mass(2:q,1:q) - (A(2:q,1:q))...
            .*overlaps_e22(2:q,1:q).^(3/2)./mass(2:q,1:q));
% Check for contacts in e_3 direction:
overlaps_e32 = twodrkhertz0906contacts3(N, q, xx1, yy1, R);
% Calculate g2_u:
g2_u(1:q,1) = dt/2*(-(A(1:q,1)).*overlaps_e32(1:q,1)...
            .^(3/2)./mass(1:q,1));
g2_u(1:(q-1),2:q)=dt/2*(A(2:q,1:(q-1)).*overlaps_e32(2:q,1:(q-1))...
            .^(3/2)./mass(2:q,1:(q-1)) - A(1:(q-1),2:q)...
            .*overlaps_e32(1:(q-1),2:q).^(3/2)./mass(1:(q-1),2:q));
g2_u(q,2:q)=dt/2*(-A(q,1:(q-1)).*overlaps_e32(q,2:q))...
            .^(3/2)./mass(q,2:q) ;
% Calculate g2_v:
g2_v(1:q,1) = -sqrt(3)*dt/2*(-(A(1:q,1)).*overlaps_e32(1:q,1)...
            .^(3/2)./mass(1:q,1));
g2_v(1:(q-1),2:q)=-sqrt(3)*dt/2*(A(2:q,1:(q-1))...
            .*overlaps_e32(2:q,1:(q-1))...
            .^(3/2)./mass(2:q,1:(q-1)) - A(1:(q-1),2:q)...
            .*overlaps_e32(1:(q-1),2:q).^(3/2)./mass(1:(q-1),2:q));
g2_v(q,2:q)=-sqrt(3)*dt/2*(-A(q,1:(q-1)).*overlaps_e32(q,2:q))...
            .^(3/2)./mass(q,2:q);
% Update temporary displacements and velocities:
xx1 = x_old + 0.5 * k2_x;
yy1 = y_old + 0.5 * k2_y;
uu1 = u_old + 0.5 * (k2_u + f2_u + g2_u);
vv1 = v_old + 0.5 * ( f2_v + g2_v);
% Calculate k3_x k3_y:
k3_x = dt * uu1;
k3_y = dt * vv1;
```

```
% Check for contacts between balls, using the new xx1 yy1 values:
% Check for contacts in e_1 direction:
overlaps_e13 = twodrkhertz0906contacts1(N, q, xx1, R);
% Calculate k3_u:
k3_u(1:q,1) = dt*(-(A(1:q,1)).*overlaps_e13(1:q,1)...
            .^(3/2)./mass(1:q,1));
k3_u(1:q,2:q)=dt*(A(1:q,1:(q-1)).*overlaps_e13(1:q,1:(q-1))...
            .^(3/2)./mass(1:q,2:q) - (A(1:q,2:q))...
            .*overlaps_e13(1:q,2:q).^(3/2)./mass(1:q,2:q));
% Check for contacts in e_2 direction:
overlaps_e23 = twodrkhertz0906contacts2(N, q, xx1, yy1, R);
% Calculate f3_u:
f3_u(1,1:q) = dt/2*(-(A(1,1:q)).*overlaps_e23(1,1:q)...
            .^(3/2)./mass(1,1:q));
f3_u(2:q,1:q)=dt/2*(A(1:(q-1),1:q).*overlaps_e23(1:(q-1),1:q)...
            .^(3/2)./mass(2:q,1:q) - (A(2:q,1:q))...
            .*overlaps_e23(2:q,1:q).^(3/2)./mass(2:q,1:q));
% Calculate f3_v:
f3_v(1,1:q) = sqrt(3)*dt/2*(-(A(1,1:q)).*overlaps_e23(1,1:q)...
            .^(3/2)./mass(1,1:q));
f3_v(2:q,1:q)=sqrt(3)*dt/2*(A(1:(q-1),1:q)...
            .*overlaps_e23(1:(q-1),1:q)...
            .^(3/2)./mass(2:q,1:q) - (A(2:q,1:q))...
            .*overlaps_e23(2:q,1:q).^(3/2)./mass(2:q,1:q));
% Check for contacts in e_3 direction:
overlaps_e33 = twodrkhertz0906contacts3(N, q, xx1, yy1, R);
% Calculate g3_u:
g3_u(1:q,1) = dt/2*(-(A(1:q,1)).*overlaps_e33(1:q,1)...
            .^(3/2)./mass(1:q,1));
g3_u(1:(q-1),2:q)=dt/2*(A(2:q,1:(q-1)).*overlaps_e33(2:q,1:(q-1))...
            .^(3/2)./mass(2:q,1:(q-1)) - A(1:(q-1),2:q)...
            .*overlaps_e33(1:(q-1),2:q).^(3/2)./mass(1:(q-1),2:q));
g3_u(q,2:q)=dt/2*(-A(q,1:(q-1)).*overlaps_e33(q,2:q))...
            .^(3/2)./mass(q,2:q) ;
```

```
% Calculate g3_v:
g3_v(1:q,1) = -sqrt(3)*dt/2*(-(A(1:q,1)).*overlaps_e33(1:q,1)...
            .^(3/2)./mass(1:q,1));
g3_v(1:(q-1),2:q)=-sqrt(3)*dt/2*(A(2:q,1:(q-1))...
            .*overlaps_e33(2:q,1:(q-1))...
            .^(3/2)./mass(2:q,1:(q-1)) - A(1:(q-1),2:q)...
            .*overlaps_e33(1:(q-1),2:q).^(3/2)./mass(1:(q-1),2:q));
g3_v(q,2:q)=-sqrt(3)*dt/2*(-A(q,1:(q-1)).*overlaps_e33(q,2:q))...
            .^(3/2)./mass(q,2:q);
% Update temporary displacements and velocities:
xx1 = x_old + k3_x;
yy1 = y_old + k3_y;
uu1 = u_old + (k3_u + f3_u + g3_u);
vv1 = v_old + ( f3_v + g3_v);
% Calculate k4 x:
k4_x = dt * uu1;
k4_y = dt * vv1;
% Check for contacts between balls using the new xx1 values:
overlaps_e14 = twodrkhertz0906contacts1(N, q, xx1, R);
% Calculate k4 v:
k4_u(1:q,1) = dt*(-(A(1:q,1)).*overlaps_e14(1:q,1)...
            .^(3/2)./mass(1:q,1));
k4_u(1:q,2:q)=dt*(A(1:q,1:(q-1)).*overlaps_e14(1:q,1:(q-1))...
            .^(3/2)./mass(1:q,2:q) - (A(1:q,2:q))...
            .*overlaps_e14(1:q,2:q).^(3/2)./mass(1:q,2:q));
% Check for contacts in e_2 direction:
overlaps_e24 = twodrkhertz0906contacts2(N, q, xx1, yy1, R);
% Calculate f4_u:
f4_u(1,1:q) = dt/2*(-(A(1,1:q)).*overlaps_e24(1,1:q)...
            .^(3/2)./mass(1,1:q));
f4_u(2:q,1:q)=dt/2*(A(1:(q-1),1:q).*overlaps_e24(1:(q-1),1:q)...
            .^(3/2)./mass(2:q,1:q) - (A(2:q,1:q))...
            .*overlaps_e24(2:q,1:q).^(3/2)./mass(2:q,1:q));
% Calculate f4_v:
```

```
    f4_v(1,1:q) = sqrt(3)*dt/2*(-(A(1,1:q))...
                .*overlaps_e24(1,1:q).^(3/2)./mass(1,1:q));
    f4_v(2:q,1:q)=sqrt(3)*dt/2*(A(1:(q-1),1:q)...
                .*overlaps_e24(1:(q-1),1:q)...
                .^(3/2)./mass(2:q,1:q) - (A(2:q,1:q))...
                .*overlaps_e24(2:q,1:q).^(3/2)./mass(2:q,1:q));
    % Check for contacts in e_3 direction:
    overlaps_e34 = twodrkhertz0906contacts3(N, q, xx1, yy1, R);
    % Calculate g4_u:
    g4_u(1:q,1) = dt/2*(-(A(1:q,1)).*overlaps_e34(1:q,1)...
                .^(3/2)./mass(1:q,1));
    g4_u(1:(q-1),2:q)=dt/2*(A(2:q,1:(q-1)).*overlaps_e34(2:q,1:(q-1))...
                .^(3/2)./mass(2:q,1:(q-1)) - A(1:(q-1),2:q)...
                .*overlaps_e34(1:(q-1),2:q).^(3/2)./mass(1:(q-1),2:q));
    g4_u(q,2:q)=dt/2*(-A(q,1:(q-1)).*overlaps_e34(q,2:q))...
                .^(3/2)./mass(q,2:q);
    % Calculate g4_v:
    g4_v(1:q,1) = -sqrt(3)*dt/2*(-(A(1:q,1)).*overlaps_e34(1:q,1)...
                .^(3/2)./mass(1:q,1));
    g4_v(1:(q-1),2:q)=-sqrt(3)*dt/2*(A(2:q,1:(q-1))...
                .*overlaps_e34(2:q,1:(q-1))...
                .^(3/2)./mass(2:q,1:(q-1)) - A(1:(q-1),2:q)...
                .*overlaps_e34(1:(q-1),2:q).^(3/2)./mass(1:(q-1),2:q));
    g4_v(q,2:q)=-sqrt(3)*dt/2*(-A(q,1:(q-1)).*overlaps_e34(q,2:q))...
                .^(3/2)./mass(q,2:q);
    % Now we go forward in time:
    u_new = u_old + (1/6) * (k1_u + 2*k2_u + 2*k3_u +k4_u)+...
            (1/6) * (f1_u + 2*f2_u + 2*f3_u +f4_u)+...
            (1/6) * (g1_u + 2*g2_u + 2*g3_u +g4_u);
    v_new = v_old +(1/6) * (f1_v + 2*f2_v + 2*f3_v +f4_v) ...
            +(1/6) * (g1_v + 2*g2_v + 2*g3_v +g4_v);
    x_new = x_old + (1/6) * (k1_x + 2*k2_x + 2*k3_x +k4_x);
    y_new = y_old + (1/6) * (k1_y + 2*k2_y + 2*k3_y +k4_y);
end
```

```
% This function calculating overlap between neighboring balls
% in e1 direction
function [new_overlaps] = twodrkhertz0906contacts1(N, q, xx1, R)
    new_overlaps = zeros(q,q);
    i=1;
    while(i<q+1)
        new_overlaps(i,1:(q-1)) = max(0, 1 + xx1(i,1:(q-1)) -...
                                  xx1(i,2:q));
        % Deal with the Nth_ball/wall interaction
        new_overlaps(i,q) = max(0, xx1(i,q)-q-(i-1)/2.0 );
        i=i+1;
    end
end

% This function calculating overlap between neighboring balls
% in e2 direction
function [new_overlaps] = twodrkhertz0906contacts2(N, q, xx, yy, R)
    new_overlaps = zeros(q,q);
    new_overlapsx = zeros(q,q);
    new_overlapsy = zeros(q,q);
    i=1;
    while(i<q+1)
        new_overlapsx(1:(q-1),i) = max(0, 0.5 + xx(1:(q-1),i) -...
                                   xx(2:q,i));
        new_overlapsy(1:(q-1),i) = max(0, yy(1:(q-1),i) -...
                                   yy(2:q,i) + sqrt(3)/2);
        i=i+1;
    end
    new_overlapsx(q,1:q)=  max(0,xx(q,1:q)-q-(q-1)/2);
    new_overlapsy(q,1:q)= max(0, yy(q,1:q)-q*sqrt(3)/2);
    new_overlaps= sqrt(new_overlapsx.^2 + new_overlapsy.^2);
end
```

```
% This function calculating overlap between neighboring balls
% in e3 direction
function [new_overlaps] = twodrkhertz0906contacts3(N, q, xx, yy, R)
    new_overlaps = zeros(q,q);
    new_overlapsx = zeros(q,q);
    new_overlapsy = zeros(q,q);
    new_overlapsx(1,1:q) = 0;
    new_overlapsy(1,1:q) = 0;
    i=2;
    while(i<q+1)
        new_overlapsx(i,1:(q-1)) = max(0, 0.5+xx(i,1:(q-1)) -...
                                   xx((i-1),2:q));
        new_overlapsy(i,1:(q-1)) = max(0, (-yy(i,1:(q-1)) +...
                                   yy((i-1),2:q)) + sqrt(3)/2);
        % Deal with the (i,q) ball
        new_overlapsx(i,q) = max(0, xx(i,q) - q - (i-1)/2);
        new_overlapsy(i,q) = max( 0, i*sqrt(3)/2- yy(i,q));
        i=i+1;
    end
    new_overlaps= sqrt(new_overlapsx.^2 + new_overlapsy.^2);
end
```

References

[1] J. Achenbach. Wave propagation in elastic solids. pages 29–33, 1984.

[2] E. C. Aifantis. On the gradient approach - relation to eringen's nonlocal theory. *International Journal of Engineering Science*, 49:1367–1377, 2011.

[3] N. Albin, A. Cherkaev, and V. Nesi. Multiphase laminates of extremal effective conductivity in two dimensions. *J. Mech. Phys. Solids*, 55(7):1513–1553, 2007.

[4] M. A. Antimonova, A. Cherkaevb, and A. B. Freidin. Phase transformations surfaces and exact energy lower bounds. *Int. J. Eng. Sci.*, 98:153–182, 2016.

[5] K. Astala and V. Nesi. Composites and quasiconformal mappings: new optimal bounds in two dimensions. *Calc. Var. Partial. Dif.*, 18(4):335–355, 2003.

[6] A. M. Balk, A. V. Cherkaev, and L. I. Slepyan. Dynamics of chains with non-monotone stress-strain relations. i. model and numerical experiments. *Journal of the Mechanics and Physics of Solids*, 49:131–148, 2001.

[7] J. M. Ball, J. C. Currie, and P. J. Olver. Null lagrangians, weak continuity, and variational problems of arbitrary order. *J. Funct. Anal.*, 41(2):135–174, 1981.

[8] J.M. Ball and F. Murat. Quasiconvexity and variational problems for multiple integrals. *J. Funct. Anal.*, 58:225–253, 1984.

[9] V. Berti, M. Fabrizio, and D. Grandi. Phase transitions in shape memory alloys: A non-isothermal ginzburg?landau model. *Physica D: Nonlinear Phenomena*, 239:95–102, 2010.

[10] C. Beyer and D. Figueroa. Design and analysis of strut-based lattice structures for vibration isolation. *J. Manuf. Sci. Eng.*, 138:121014, 2016.

[11] K. Bhattacharya. Comparison of the geometrically nonlinear and linear theories of martensitic transformation. *Continuum Mechanics and Thermodynamics*, 5:205–242, 1993.

[12] K. Bhattacharya. Microstructure of martensite. pages 1–87, 2004.

[13] K. Bhattacharya and R. V. Kohn. Symmetry, texture and the recoverable strain of shape-memory polycrystals. *Acta Materialia*, 44:529–542, 1996.

[14] C. Bil, K. Massey, and E. J. Abdullah. Wing morphing control with shape memory alloy actuators. *Journal of Intelligent Material Systems and Structures*, 24:879–898, 2013.

[15] V. Birman. Review of mechanics of shape memory alloy structures. *Appl. Mech. Rev.*, 50, 1997.

[16] R. W. Boyd. Nonlinear optics. *Journal of the Mechanics and Physics of Solids*, 2008.

[17] I. V. Chenchiah and K. Bhattacharya. The relaxation of two-well energies with possibly unequal moduli. *Arch Rational Mech Anal*, 187:409–479, 2008.

[18] A. Cherkaev. Bounds for effective properties of multimaterial two-dimensional conducting composites. *Mech. Mater.*, 41(4):411–433, 2009.

[19] A. Cherkaev and G. Dzierżanowski. Three-phase plane composites of minimal elastic stress energy: High-porosity structures. *Int. J. Solids. Struct.*, 50(25):4145–4160, 2013.

[20] A. Cherkaev and Y. Zhang. Optimal anisotropic three-phase conducting composites: Plane problem. *Int. J. Solids Struct.*, 48(20):2800–2813, 2011.

[21] B. G. Compton and J. A. Lewis. 3d-printing of lightweight cellular composites. *Adv. Mater.*, 26:5930–5935, 2014.

[22] C. Daraio, V. F. Nesterenko, E. B. Herbold, and S. Jin. Strongly nonlinear waves in a chain of teflon beads. *Phys. Rev. E*, 72, 2005.

[23] C. Daraio, V. F. Nesterenko, E. B. Herbold, and S. Jin. Energy trapping and shock disintegration in a composite granular medium. *Phys. Rev. Lett.*, 96, 2006.

[24] T. Dauxois and M. Peyrard. *Physics of Solitons*. Cambridge University Press, 2006.

[25] J. L. Ericksen. Equilibrium of bars. *Journal of Elasticity*, 5:3–4, 1975.

[26] J. L. Ericksen. Some phase transitions in crystals. *Arch. Rational Mech. Anal.*, 73:99–124, 1980.

[27] G. A. Francfort and F. Murat. Homogenization and optimal bounds in linear elasticity. *Arch. Ration. Mech. An.*, 94(4):307–334, 1986.

[28] G. Friesecke and K. Matthies. Geometric solitary waves in a 2d mass-spring lattice. *Discrete and Continuous Dynamical Systems-Series B*, 3:105–114, 2003.

[29] Y. Furuya. Design and material evaluation of shape memory composites. *Journal of Intelligent Material Systems and Structures*, 7:321–330, 1996.

[30] H. Gao, Y. Huang, W. D. Nix, and J. W. Hutchinson. Mechanism-based strain gradient plasticity-i. theory. *Journal of the Mechanics and Physics of Solids*, 47:1239–1263, 1998.

[31] L. V. Gibiansky and O. Sigmund. Multiphase composites with extremal bulk modulus. *J. Mech. Phys. Solids*, 48(3):461–498, 2000.

[32] Y. Grabovsky. The g-closure of two well-ordered, anisotropic conductors. *Proc. R. Soc. Edinb. A*, 123(3):423–432, 1993.

[33] Y. Grabovsky and R. V. Kohn. Microstructures minimizing the energy of a two phase elastic composite in two space dimensions. I: the confocal ellipse construction. *J. Mech. Phys. Solids*, 43(6):933–947, 1995.

[34] U. Harbola, A. Rosas, A. H. Romero, M. Esposito, and K. Lindenberg. Pulse propagation in decorated granular chains: An analytical approcah. *Phys. Rev. E*, 80, 2009.

[35] D. J. Hartl and D. C. Lagoudas. Aerospace applications of shape memory alloys. *Proceedings of the Institution of Mechanical Engineers, Part G: Journal of Aerospace Engineering*, 221:535–552, 2007.

[36] Z. Hashin. The elastic moduli of heterogeneous materials. *J. Appl. Mech.*, 29(1):143–150, 1962.

[37] Z. Hashin. On elastic behaviour of fibre reinforced materials of arbitrary transverse phase geometry. *J. Mech. Phys. Solids*, 13:119–134, 1965.

[38] Z. Hashin and S. Shtrikman. A variational approach to the theory of the elastic behaviour of polycrystals. *J. Mech. Phys. Solids*, 10(4):343–352, 1962.

[39] Z. Hashin and S. Shtrikman. A variational approach to the theory of the elastic behaviour of multiphase materials. *J. Mech. Phys. Solids*, 11(2):127–140, 1963.

[40] M. Helou and S. Kara. Design, analysis and manufacturing of lattice structures: an overview. *International Journal of Computer Integrated Manufacturing*, 31, 2018.

[41] R. Hill. The elastic behaviour of a crystalline aggregate. *Proc. Phys. Soc. A.*, 65(5):349, 1952.

[42] J. Hong. Universal power-law decay of the impulse energy in granular protectors. *Phys. Rev. Lett.*, 94, 2005.

[43] J. B. Hopkins, L. A. Shaw, T. H. Weisgraber, G. R. Farquar, C. D. Harvey, and C. M. Spadaccini. Organizing cells within non-periodic microarchitectured materials that achieve graded thermal expansions. *ASME. International Design Engineering Technical Conferences and Computers and Information in Engineering Conference*, 2B, 2015.

[44] J. B. Hopkins, Y. Song, H. Lee, C. M. Spadaccini, and N. X. Fang. Polytope sector-based synthesis and analysis of microstructural architectures with tunable thermal conductivity and expansion. *Journal of Mechanical Design*, 138:051401, 2016.

[45] K. C. Hwang, H. Jiang, Y. Huang, H. Gao, and N. Hu. A finite deformation theory of strain gradient plasticity. *Journal of the Mechanics and Physics of Solids*, 50:81–99, 2002.

[46] T. Ioannidou, J. Pouget, and E. Aifantis. Soliton dynamics in a 2d lattice model with nonlinear interactions. *J. Phys. A: Math. Gen.*, 36:643–652, 2003.

[47] R. D. James. Finite deformation by mechanical twinning. *Archive for Rational Mechanics and Analysis*, 77(2):143–176, 1981.

[48] R. D. James. Displacive phase transformations in solids. *J. Mech. Phys. Solids*, 34:359–394, 1986.

[49] R. D. James. The stability and metastability of quartz, metastability and in- completely posed problems (ed. antman, s., ericksen, j. l., kinderlehrer, d. and muller, i.). *IMA*, 3:147–176, 1987.

[50] R. D. James and K. F. Hane. Martensitic transformations and shape-memory materials. *Acta mater.*, 48:197–222, 2000.

[51] P. G. Kevrekidis. Non-linear waves in lattices: past, present, future. *Applied Mathematics*, 76:389–423, Apr 2011.

[52] D. Khatria, C. Daraioab, and P. Rizzoc. Coupling of highly nonlinear waves with linear elastic media. *Proc. SPIE*, 7292, 2009.

[53] M. Kohl. *Shape memory microactuators*. Springer Science & Business Media, 2013.

[54] I. A. Kunin. *The Theory of Elastic Media with Microstructure and the Theory of Dislocations*. Springer Berlin Heidelberg, 1975.

[55] A. Leonard, C. Chong, P. G. Kevrekidis, and C. Daraio. Traveling waves in 2d hexagonal granular crystal lattices. *Granular Matter*, 16, 2014.

[56] A. Leonard and C. Daraio. Stress wave anisotropy in centered square highly nonlinear granular systems. *Phys. Rev. Lett.*, 108, 2012.

[57] A. Leonard, F. Fraternali, and C. Daraio. Directional wave propagation in a highly nonlinear square packing of spheres. *Experimental Mechanics*, 53, 2013.

[58] L. Liu. Effective conductivities of two-phase composites with a singular phase. *J. Appl. Phys.*, 105(10):103503, 2009.

[59] L. Liu. Hashin–shtrikman bounds and their attainability for multi-phase composites. In *Proc. R. Soc. Lond. A Math Phys. Sci*, volume 466, pages 3693–3713. The Royal Society, 2010.

[60] L. Liu. New optimal microstructures and restrictions on the attainable hashin-shtrikman bounds for multiphase composite materials. 3:1–10, 07 2011.

[61] L. Liu, R. D. James, and P. H. Leo. New extremal inclusions and their applications to two-phase composites. *Arch. Rational Mech. Anal.(accepted)*, 2008.

[62] J. K. Lucek and K. J. Blow. Soliton self-frequency shift in telecommunications fiber. *Phys. Rev. A*, 45:6666–6674, 1992.

[63] K. A. Lurie and A. V. Cherkaev. G-closure of a set of anisotropically conducting media in the two-dimensional case. *J. Optim. Theory Appl.*, 42(2):283–304, 1984.

[64] K. A. Lurie and A. V. Cherkaev. Optimization of properties of multicomponent isotropic composites. *J. Optim. Theory Appl.*, 46(4):571–580, 1985.

[65] D. Mahmoud and M. A. Elbestawi. Lattice structures and functionally graded materials applications in additive manufacturing of orthopedic implants: A review. *J. Manuf. Mater. Process.*, 1:1020013, 2017.

[66] E. H. Mansfield. Neutral iioles in plane sheet reinforced iioles which are elastically equivalent to the uncut sheet. *Q. J. Mech. Appl. Math.*, 6(3):370–378, 1953.

[67] D. Mantovani. Shape memory alloys: Properties and biomedical applications. *JOM*, 52:36–44, 2000.

[68] G. W. Milton. Bounds on the electromagnetic, elastic, and other properties of two-component composites. *Phys. Rev. Lett.*, 46(8):542, 1981.

[69] G. W. Milton. Modelling the properties of composites by laminates. *Homogenization and effective moduli of materials and media*, 1:150–174, 1986.

[70] G. W. Milton. Composite materials with poisson's ratios close to -1. *J. Mech. Phys. Solids*, 40(5):1105–1137, 1992.

[71] G. W. Milton and A. Cherkaev. Which elasticity tensors are realizable? *J. Eng. Mater-T. ASME*, 117(4):483–493, 1995.

[72] G. W. Milton, W. Graeme, and R. V. Kohn. Variational bounds on the effective moduli of anisotropic composites. *J. Mech. Phys. Solids*, 36(6):597–629, 1988.

[73] J. M.Jani, M. Leary, A. Subic, and M. A. Gibson. A review of shape memory alloy research, applications and opportunities. *Materials and Design*, 56:1078–1113, 2014.

[74] NB Morgan. Medical shape memory alloy applications?the market and its products. *Materials Science and Engineering: A*, 378(1-2):16–23, 2004.

[75] Ali H Nayfeh and P Frank Pai. *Linear and nonlinear structural mechanics*. John Wiley & Sons, 2008.

[76] V. Nesi. Bounds on the effective conductivity of two-dimensional composites made of n $\geq$ 3 isotropic phases in prescribed volume fraction: the weighted translation method. *Proc. R. Soc. Edinb. A*, 1995.

[77] V. F. Nesterenko. Propagation of nonlinear compression pulses in granular media. *Applied Mechanics and Technical Physics*, 24:733–743, 1983.

[78] V. F. Nesterenko. Dynamics of heterogeneous materials. pages 1–27, 2001.

[79] V. F. Nesterenko. Waves in strongly nonlinear discrete systems. *Phil. Trans. R. Soc. A*, 376, 2018.

[80] V. F. Nesterenko, C. Daraio, E. B. Herbold, and S. Jin. Anomalous wave reflection at the interface of two strongly nonlinear granular media. *Phys. Rev. Lett.*, 95, 2005.

[81] X. Ni, P. Rizzo, J. Yang, D. Katri, and C. Daraio. Monitoring the hydration of cement using highly nonlinear solitary waves. *NDT and E International*, 52, 2012.

[82] A. N. Norris. A differential scheme for the effective moduli of composites. *Mech. Mater.*, 4(1):1–16, 1985.

[83] K. Otsuka and T. Kakeshita. Science and technology of shape-memory alloys: New developments. *MRS Bulletin*, 27:91–100, 2002.

[84] K. Otsuka and X. Ren. Physical metallurgy of ti?ni-based shape memory alloys. *Progress inMaterials Science*, 50:511–678, 2005.

[85] P. Pedregal. Partial minimization for vector variational problems. *Numerical Functional Analysis and Optimization*, 27:437–449, 2006.

[86] M. A. Porter, C. Daraio, I. Szelengowicz, E. B. Herbold, and P. G. Kevrekidis. Highly nonlinear solitary waves in heterogeneous periodic granular media. *Phys. Rev. E*, 77, 2008.

[87] A. Reuss. Berechnung der fließgrenze von mischkristallen auf grund der plastizitätsbedingung für einkristalle. *ZAMM-Journal of Applied Mathematics and Mechanics/Zeitschrift für Angewandte Mathematik und Mechanik*, 9(1):49–58, 1929.

[88] D. Rosen, S. Johnston, and M. Reed. Design of general lattice structures for lightweight and compliance applications. *Rapid Manufacturing Conference*, 2006.

[89] P. Rosenau. Hamiltonian dynamics of dense chains and lattices: or how to correct the continuum. *Phys. Lett. A*, 311:39–52, 2003.

[90] S. Sen, J. Hong, J. Bang, E. Avalos, and R. Doney. Solitary waves in the granular chain. *Phys. Rep*, 462:21, 2008.

[91] M. Shoaib and L. Kari. Discrete element simulation of elasto-plastic shock wave propagation in spherical particles. *Advances in Acoustics and Vibration*, 2011, 2011.

[92] O. Sigmund. A new class of extremal composites. *J. Mech. Phys. Solids*, 48(2):397–428, 2000.

[93] O. Sigmund and S. Torquato. Composites with extremal thermal expansion coefficients. *Appl. Phys. Lett.*, 69(21):3203–3205, 1996.

[94] O. Sigmund and S. Torquato. Design of materials with extreme thermal expansion using a three-phase topology optimization method. *J. Mech. Phys. Solids*, 45(6):1037–1067, 1997.

[95] O. Sigmund and S. Torquato. Design of smart composite materials using topology optimization. *Smart Mater. Struct.*, 8(3):365, 1999.

[96] S. Singamaneni and V. V. Tsukruk. Buckling instabilities in periodic composite polymeric materials. *Soft Matter*, 6:5681–5692, 2010.

[97] M. Sreekumar, T. Nagarajan, M. Singaperumal, M. Zoppi, and R. Molfino. Critical review of current trends in shape memory alloy actuators for intelligent robots. *Industrial Robot*, 34(4):285–294, 2007.

[98] D. Stoeckel. Shape memory actuators for automotive applications. *Materials and Design*, 11:302–307, 1990.

[99] T. Tadaki, K. Otsuka, and K. Shimizu. Shape memory alloys. *Annual Review of Materials Science*, 18:25–45, 1988.

[100] D. Talbot, J. R. Willis, and V. Nesi. On improving the hashin-shtrikman bounds for the effective properties of three-phase composite media. *IMA. J. Appl. Math*, 54(1):97–107, 1995.

[101] S. Timoshenko and J. M. Gere. *Theory of Elastic Stability*. New York: McGraw-Hill, 1961.

[102] David Tong. Tasi lectures on solitons: Instantons, monopoles, vortices and kinks. *Lecture Notes*, 2005.

[103] L. Truskinovsky and G. Zanzotto. Ericken's bar revisited: energy wiggles. *J. Mech. Phys. Solids*, 44:1371–1408, 1996.

[104] S. Vigdergauz. Optimal stiffening of holes under equibiaxial tension. *Int. J. Solids. Struct*, 30(4):569–577, 1993.

[105] W. Voigt. Ueber die beziehung zwischen den beiden elasticitätsconstanten isotroper körper. *Ann Phys-Berlin*, 274(12):573–587, 1889.

[106] P. S. Wahyudin, J. Wu, B. Zhao, I. Maskery, W. Elmadih, and R. Leach. Design and analysis of strut-based lattice structures for vibration isolation. *Precision Engineering*, 52:494–506, 2018.

[107] L. J. Walpole. On bounds for the overall elastic moduli of inhomogeneous systems–I. *J. Mech. Phys. Solids*, 14(3):151–162, 1966.

[108] J. Yang, D. Khatri, P. Anzel, and C. Daraio. Interaction of highly nonlinear solitary waves with thin plates. *International Journal of Solids and Structures*, 49, 2012.